# PALEOTEMPERATURE, VEGETATION CHANGE, FIRE HISTORY, AND LAKE PRODUCTIVITY FOR THE LAST 14,500 YEARS AT GOLD LAKE, PACIFIC NORTHWEST, USA

by

JAMILA BAIG

A DISSERTATION

Presented to the Environmental Studies Program
and the Division of Graduate Studies of the University of Oregon
in partial fulfillment of the requirements
for the degree of
Doctor of Philosophy

September 2023

DISSERTATION APPROVAL PAGE

Student: Jamila Baig

Title: Paleotemperature, Vegetation Change, Fire History, and Lake Productivity for the last 14, 500 years at Gold Lake, Pacific Northwest, USA

This dissertation has been accepted and approved in partial fulfillment of the requirements for the Doctor of Philosophy degree in the Environmental Studies Program by:

| | |
|---|---|
| Daniel Gavin | Chairperson & Advisor |
| Patricia McDowell | Co-advisor and core member |
| Scott Bridgham | Core Member |
| Lucas Silva | Core Member |
| Michelle Wood | Institutional Representative |

and

| | |
|---|---|
| Krista Chronister | Vice Provost for Graduate Studies |

Original approval signatures are on file with the University of Oregon Graduate School.

Degree awarded September 2023

DISSERTATION ABSTRACT

Jamila Baig

Doctor of Philosophy

Environmental Studies Program

September 2023

Title: Paleotemperature, Vegetation Change, Fire History, and Lake Productivity for the last 14, 500 years at Gold Lake, Pacific Northwest, USA

**Abstract**

The postglacial history of vegetation, wildfire, and climate in the Cascade Range (Oregon) is only partly understood. This study uses high-resolution analysis from a 13-meter, 14,500-year sediment core from Gold Lake to reconstruct forest vegetation, fire, and climate using four traditional palaeoecological methods: pollen, charcoal, organic matter variables, and a biological variable chironomid (midges living in the lake). As the response of these proxies differs, this multiproxy approach is vital to have a complete picture of past environments. The occurrence of three tephra layers, including a 78-cm airfall Mazama tephra and highly laminated segments, allows us to study tephra impacts at a fine temporal resolution. This study is the first attempt in Oregon to reconstruct paleotemperature using chironomids.

The high-resolution macroscopic charcoal and pollen analysis reveals minimal variation in pollen spectra during the Late Glacial and Younger Dryas periods. However, the early Holocene shows a sudden increase in *Pseudotsuga*, indicating warmer conditions, while the late Holocene shows an increase in *Tsuga heterophylla* and *Tsuga mertensiana*, suggesting the onset of moist conditions. The charcoal data indicate periods of large fire peaks during the Late Glacial, pre-, and post-Mazama eruption and since 4,000 years ago. Surprisingly, low fire activity is observed during the early Holocene, which contradicts expectations based on regional evidence of warmer and drier summers. The deposition of the Mazama tephra resulted in changes to the non-arboreal pollen composition, while arboreal taxa were minimally affected.

The paleotemperature reconstruction reveals variations in taxon richness of chironomids. The reconstructed midge-based mean July air temperature (MJAT) at Gold Lake ranged between 9.4 and 13.2°C, with the Late Glacial period being 2-3°C colder than present. The transition into the early Holocene indicates a temperature increase with MJAT varying between 10.7°C and 13.1°C. The analysis of organic geochemistry reveals variability in $\delta^{13}C_{org}$ and $\delta^{15}N$, reflecting changes in aquatic productivity. The base of the core following deglaciation shows low terrestrial input and high aquatic productivity, while the Holocene warming period is associated with decreased $\delta^{15}N$ and increased input from cyanobacteria. The thick Mazama tephra enhances diatom production and subsequent fluctuations in mass accumulation rate. The late Holocene exhibits high aquatic productivity, potentially influenced by increased forest fires and nutrient runoff.

This multiproxy approach significantly contributes to understanding climate change and ecosystem dynamics in the Cascade Range of Oregon based on high-resolution analysis of sediment records from Gold Lake.

This dissertation includes both previously published/unpublished and co-authored material.

CURRICULUM VITAE

NAME OF AUTHOR: Jamila Baig

GRADUATE AND UNDERGRADUATE SCHOOLS ATTENDED:

University of Oregon, Eugene
Karakoram International University, Gilgit, Pakistan
University of Peshawar, Pakistan
University of Punjab, Pakistan

DEGREES AWARDED:

Doctor of Philosophy, 2023, Environmental Sciences, Studies, and Policy, University of Oregon
Master of Science, Biological Sciences, 2012, Karakoram International University, Gilgit, Pakistan
Master of Science, Zoology, 2000, University of Peshawar, Pakistan
Bachelor of Science, Zoology, Botany & Geography,1998, University of Punjab, Pakistan

AREAS OF SPECIAL INTEREST:

Paleoecology, Pollen, Palynology, Paleoclimatology, Paleolimnology, Forest Fire, Paleotemperature reconstruction, Chironomids, Climate Change, High Altitude Lakes, Glaciers, Organic Geochemistry

PROFESSIONAL EXPERIENCE:

Lecturer Biology, Aga Khan Higher Secondary School Hunza, Pakistan, 2001-2005

Lecturer Zoology, Federal Government Degree College Hunza, Pakistan, 2005-2008

Lecturer Zoology, Karakoram International University, Gilgit, Pakistan, 2008-2016

Teaching Assistant, University of Oregon, Environmental Sciences, Studies, and Policy, 2017-2023

Instructor, University of Oregon, Department of Geography, Summer 2019

GRANTS, AWARDS, AND HONORS:

Grant on Climate Change and Glaciology, a collaborative project between the University of Oregon and Karakoram International University, Pakistan (Developed this project with two other colleagues, working as Assistant Project Director), US$ 500000, 2022-2025

Sean Rocks Memorial Scholarship, University of Oregon, USA, 2022-2023

Lokey Doctoral Science Fellowship, University of Oregon, USA, 2021-2022

Oregon Lakes Association Scholarship, University of Oregon, USA, 2022

Soderwall Environmental Studies Fund, University of Oregon, USA, 2021

Rippey Geography Endowment Fund, University of Oregon, USA, 2019 & 2021

David Easly Memorial Award, University of Oregon, USA, 2017 & 2022

Global Oregon International Research Award, University of Oregon, USA, 2017

First-year Graduate Fellowship, University of Oregon, USA, 2016-2017

Young Ecologist Research Scholarship for M. Phil research, WWF-Pakistan, 2012-2013

Co-PI on "Threatened birds of Central Karakoram National Park, their Conservation and Management Strategies" funded by SEED project of EVK2CNR (Italian project), 2012-2014

PUBLICATIONS:

**Baig, J**., & Gavin, D. G. (2023). Post-glacial vegetation and fire history with a high-resolution analysis of tephra impacts, High Cascade Range, Oregon, USA. Quaternary Science Reviews, 303, 107970.

**Baig, J**, Gavin, D.G., Walker, I., Porinchu, D.F., Bartlein, P. Manuscript in preparation for Journal of Quaternary Science. Chironomid-Inferred Postglacial Temperature Reconstruction From Gold Lake, Oregon, USA.

**Baig, J** & Gavin, D.G. Manuscript in preparation for Journal of Quaternary Science. Paleolimnological History Of Gold Lake Using Geochemical Signatures of Organic Matter, Oregon, USA.

Alam, A., **Baig, J**., Din, S. U., Arshad, M., Adnan, M., & Khan, A. (2016). Relative abundance of benthic macroinvertebrates in relation to the abiotic environment in Hussainabad nallah, Hunza, Gilgit Baltistan, Pakistan. Int J Biosci, 9(3), 185-193.

Naseer, F., **Baig, J**., Din, S. U., Nafees, M. A., Alam, A., Hameed, N., ... & Shah, S. R. A. (2016). Impact of water quality on the distribution of macro-invertebrate in Jutial nallah, Gilgit-Baltistan, Pakistan. Int J Biosci, 9(6), 451-459.

**Baig, J**., Shah, A., & Haq, M. (2011). Reduction in Iodine Deficiency Disorders: A Prospective Study of 2550 School Children in Northern Areas. Proc. Pakistan Congr. Zool, 31, 89-94.

**Baig, J**., & Shahzadi. (2011). Efficacy of (Dirhinus Giffardii) On Biological Control of Fruit Fly in Laboratory Conditions. Proc. Pakistan Congr. Zool, 31, 125-131.

Bahadur, S., **Baig, J**., & Husain, S. (2011). Socio-Economic Impact of Trophy Hunting on Communities in Gilgit Baltistan. Proc. Pakistan Congr. Zool, 31, 71-77.

ACKNOWLEDGMENTS

I am deeply grateful to my supervisor, Dan Gavin, for his exceptional professional guidance, unwavering moral and financial support, and his remarkable kindness and patience towards all his students, including myself. From our first meeting in 2015 to our field work at Gold Lake, teaching me to process and identify pollen with patience and explaining every step to run complicated “R” codes, Dan has consistently made me feel welcomed and supported. In particular, Dan's assistance in collecting, processing, and identifying data is instrumental. Supporting my ambitious ideas to take a multiproxy approach for my dissertation, he left no stone unturned to support me in completing this project. This project and the Ph.D. journey would not have been possible without his support, so I call him my “MENTOR.” This journey does not end with the completion of a Ph.D.; I am looking forward to working on many projects in the future.

I extend my heartfelt appreciation to my co-advisor, Pat McDowell, who helped me survive a shift in the dissertation aspect after two years of working on a proposal in a different direction and ensuring I am ready to work on a new project. Thank you for all your support and for guiding me in the right direction.

I am thankful to my committee members, Lucas Silva, Scott Bridgham, and Michelle Wood, for their invaluable academic guidance and unwavering support. Despite unexpected circumstances, such as the pandemic and family responsibilities, my committee members were understanding and supportive, which I sincerely appreciate.

I want to thank Prof. Ian Walker (University of British Columbia) for his support and guidance in identifying chironomid head capsules, spending hours on Zoom, and contributing to the chironomid manuscript. My thanks go to Prof. David Porinchu (University of Georgia) for helping me identify chironomids and for editing a manuscript on chironomids.

I am genuinely grateful to my lab mates Geoffrey Johnson, Lauren Hendricks, Buzz Nanavati, and Erin Herring. Thanks to dear friends Chantel Saban and Monika Ruwaimana for every moment we shared, crying and laughing, and for the memorable food and chai we had.

Finally, I want to express my deepest gratitude to my husband, Amir Ali, for his

unwavering support throughout this journey. He sacrificed a lot so that we could get the education we have today. Without his love and encouragement, I would not have been able to achieve what I have.

To my children, Zain Shah and Farheen Shah, who constantly fill our lives with immeasurable joy and constantly remind us of what truly matters. They were great support during this journey and allowed me to spend hours and hours away from them to complete my work. My son, Zain Shah, with whom I shared the commencement ceremony 2023 at the University of Oregon, two ducks from a family, is a lifelong memory that we will always cherish.

We acknowledged the funding support provided by the University of Oregon, Lokey Doctoral Science Fellowship, Oregon's Lake Association Scholarship, David Easly Memorial Award, Sean Rocks Memorial Scholarship, Rippey Geography Endowment Fund, Soderwall Environmental Studies Fund, and First-year Graduate Fellowship, University of Oregon, USA.

For Zaibul and Abdullah Baig (my parents), whose vision and hard work led me to achieve all endeavors in my life,

and

for Amir Ali, Zain, and Farheen, my constant support pillars.

TABLE OF CONTENTS

LIST OF FIGURES

Figure Page

LIST OF TABLES

Table Page

LIST OF SUPPLEMENTARY TABLES

Supplementary Table Page

LIST OF FIGURES

Figure Page

# I. INTRODUCTION

The history of vegetation, wildfire, and climate in the Cascade Range (Oregon) is only partly understood. During the transition from the Last Glacial Maximum about 21,000 years ago to the present interglacial stage, the Pacific Northwest has not only experienced a significant change in vegetational composition, but it also has resulted in a shift of the biogeographic range of certain species (Whitlock, 1992). Lake sediments are used to interpret past environmental conditions using the information stored in the sediment profile, including fossilized chironomids, pollen (Smol et al., 2001), and organic matter of the lake (Meyers, 2003). These proxies provide information about changes within the lakes and their surroundings, including lake catchment and terrestrial vegetation that directly and indirectly affect the lake ecosystem. As the response of these two proxies is different from each other in terms of time and scale (Birks & Birks, 2008), a multiproxy approach is vital to have a complete picture of community ecology by detecting the weaknesses and emphasizing the strengths of each proxy (Lotter, 2003). These proxies provide a wide range of environmental information like lake trophic status, lake development, eutrophication, temperature changes, vegetation change, fire, and lake productivity (Walker & Mathewes, 1987; Stahl, 1959; Bryce, 1962; Walker & Paterson, 1983; Meyers, 2003).

The Pacific Northwest of the United States has many lakes, making it a potential place for answering fundamental palaeoecological questions related to coupled climate-ecosystem transitions since the Last Glacial Maximum. For this dissertation, the Pacific Northwest is defined as a geographical region in North America that includes the states of Washington, Oregon, and Idaho in the United States. The region is characterized by its proximity to the Pacific Ocean, lush forests, diverse ecosystems, and landscapes, including marked ecological gradients from plains to mountains and from deserts to temperate rainforests. In this broad region, almost every lake studied to date has evidence of three major volcanic eruptions in the Pacific Northwest, including St Helens (Southwestern Washington), Mount Mazama (Southwestern Oregon), and Glacier Peak (Washington Cascade Range), which provide a helpful dating tool alongside radiocarbon dating (Sarna-Wojcicki et al., 1983). Studies of these lakes have provided many insights into the long-term ecology and climate history of the Pacific Northwest. Below, I introduce some of these themes.

The Pacific Northwest has many lakes, making it a potential place for answering some palaeoecological questions since the Last Glacial Maximum. Almost every studied lake has evidence of three major volcanic eruptions in the Pacific Northwest, including St Helens (Southwestern Washington), Mount Mazama (Southwestern Oregon), and Glacier Peak (Washington Cascade Range), which provide a helpful dating tool alongside radiocarbon dating (Sarna-Wojcicki et al., 1983). Studies of these lakes have provided many insights into the long-term ecology and climate history of the Pacific Northwest. Below, I introduce some of these themes.

**Climate-fire-vegetation linkages**

Understanding the link between climate, fire, and vegetation is crucial to understand the impacts on the region's ecosystem (Gavin et al., 2013; Whitlock et al., 2015; Lucas, 2022). The response of preserved pollen and charcoal in lake sediment shows that fire and volcanic eruptions have substantially altered vegetation in the Cascade Range of the Pacific Northwest (Agee, 1993) as the intensity of wild fires in the Pacific Northwest is directly impacted by climate variability (Lucas, 2022). From the Bolling-Allerod (14.4 -12.9 ka) to the Holocene (11.6 ka), insolation and jet stream position caused seasonal changes in temperature and precipitation, resulting in major biotic reorganization (Kutzbach et al., 1998).

**Tephra impacts on lake ecosystems**

Tephra consists of fragmented material of various size and ash that is released during a volcanic eruption and have various degree of impact on terrestrial and aquatic ecosystems (Rose et al., 2009; Delmelle et al., 2001; Egan et al., 2016). Redeposition of tephra from vast catchments adds progressively to the lake ecology, changing it over time (Telford et al., 2004), whereas lakes with a limited catchment area will be less responsive to this process. Alterations in the lake's biotic reaction to tephra can have long-term or short-term effects on algae due to shifts in nutrient input (Blinman et al., 1979). For example, in alpine lakes in British Columbia, a dramatic rise in diatoms owing to silica fertilization persisted for 300 years (Hickman & Reasoner, 1994), but in European lakes, the reaction was short-lived and measured in decades rather than centuries (Lotter et al., 1995).

**Multiproxy climate reconstruction using pollen and chironomids**

Fossil pollen has been used since 1916 to trace the abundance of plants and changes in a vegetational pattern, which can be used to infer past changes and provide important analogs for a vegetational response to climate change in the future (Overpeck et al., 1991). Fossil pollen data helps understand the relationship between past vegetation and climate change as a direct and indirect proxy (Davis & Shaw, 2001). The summer air and lake water temperature significantly affect the distribution of larvae in the midge family Chironomidae (Walker et al., 1997). Remains of chironomid larvae, particularly the fossilized head capsule, preserve well in quaternary lake sediments and remain identifiable, typically to genus, species-group, or morphotype level (Brooks et al., 2007). Paleotemperature can be reconstructed using chironomid taxa because they require a specific temperature to complete different life cycle stages, including pupation, larval, and emergence into an adult fly that affect their abundance and distribution (Walker & Cwynar, 2006). This relationship is then used to develop a transfer function for air and water temperature (Brooks & Birks, 2001; Walker et al., 1993).

Multiproxy studies have become a powerful tool to assess environmental and climate change. The multiproxy approach helps reconstruct past environments, make future predictions, and understand different aspects of ecosystems concerning climate change and major events in the past. Multiproxy studies are more helpful than a single proxy because they provide a comprehensive overview of the ecosystem as a community due to their multiple interactions (Birks & Birks, 2006).

A powerful example of this approach was a comparison of two independent multiproxy studies conducted in Switzerland (Lotter et al., 2000) and Norway (Birks & Ammann, 2000), included pollen, chironomids, and Cladocera, an order of microcrustaceans to infer changes that occurred during the Younger Dryas event. Birks & Ammann, 2000 combined both data sets and inferred a similar pattern of fall in temperature during Younger Dryas and a sharp rise after this event with a minor difference between values of pollen and chironomids compared to Cladocera. These results show how independent terrestrial and aquatic origin climate proxies may correspond. There was an increased abundance of aquatic organisms with increased lake productivity due to a temperature rise, and it was correlated with the interaction between different proxies (Smol et al., 2005). Chironomids can produce more reliable July temperature

estimates than pollen, even if no modern analogs are available (Lotter et al., 1999). Thus, palaeoecological research of fossilized chironomid assemblages can reconstruct past lake fauna changes and indirectly reveal past temperature variations (Cwynar & Levesque, 1995; Porinchu et al., 2003).

This study will be the first attempt to reconstruct temperature for the past 14,500 years using a fossilized chironomid head capsule in Oregon. While much work has been done in Canada, Europe, and other parts of the world, the only chironomid reconstructions in the USA have been in California, Colorado, Nevada, and Utah (Haskett & Porinchu, 2014; Porinchu et al., 2010). It will be helpful to see how temperature has changed quantitatively over the Last Glacial Maximum and Holocene and how chironomid composition changed in response to temperature change.

**Sediment organic matter and lake productivity**

The presence of organic matter in lakes indicates lake productivity, climate change, and the adjacent vegetation. Lake sediment organic matter, even if only a small portion of total lake sediment, contains stable isotopes, elements, and chemical indicators that provide paleoenvironmental data about the lake and its surroundings (Meyers, 2003). Lake sediment processes that affect organic matter are affected by higher sedimentation and primary production than in oceans. Clastic sediment particles can dilute organic matter, while carbonate mineral dissolution can concentrate it (Dean, 1999). As for reconstructing climate, multiple proxies related to lake productivity ($\delta^{13}C_{org}$, $\delta^{15}N$, C/ N ratio, and mass accumulation rates) can be used to reconstruct lake ecosystem productivity through time.

**The Gold Lake research site and overall project goals**

Gold Lake is 38.9 hectares in size and has a watershed area of 48.4 $km^2$ located in the Cascade Range (43° 37' 57"N, 122° 02' 36" W) in a glacially carved hollow in basaltic andesite at an elevation of 1465m a.s.l. It gets its water from nearby springs and Salt Creek, which runs through Gold Lake Bog on the lake's northeastern shore, and due to having high phosphorus (0.047 mg/l) and chlorophyll a (1.9 mg/l), it is highly productive (Johnson et al., 1985).

A 13-meter-long core of lake sediments from the present to approximately 14,500 years ago was obtained from the lake in the summer of 2018. The core has outstanding properties, including a high sedimentation rate (13 meters in 14.5 ka) that allows detailed sampling, sections

of varved sediment (annual layering that allows sampling from a single year for detailed studies), and well-preserved layers of tephra from the Mount Mazama eruption, Llao Rock eruption, and Rock Mesa eruption. The multiproxy approach using pollen, chironomids, wildfire charcoal, and geochemical indicators helps reconstruct past environments, make future predictions, and understand different aspects of ecosystems concerning climate change and significant events in the past.

This study aims to reconstruct paleotemperature, paleotemperature reconstruction, vegetation change, fire history, and lake productivity using multiple proxies (chironomids, pollen, charcoal, LOI, carbon to nitrogen ratio (C/N ratio), total organic carbon (TOC), total nitrogen (TN), $\delta^{13}C_{org}$, and $\delta^{15}N$) from Gold Lake. There have been several pollen studies in the region regarding vegetation change and its relation to climate change and other disturbances, but no work has been done so far in Oregon to reconstruct temperature based on chironomids.

According to Whitlock (1992), vegetation change can be studied at a very fine temporal scale with the help of varved lake sediments to see the sensitivity of vegetation to decadal and century-scale environmental changes. A two-meter section near the middle of the Gold Lake sediment core is highly laminated. Detailed analysis of the varved section will enable us to see vegetational responses to environmental changes on a short and long-term time scale and to see succession in the study area. In addition, the large eruption from Mt. Mazama 7600 years ago and several other small tephras are found in the cores. This allows us to examine the effects of volcanic disturbances on terrestrial vegetation and the aquatic environment.

To characterize its palaeoecological history, I interpret the 14,500-year sediment record of Gold Lake, a mesotrophic lake with high aquatic production. The rapid sedimentation rate at Gold Lake and thicker Mazama tephra than in prior studies allow this record to analyze plant and fire responses to tephra at fine temporal resolution. I aimed to reconstruct postglacial plant change, fire history, temperature, and lake productivity at multi-centennial and sub-decadal resolutions.

**Organization of the dissertation**

This dissertation is organized into three main chapters. Jamila Baig and Daniel Gavin have published chapter II. Chapter III is in the process of submission by Jamila Baig, Daniel

Gavin, Ian Walker, David Porinchu, and Patrick Bartlein. Chapter IV is also in the submission process by Jamila Baig and Daniel Gavin in the Journal of Quaternary Sciences.

Chapter II will use the multiproxy (pollen, charcoal, LOI, and magnetic susceptibility) approach to answer the following questions. How has the terrestrial vegetation changed over the last 14,500 years in Gold Lake's vicinity, and how has fire history shaped the current vegetation pattern? This chapter included a high-resolution analysis of vegetation around the Mazama and Llao rock eruption, while charcoal has been analyzed at high resolution throughout the core at 1 cm resolution (ca. 10 yrs). This will help us to answer the following questions: How has the terrestrial vegetation responded and changed after the significant disturbance of the Mount Mazama eruption and Llao rock eruption, for which there is evidence in the lake sediments? I have 78 cm of Mazama tephra, 1 cm of Llao rock eruption, and 1 cm of Rock Mesa eruption in the core. Using a high-resolution analysis of laminated (finely layered) sections of the lake cores below and above the Mazama tephra layer will enable me to address succession at a fine time scale before and after this critical disturbance event, addressing both the tree (arboreal) and non-arboreal components of vegetation and the response of fire to the tephra, as well.

Chapter III describes a paleotemperature reconstruction using fossilized chironomids in Oregon for the first time. The goal of this chapter is to answer the following questions. Has the air and lake water temperature changed over the last 14,500 years based on fossilized chironomids in Gold Lake? Does paleotemperature show a similar or different change pattern compared to other studied lakes in western North America, British Columbia, and other nearby regions? I employ Inter-Mountain West's midge-based training data set (Haskett & Porinchu, 2014) and propose an inference model for mean July air temperature (MJAT) utilizing better elevation-adjusted temperature estimations. I compare our reconstruction with regional paleoclimate work to analyze high-elevation climate controls.

Chapter IV describes Gold Lake's paleolimnology and biological productivity over time. Gold Lake, one of the most productive lakes in the High Cascade Range, is ideal for studying lake sediment's reaction to many environmental conditions. This article develops high-resolution lake productivity records utilizing several proxies in lacustrine lake sediment with diverse causes impacting its concentration since the Late Glacial epoch. I addressed the following questions: How have lake chemistry and biological productivity (total organic carbon (TOC), total nitrogen (TN), $\delta^{13}C_{org}$, and $\delta^{15}N$, C/N ratio, carbon mass accumulation rate (CMAR) of Gold Lake varied

over the last 14,500 years? How and why is Gold Lake's paleolimnology similar to or different from other Pacific Northwest lakes?

## References


Agee, J. K. (1993). Fire Ecology of Pacific Northwest Forests. In *International Journal of Wildland Fire* (Vol. 4, Issue 3, pp. 113–136). https://doi.org/10.1071/wf9940195

Birks, H. H., & Ammann, B. (2000). Two terrestrial records of rapid climatic change during the glacial- Holocene transition (14,0009,000 calendar years B.P.) from Europe. *Proceedings of the National Academy of Sciences of the United States of America*, *97*(4), 1390–1394. https://doi.org/10.1073/pnas.97.4.1390

Birks, H. H., Battarbee, R. W., & Birks, H. J. B. (2000). The development of the aquatic ecosystem at Kråkenes Lake, western Norway, during the late glacial and early Holocene-a synthesis. Journal of Paleolimnology, 23(1), 91.

Birks, H. H., & Birks, H. J. B. (2006). Multi-proxy studies in palaeolimnology. *Vegetation History and Archaeobotany*, *15*(4), 235–251. https://doi.org/10.1007/s00334-006-0066-6

Birks, H. J. B., & Birks, H. H. (2008). Biological responses to rapid climate change at the Younger Dryas-Holocene transition at Kråkenes, western Norway. *Holocene*, *18*(1), 19–30. https://doi.org/10.1177/0959683607085572

Blinman, E., Mehringer Jr, P. J., & Sheppard, J. C. (1979). Pollen influx and the deposition of Mazama and Glacier Peak tephra. In P. . Shets & D. K. K. Grayson (Eds.), *Volcanic activity and human ecology* (pp. 393–425). Academic Press.

Brooks, S. J., Langdon, P. G., & Heiri, O. (2007). *The identification and use of palaearctic chironomidae larvae in palaeoecology (Technical guide / quaternary research association, no. 10)*. Quaternary Research Association.

Brooks, Stephen J., & Birks, H. J. B. (2001). Chironomid-inferred air temperatures from Lateglacial and Holocene sites in north-west Europe: Progress and problems. *Quaternary Science Reviews*.

Bryce, D. (1962). Chironomidae (Diptera) from freshwater sediments with special reference to Malham Tarn (Yorks). *Trans. Soc. Br. Entomol*, *15*, 41–54.

Cwynar, L. C., & Levesque, A. J. (1995). Chironomid evidence for late-glacial climatic reversals in maine. *Quaternary Research*, *43*(3), 405–413. https://doi.org/10.1006/qres.1995.1046

Davis, M. B., & Shaw, R. G. (2001). Range shifts and adaptive responses to quaternary climate change. *Science*, *292*(5517), 673–679. https://doi.org/10.1126/science.292.5517.673

Dean, W. E. (1999). The carbon cycle and biogeochemical dynamics in lake sediments. Journal of paleolimnology, 21, 375-393.

Delmelle, P., Stix, J., Bourque, C. P. A., Baxter, P. J., Garcia-Alvarez, J., & Barquero, J. (2001). Dry deposition and heavy acid loading in the vicinity of Masaya Volcano, a major sulfur and chlorine source in Nicaragua. Environmental science & technology, 35(7), 1289-1293.

Gavin, D. G., Brubaker, L. B., & Greenwald, D. N. (2013). Postglacial climate and fire-mediated vegetation change on the western Olympic Peninsula, Washington (USA). *Ecological Monographs*, *83*(4), 471–489. https://doi.org/10.1890/12-1742.1

Haskett, D. R., & Porinchu, D. F. (2014). A quantitative midge-based reconstruction of mean July air temperature from a high-elevation site in central Colorado, USA, for MIS 6 and 5. *Quaternary Research*, *82*(3), 580–591. https://doi.org/10.1016/j.yqres.2014.05.002

Hickman, M., & Reasoner, M. A. (1994). Diatom responses to late Quaternary vegetation and climate change, and to deposition of two tephras in an alpine and a sub-alpine lake in Yoho National Park, British Columbia. *Journal of Paleolimnology 1994 11:2*, *11*(2), 173–188. https://doi.org/10.1007/BF00686864

Johnson, D. M. (1985). Atlas of Oregon lakes. Oregon State University Press.

Kutzbach, J., Gallimore, R., Harrison, S., Behling, P., Selin, R., & Laarif, F. (1998). Climate and biome simulations for the past 21,000 years. *Quaternary Science Reviews*, *17*(6–7), 473–506. https://doi.org/10.1016/S0277-3791(98)00009-2

Lotter, A. F., Birks, H. J. B., & Zolitschka, B. (1995). Late-glacial pollen and diatom changes in response to two different environmental perturbations: volcanic eruption and Younger Dryas cooling. *Journal of Paleolimnology 1995 14:1*, *14*(1), 23–47. https://doi.org/10.1007/BF00682592

Lotter, A. F, Birks, H. J. B., Eicher, U., Hofmann, W., Schwander, J., & Wick, L. (2000). Younger Dryas and Allerod summer temperatures at Gerzensee (Switzerland) inferred from fossil pollen and cladoceran assemblages. *Palaeogeography, Palaeoclimatology, Palaeoecology*, *159*(3–4), 349–361. https://doi.org/10.1016/S0031-0182(00)00093-6

Lotter, André F. (2003). Multi-proxy climatic reconstructions. In *Mackay, A., Battarbee, R.W., Birks, H.J.B., Oldfield, F. (Eds.), Global Change in the Holocene* (pp. 373–383).

Lotter, André F., Walker, I. R., Brooks, S. J., & Hofmann, W. (1999). An intercontinental comparison of chironomid palaeotemperature inference models: Europe vs North America. *Quaternary Science Reviews*, *18*(6), 717–735. https://doi.org/10.1016/S0277-3791(98)00044-4

Silva, L. C. (2022). Expanding the scope of biogeochemical research to accelerate atmospheric carbon capture. Biogeochemistry, 161(1), 19-40.

Meyers, P. A. (2003). Applications of organic geochemistry to paleolimnological reconstructions: A summary of examples from the Laurentian Great Lakes. *Organic Geochemistry*, *34*(2), 261–289. https://doi.org/10.1016/S0146-6380(02)00168-7

Overpeck, J. T., Bartlein, P. J., & Webb, T. I. (1991). Potential magnitude of future vegetation change in eastern North America: Comparisons with the past. *Science*, *254*, 692–695.

Porinchu, D. F., MacDonald, G. M., Bloom, A. M., & Moser, K. A. (2003). Late Pleistocene and early Holocene climate and limnological changes in the Sierra Nevada, California, USA inferred from midges (Insecta: Diptera: Chironomidae). *Palaeogeography, Palaeoclimatology, Palaeoecology*, *198*(3–4), 403–422. https://doi.org/10.1016/S0031-0182(03)00481-4

Porinchu, D. F., Reinemann, S., Mark, B. G., Box, J. E., & Rolland, N. (2010). Application of a midge-based

inference model for air temperature reveals evidence of late-20th century warming in sub-alpine lakes in the central Great Basin, United States. *Quaternary International*, *215*(1–2), 15–26. https://doi.org/10.1016/j.quaint.2009.07.021

Rose, W. I., & Durant, A. J. (2009). Fine ash content of explosive eruptions. Journal of Volcanology and Geothermal Research, 186(1-2), 32-39.

Sarna-Wojcicki, Andrei M., Champion, D.E & Davis, J. O. (1983). Holocene volcanism in the conterminous United States and the role of silicic volcanic ash layers in correlation of latest-Pleistocene and Holocene deposits. In *In J. H.E. Wright (Ed.), Late-Quaternary Environments of the United State* (pp. 52–77). University of Minnesota Press, Minneapolis.

Smol, J. P., Birks, H. J. B., & Last, W. M. (Eds.). (2001). *Tracking Environmental Change Using Lake Sediments* (Vol. 4). Springer Netherlands. https://doi.org/10.1007/0-306-47671-1

Smol, J. P., Wolfe, A. P., Birks, H. J. B., Douglas, M. S., Jones, V. J., Korhola, A., ... & Weckström, J. (2005). Climate-driven regime shifts in the biological communities of arctic lakes. Proceedings of the National Academy of Sciences, 102(12), 4397-4402.

Stahl, J. B. (1959). The developmental history of the chironomid and Chaoborus faunas of Myers Lake. *Invest. Indiana Lakes Streams*, *5*, 47–102.

Telford, R. J., Barker, P., Metcalfe, S., & Newton, A. (2004). Lacustrine responses to tephra deposition: examples from Mexico. *Quat Sci Rev*, *23*(23–24), 2337–2353. https://doi.org/10.1016/j.quascirev.2004.03.014

Walker, I. R., Reavie, E. D., Palmer, S., & Nordin, R. N. (1993). A palaeoenvironmental assessment of human impact on Wood Lake, okanagan valley, British Columbia, Canada. Quaternary International, 20, 51-70.

Walker, Ian R., & Cwynar, L. C. (2006). Midges and palaeotemperature reconstruction—the North American experience. *Quaternary Science Reviews*, *25*(15–16), 1911–1925. https://doi.org/10.1016/j.quascirev.2006.01.014

Walker, I. R., Levesque, A. J., Cwynar, L. C., & Lotter, A. F. (1997). An expanded surface-water palaeotemperature inference model for use with fossil midges from eastern Canada. Journal of Paleolimnology, 18(2), 165-178.

Walker, Ian R, & Paterson, C. G. (1983). Post-Glacial Chironomid Succession in Two Small, Humic Lakes in the New Brunswick-Nova Post-glacial Chironomid Succession in Two Small, Humic Lakes in the New Brunswick -Nova Scotia (Canada) Border Area'. *Source: Freshwater Invertebrate Biology*, *2*(2), 61–73. http://www.jstor.org/stable/1467111

Whitlock, C. (1992). Vegetational and climatic history of the Pacific Northwest during the last 20 000 years: implications for understanding present-day biodiversity. *Northwest Environmental Journal*, *8*(1), 5–28.

Whitlock, Cathy, McWethy, D. B., Tepley, A. J., Veblen, T. T., Holz, A., McGlone, M. S., Perry, G. L. W., Wilmshurst, J. M., & Wood, S. W. (2015). Past and present vulnerability of closed-canopy temperate forests to altered fire regimes: A comparison of the pacific Northwest, New Zealand, and Patagonia. *BioScience*, *65*(2), 151–163. https://doi.org/10.1093/biosci/biu194

# II. POSTGLACIAL VEGETATION AND FIRE HISTORY WITH A HIGH-RESOLUTION ANALYSIS OF TEPHRA IMPACTS, HIGH CASCADE RANGE, OREGON, USA

Published as Baig, J., & Gavin, D. G. (2023). Postglacial vegetation and fire history with a high-resolution analysis of tephra impacts, high Cascade Range, Oregon, USA. Quaternary Science Reviews, 303, 107970.

JB and DGG conceptualized the study and devised the methodology. JB acquired the funding while curation, analysis, and visualization of the data were done with the help of DGG. JB wrote the original manuscript, and DGG reviewed, edited, and contributed to the final manuscript.

## Introduction

It is well understood that climate and fire regimes have driven postglacial vegetation change in the Pacific Northwest USA (Whitlock, 1992; Walsh et al., 2015). It is also well-understood how soil and landscape attributes can influence Holocene vegetation trajectories (Brubaker, 1975; Tweiten et al., 2015). It is less clear how dramatic changes in soil, via significant additions of volcanic tephra, have influenced vegetation and fire during postglacial vegetation changes. In particular, Mt Mazama in the southern Oregon Cascade Range, at 7.63 ka (thousands of calibrated years before 1950 AD), in one of the largest volcanic eruptions of the Holocene, deposited > 50 cm of tephra within 100 km of the volcano (Egan et al., 2015; Buckland et al., 2020), and emplaced a new soil parent material that differed substantially from pre-eruption soils (McDaniel et al., 2005).

Among the various natural disturbances that alter an ecosystem, fire and volcanic eruptions have greatly affected vegetation in the Cascade Range of the Pacific Northwest (Agee, 1993), which is reflected by the response of fossilized pollen and charcoal in lake sediment (Egan et al., 2016). The postglacial vegetation history of this region reveals major biotic

reorganization occurred from the Bolling-Allerod (14.4 -12.9 ka) to the Holocene (11.6 ka), where seasonal changes in temperature and precipitation occurred due to the direct effects of insolation and jet stream position (Kutzbach et al., 1998). Over time, fire was an additional factor to climate, causing significant changes in vegetation cover, so it is essential to understand the relationship between climate, fire, and vegetation (Gavin et al., 2013; Whitlock et al., 2015). For example, *Alnus rubra*, *Pinus contorta,* and *Pseudotsuga* had individualistic responses to changing climate but maintained their presence within the mountainous landscape (Whitlock, 1992). Furthermore, postglacial climate change may manifest differently across large regions, especially regions with major continentality and topographic gradients, such as in the Pacific Northwest. In addition, non-equilibrium responses of vegetation and fire to environmental change and the individualistic responses of each taxon to perturbations such as climate, fire, and tephra (Chapin and Shaver, 1985; Webb, 1986) must be considered when interpreting sediment records.

The impact of airfall tephra deposition on vegetation varies greatly, depending on several factors, including tephra thickness (Thorarinsson, 1979), distance from eruption (Millar et al., 2006), response and sensitivity of vegetation (Harris and Couvering, 1995; Antos and Zobel, 1986; Hotes et al., 2006), and a negative impact on soil fertility by limiting nutrient availability due to tephra thickness (Crisafulli et al., 2015). Effects of tephra may include direct damage (e.g., stripping of foliage and twigs from the canopy), burial of plants, and soil alteration. Small plants are affected greatly, as shown by only partial recovery of the understory plant community 20 years after 15 cm of tephra deposition from 1980 Mount Saint Helens (Antos and Zobel, 2005). During the burial period, some plant species may persist by modifying their growth to penetrate the tephra with rhizomes or establishing adventitious roots, while other species require seed dispersal to reestablish (Mack, 1981; Antos and Zobel, 1986).

The lake's biotic response to tephra also varies from long-term to short-term impacts related to nutrient contribution changes that affect algae (Blinman et al., 1979). For example, a sudden increase in diatoms due to silica fertilization lasted for 300 years in alpine lakes in British Columbia (Hickman and Reasoner, 1994), while a short-term decadal response was observed in European lakes (Lotter et al., 1995). Lake catchment area plays a vital role in the modification of

the lake ecosystem as redeposition of tephra from large catchments is added gradually to the lake ecosystem, while lakes with a small catchment area will be less sensitive to this mechanism (Telford et al., 2004).

Several studies have addressed the impact of the Mazama tephra deposition on terrestrial vegetation using pollen records. Egan et al. (2016) reviewed tephra impacts on vegetation and identified eight studies where tephra affected arboreal pollen minimally (e.g., a decline in *Pinus* percentage). Long et al. (2014) found that a moderate amount of Mazama tephra in dry forest in the eastern Oregon Cascades did not change the forest composition. The greatest impact of the Mazama tephra on a forest was detected at Dismal Lake, Idaho, where there were abrupt and persistent changes in pollen assemblages (loss of *Pseudotsuga* and *Abies* and an increase in disturbance-adapted species) after both the Glacier Peak tephra and the Mazama tephra (Herring, 2014). In contrast, there was no detectable impact on arboreal pollen at Lost Trail Pass, a drier site in Idaho that received less tephra (Mehringer, 1977). Several studies report a major impact of Mazama tephra on non-arboreal pollen (Egan et al., 2016; Long et al., 2014) and a large impact on open vegetation communities, including a decline in PAR and charcoal levels (Oetelaar and Beaudoin, 2005; Power et al., 2011). Dead Horse Lake's diverse grass and shrub pollen assemblage never recovered following the Mazama tephra (Minckley et al., 2007). These studies are consistent with observations after the 1980 Mount Saint Helens tephra deposition, where understory species were most affected (Antos and Zobel, 1986; Zobel and Antos, 1997). Furthermore, the tephra addition's effect on vegetation may depend on pre-existing soil texture. Gavin et al. (2001) suggested that Mazama tephra's addition to alpine talus fields accelerated subalpine forest establishment. Similarly, fine Mazama tephra deposition was shown to affect lake hydrology by increasing available soil water capacity (Steinman et al., 2019). Overall, response to tephra is not homogenous because several species- and site-specific factors contribute to plant species responses (Antos and Zobel, 2005).

Though too numerous to review here, palaeoecological studies of the impact of airfall tephra from other regions have found significant impacts on vegetation. Birks and Lotter (1994) found a statistically significant impact of tephra deposition on pollen assemblages at a site proximal to the volcano (< 60 km, 80 mm of tephra) but no effect at more distal sites. Allen and

Huntley (2017) compared the pollen-assemblage responses to a series of tephras in a varve record from Italy, showing longer recovery times of a century for thicker tephras and during times of woodland vegetation (as opposed to forest or herbaceous vegetation). Other studies show that the effects of tephra may last from a few decades (Giles et al., 1999) to millennia due to the deposition of a small amount of tephra layers (Kilian et al., 2006). Lastly, tephra depositions greatly affect peatlands but depend on tephra thickness (Hotes et al., 2006).

Despite many studies of tephra's impact on vegetation, few studies have addressed tephra's impacts on forest fire occurrence. Tephra-induced branch fall or mortality may increase fuels and increase the likelihood of fire. Recent eruptions have shown that volcanic lightning may occur tens of km from a volcano (Cimarelli and Genareau, 2022). Hallett et al. (1997) suggested a fire concurrent with ashfall in British Columbia could explain charcoal particles embedded in the Mazama tephra. Charcoal peaks adjacent to the Mazama tephra at Three Creeks and Breitenbush lakes suggest the tephra may have increased the likelihood of fire, though no such peaks were associated with the tephra at two other sites (Long et al., 2014). In contrast with these studies, deeper tephras may bury surface fuels and reduce the likelihood of fire, as found at Foy Lake, Montana (Power et al., 2011).

In this paper, I describe the palaeoecological history of Gold Lake, a mesotrophic lake with high aquatic productivity, based on the interpretation of a 14,400 years long record of pollen, charcoal, and sediment properties (Fig. 2.1). Gold Lake occurs 77 km N of Crater Lake (the source of the Mazama tephra) along the main direction of tephra deposition, and a nearby site received a thicker air fall tephra (64 cm) than occurs at most other palaeoecological sites (Buckland et al., 2020). Just east of Gold Lake, a "poor site" lodgepole pine (*Pinus contorta*) "Pumice Plateau" vegetation type is attributable to a thick Mazama tephra (Fig. 2.1B; Franklin and Dyrness, 1988). Given the high sedimentation rate at Gold Lake, in combination with a thicker Mazama tephra than in any previous study, this record offers the chance to study vegetation and fire responses to tephra at a fine temporal resolution. Our objective is to reconstruct vegetation change and fire history over the postglacial period at a relatively low (multi-centennial) resolution and surrounding the Mazama tephra at a relatively high (sub-decadal) resolution. I hypothesized that Mazama tephra would have a greater impact on non-

arboreal taxa with minimal impact on regional forest composition, though tephra deposition would result in decreased forest fires due to the abrupt loss of surface fuel.

## Materials and Methods

### Study Site Description

Gold Lake is in a glacially scoured depression in basaltic andesite at an elevation of 1465 m a.s.l. in the Cascade Range (43° 37' 57"N, 122° 02' 36"W), with a lake area of 38.9 ha and a watershed area of 48.4 $km^2$. Located in the Willamette National Forest, Gold Lake receives water from adjacent springs and Salt Creek, passing through Gold Lake Bog on its northeast side. It has an oval-shaped basin with the deepest area (12 m) on the southeastern edge. As water enters after passing through Gold Lake Bog, particulate and dissolved organic matter enters the lake, supporting higher productivity than most other lakes in the Cascade Range. A high concentration of phosphorous (0.047 mg/l) and chlorophyll a (1.9 mg/l) classifies the lake as mesotrophic (Johnson et al., 1985).

There is a large variation in temperature and precipitation within the Cascade Range that decreases and increases respectively from low to high elevation, resulting in distinct vegetation zonation (Fig. 2.1B). At the lowest elevation within the Willamette Valley (120-240 m elevation), *Quercus* Woodlands consists of Oregon white oak (*Quercus garryana*), Douglas-fir (*Pseudotsuga menziesii*), Bigleaf maple (*Acer macrophyllum*), Oregon ash (*Fraxinus latifolia*), and red alder (*Alnus rubra*). The *Tsuga heterophylla* Zone at 250-1000 m is the most spatially extensive in the region and consists of extensive stands of *Pseudotsuga menziesii* with *T. heterophylla* and western redcedar (*Thuja plicata*). The *Abies amabilis* Zone at 1000-1500 m elevation is marked by the highly shade-tolerant Pacific silver fir (*Abies amabilis).* Finally, the *Tsuga mertensiana* Zone at 1500-2000 m elevation is dominated by mountain hemlock (*Tsuga mertensiana*) and marked by deep snowpack persisting to May or June in most years. Gold Lake is at a transitional zone between the *Abies amabilis* and *Tsuga mertensiana* zones (Franklin and Dyrness, 1988) and only 10 km west of a steep precipitation gradient and *Pinus* forests (Fig. 2.1B). Gold Lake is surrounded by *Abies procera, Abies amabilis, Picea engelmannii, Tsuga mertensiana,* with minor amounts of *Pseudotsuga, Tsuga heterophylla, Abies concolor, Abies*

*lasiocarpa*, and *Pinus contorta*. The stand appears to be an uneven-aged old-growth forest with no stand-structural or fire-scar evidence of recent fire.

Sea and Whitlock (1995) reconstructed Gold Lake Bog's vegetational and climate history from a pollen record of a 10,500-year core that bottomed out in sand and clay. The study reconstructed a subalpine forest dominated by *Pinus* and *Abies* from 10.5 to 4.47 ka. After 4.47 ka, it shows an increased percentage of *Tsuga mertensiana*, *Picea*, *Abies*, *Pseudotsuga*, and *Tsuga heterophylla*, resembling the modern vegetation in the High Cascade Range.

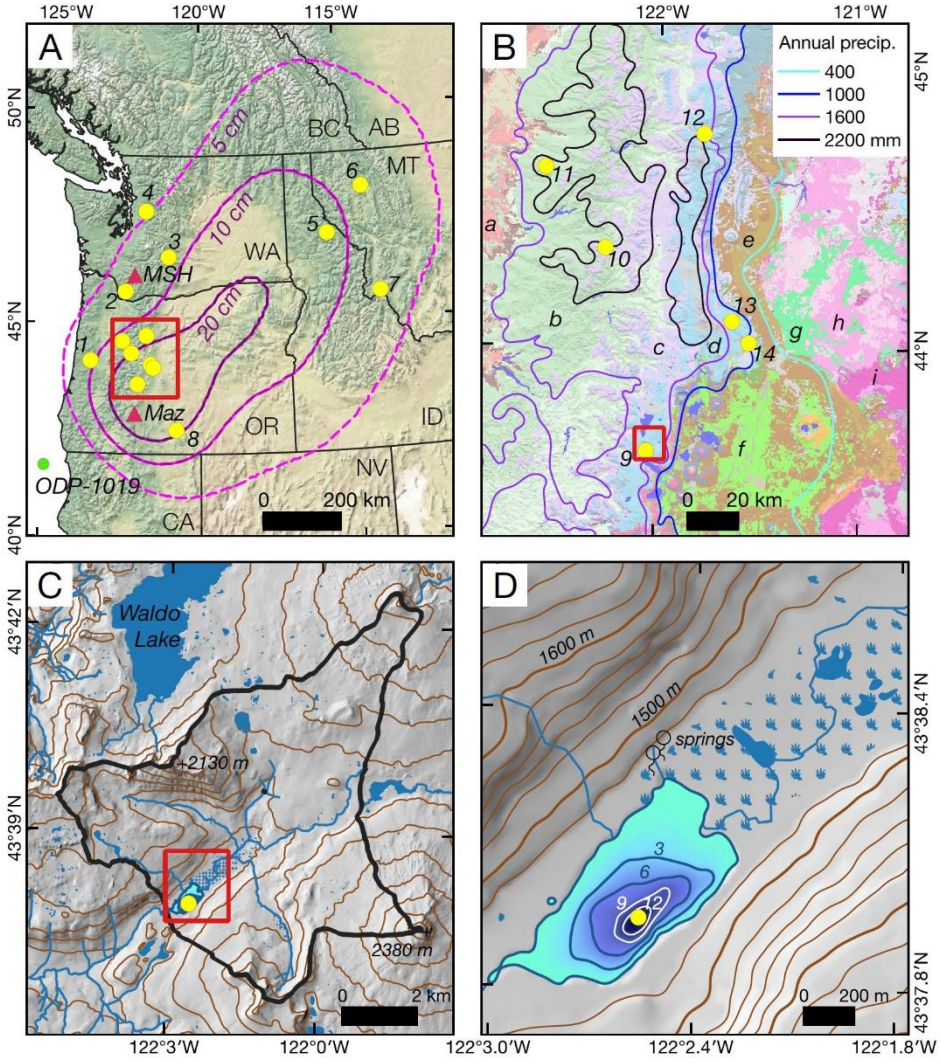


**Figure 2. 1** (A) The Pacific Northwest showing forest distribution (green) on shaded relief, study sites mentioned in the text (numbers), and isopach contours of Mt. Mazama airfall tephra (Buckland et al. 2020). Also shown are the

locations of Mount Mazama (Maz), Mount Saint Helens (MSH, and the marine core site ODP-1089. The red box indicates the extent of map B. (B) The central Oregon High Cascade forest zones (color background; Rollins et al., 2009), study sites mentioned in the text (numbers), and mean annual precipitation (contours). The red box indicates the extent of map C. Locations in maps A and B are 1: Little Lake (Long et al., 1998; Grigg and Whitlock, 1998); 2: Battle Ground Lake (Walsh et al., 2008); 3: Long Lake (Rushton and Walsh, 2021); 4: Moss Lake (Egan et al., 2016); 5: Dismal Lake (Herring, 2014); 6: Foy Lake (Power et al., 2011); 7: Lost Trail Pass Bog (Mehringer, 1977); 8: Dead Horse Lake (Minckley et al., 2007); 9: Gold Lake (this study); 10: Gordon Lake (Grigg and Whitlock, 1998); 11: Indian Prairie Fen (Sea and Whitlock, 1995); 12: Breitenbush Lake (Minckley and Long, 2016); 13: Three Creeks Lake (Long et al., 2011, 2014); 14: Tumulo Lake (Long et al., 2011). The major vegetation zones, following Franklin and Dyrness (1992), are a: Quercus Woodland; b: Tsuga heterophylla Zone; c: Abies amabilis Zone; d: Tsuga mertensiana Zone; e: Abies grandis and Pinus ponderosa Zones; f: Pinus contorta Zone; g: Juniperus occidentalis Zone; h: Artemisia tridentata steppe; i: Montane Artemisia tridentata Steppe. (C) Shaded relief map with a 100-m contour interval, showing the 48.4 km2 Gold Lake watershed (black line) and 100-m contour interval. The red box indicates the extent of map D. (D) Bathymetric map of Gold Lake (3 m contour interval; Johnson et al., 1985), core location (yellow circle), and the location of the Gold Lake Bog wetland studied by Sea and Whitlock (1995). Springs on the north side of the lake are indicated.

### Field Collection

Sediment cores were obtained from a platform on inflatable rafts anchored over the deepest point of Gold Lake (Fig. 2.1). Two parallel piston cores were recovered in June 2018. Cores were collected using a square-rod piston corer. Each 1-meter core drive was extruded on the raft, measured, and briefly described. Sediment cores were covered in plastic wrap within PVC pipe halves and labeled. A surface core was collected in a clear polycarbonate tube fitted with a piston, which was transported to the lakeshore and sectioned into bags at 1 cm intervals. The piston cores were transported to the laboratory at the University of Oregon and stored in a refrigerator at 4°C.

## Laboratory Analysis

### Core Processing, Magnetic Susceptibility, and Loss-on-ignition

All core drives were longitudinally split into working and archive core halves. The sediment was classified by visual observation and organic matter analysis (described below) following the terminology of Schnurrenberger et al. (2003). Later, core images were obtained using a line scan camera at the Marine Core Repository, Oregon State University. Tie-points

between the parallel cores were identified to develop an uninterrupted stratigraphy, except for the lower 5-meter core drives for which a parallel core did not exist. PSICAT, CORELYZER, and Feldman software were used to analyze line scan images to find tie points and generate a composite lake core with all the lithological characters noted during visual observation. Magnetic susceptibility profiles at 1-cm intervals (measured in a Sapphire Instruments cup meter) and field measurements of core depths were used to locate the tie-point from the surface core and the uppermost piston core drive. All surface-core samples and an initial 50 cm of the first Livingstone drive were used for this purpose.

LOI is used to determine the bulk density, organic content, and carbonate content of the lake sediment (Dean, 1974). Subsamples (1 $cm^3$) of lake sediment were placed in crucibles, dried at 80 °C, and then combusted at 550 °C for two hours to determine organic content. Samples were weighed after each step to calculate the percent organic matter. One hundred seventy-eight samples were analyzed at every 5 cm in the pre-Mazama section while at every 10 cm in the post-Mazama section.

Magnetic susceptibility is strongly affected by the presence of paramagnetic minerals and provides information about clastic input from soil erosion (Gedye et al., 2000). Magnetic susceptibility was measured using a Sapphire cup meter at every cm in the top 50 cm of core (2 $cm^3$), every 10 cm (1 $cm^3$) post-Mazama, and at every 5 cm (1 $cm^3$) pre-Mazama (total 208 samples).

**Radiocarbon dating and age model development**

Other than the major climactic Mazama tephra, two additional thinner tephras occurred in the Gold Lake core. These tephras were identified by electron microprobe analysis at Washington State University and the University of Oregon.

To develop an age-depth model, 13 samples for radiocarbon dating were obtained, which consisted of charcoal, identifiable plant material, pollen isolates, and bulk sediment (Table 1). Bulk sediment (3 $cm^3$) in 5 cases and pollen extract (3 $cm^3$) in 3 cases were used where sieving failed to produce macrofossils (Brown et al., 1989). The bulk-sediment samples were sieved at 150 μm, treated with 10% HCL followed by 10% KOH (twice), and washed with distilled water. Pollen-extract samples were treated as for the 150- μm samples but were sieved at 40 μm and

treated with a weak bleach solution. Before submitting to radiocarbon laboratories, all charcoal and macrofossils (5 samples) were pretreated with 10% HCl and 10% KOH. A batch of five radiocarbon dates (macrofossil, pollen, and bulk sediment) was sent to NOSAMS at Woods Hole Oceanographic Institute (Woods Hole, MA), while the other batch of eight radiocarbon dates was sent to Direct AMS (Bothell, WA). Part of the core following the Mazama tephra was coarsely laminated. The laminations counts were confirmed from independent visual inspection by JB, and DGG Ages at 10-cm intervals were estimated and were added to the age-depth model as a calendar year using the Mazama eruption (7633±25 cal yr BP; Egan et al., 2015) as a baseline. To account for increasing uncertainty along the varve sequence, the 25-year error was incremented by two years per 10 cm (ca. 5% error). Although varves were counted at 732-504 cm, they were used only up to 570 cm because, above that point, varves became less distinct, and counts differed between researchers. Post-Llao Rock eruption laminations were also counted and added to the age-depth model. Three radiocarbon dates were obtained within 732-570 cm to verify that the counted laminations are annual. An age model was built using Bacon software using 11 radiocarbon ages, 17 varve-age estimates (at 10 cm intervals), and the age of the Mazama tephra. The age-depth model was built using Bacon for R (Blaauw and Christen, 2011), a Bayesian statistical software. Three tephra layers were modeled as intervals of instantaneous deposition. The program applied the INTCAL20 calibration curve (Reimer et al., 2009).

**Table 2. 1. Radiocarbon dates and varve-counts used in the age-depth model for Gold Lake, Oregon.** Varve ages every 10 cm; assume a Mazama tephra age of 7633±25 cal yr BP.

| Lab code | Depth (cm) | Dated material | $^{14}$C date (yr BP)[a] | Median age (cal yr BP)[b] | 2σ Age range (cal yr BP) |
|---|---|---|---|---|---|
| D-AMS 041766 | 173-174 | wood | 1727±30 | 1637 | 1542-1731 |
| OS-166898 | 300-301 | Pollen >40 µm | 2970±20 | 3153 | 3039-3317 |
| OS-169236 | 504-505 | Pollen >40 µm | 5740±35 | 6401 | 6202-6530 |
| D-AMS 041769 | 590-591 | sediment >150µm | 6200±27 | 7066 | 7019-7114 |
| D-AMS 041767 | 678-679 | wood | 6409±27 | 7405 | 7374-7432 |
| D-AMS 041770 | 678-679 | sediment >150 µm | 6778±39 | Rejected (older than Mazama) | |
| D-AMS 041771 | 715-717 | sediment >150 µm | 6628±33 | 7554 | 7521-7584 |

| | | | | | |
|---|---|---|---|---|---|
| Mazama | 732-810 | Egan et al. (2015) | | 7633±25 | |
| OS-169237 | 831-832 | Pollen >40 µm | 6840±110 | 7728 | 7682-7780 |
| D-AMS 041768 | 959-960 | Pinus needle, seed | 8178±47 | 9226 | 9044-9398 |
| D-AMS 041772 | 1086-1088 | sediment >150 µm | 10166±34 | 11743 | 11,399-11,915 |
| OS-163361 | 1166-1168 | Charcoal | 10950±200 | 12832 | 12,571-13,077 |
| D-AMS 041773 | 1252-1254 | sediment >150 µm | 12076±43 | 13894 | 13,770-14,057 |
| OS-163361 | 1292-1300 | Charcoal | 14,700±600 | Rejected (large error) | |
| Manually counted varves | 570 | | | 7021±57 | |
| counted varves | 580 | | | 7045±55 | |
| counted varves | 590 | | | 7080±53 | |
| counted varves | 600 | | | 7108±51 | |
| counted varves | 608 | | | 7138±49 | |
| counted varves | 620 | | | 7183±47 | |
| counted varves | 630 | | | 7217±45 | |
| counted varves | 642 | | | 7257±43 | |
| counted varves | 650 | | | 7288±41 | |
| counted varves | 660 | | | 7326±39 | |
| counted varves | 670 | | | 7370±37 | |
| counted varves | 680 | | | 7414±35 | |
| counted varves | 690 | | | 7454±33 | |
| counted varves | 700 | | | 7488±31 | |
| counted varves | 710 | | | 7533±29 | |
| counted varves | 718 | | | 7563±27 | |
| counted varves | 830 | | | 7698±27 | |

[a] Radiocarbon age determination from DirectAMS, Bothell, WA (D-AMS codes), and NOSAMS at Woods Hole Oceanographic Institute, Woods Hole, MA (OS codes)
[b] Calendar ages determined using IntCal20 calibration curve (Reimer et al., 2020)

**Pollen Analysis**

Pollen analysis was conducted on 50 samples (0.5-1.5 $cm^3$), including 26 samples at 50 cm intervals and 24 samples at the Mazama tephra at every 1 cm (12 samples each before and after the tephra). The ages and sedimentation rates for these high-resolution samples are based on the manually counted varves, as opposed to the Bacon model output. For data analysis and visualization, the samples directly before and directly following the Mazama tephra were added to the 50-cm data set to include the immediate effect of tephra on vegetation in the presentation of the long-core pollen record. Exotic *Lycopodium* (batch 3638) spike tablets were added to the samples to compute pollen concentrations. Pollen processing was completed following the standard chemical digestion procedure outlined by Faegri et al. (1989), except the sediment samples were not sieved before chemical digestion. After processing, pollen was stained, preserved in silicone oil, and examined under 400X magnification for identification. Pollen was identified to the lowest taxonomic level possible by comparing them to the pollen reference collection at the Paleoecology Laboratory at the University of Oregon and with the help of published keys (Bassett et al., 1978; Erdtman, 1969; Kapp, 1969; Moore et al., 1991). Some of the pollen was identified using an online reference collection provided by the Global Pollen Project (https://globalpollenproject.org/). Aquatic palynomorphs (algae, *Equisetum*, *Isoëtes*, and *Pediastrum*) were identified but are not included in this analysis of terrestrial vegetation change.

Pollen zones were identified using stratigraphically constrained cluster analysis on the 19 most abundant taxa using rioja software in the R statistical package (Juggins, 2009). The number of statistically significant pollen zones was assessed using the broken stick method in rioja (Bennett, 1996). A pollen diagram was generated using TILIA software (https://www.tiliait.com/). PAR (grains/$cm^2$/yr) was calculated from pollen concentration and the sedimentation rate from the Bacon age-depth model (cm/yr) (Bennett and Willis, 2001). Nonmetric multidimensional scaling (NMDS) using the chord distance (Prentice, 1980; Gavin et

al., 2013) was applied to the most abundant terrestrial pollen taxa (excluding aquatics and cryptograms) that comprise 95% of the pollen grains identified. Taxa were selected in this manner to focus on terrestrial vegetation response and remove the influence of rare sporadically-occurring pollen types on the ordination. NMDS was applied separately to the coarse-resolution and the fine-resolution data sets using the same taxa set.

### Charcoal Analysis

To reconstruct the fire history, a high-resolution macroscopic charcoal analysis was made following the protocol described in Whitlock and Larsen (2001). Contiguous subsampling of sediment (1-2 $cm^3$) was made at every cm for the non-tephra core segments (1224 samples). These samples were soaked in a 5% sodium hexametaphosphate solution for 24 hours, followed by 3% hydrogen peroxide, and then washed through 125 and 250 μm meshes. Samples were examined under 50X magnification, and charcoal was counted. Charcoal counts were converted into concentration data (particles/$cm^3$). The charcoal accumulation rate (CHAR: particles/$cm^2$/yr) was calculated by dividing the charcoal concentration by sample deposition time (yr /cm).

CharAnalysis software (Higuera, 2009) was used for peak detection. Two analyses were performed: for the entire core and for a period of high sedimentation around the Mazama tephra (8 ka to 6 ka). For the full-core analysis, charcoal data were resampled to an interval of ten years, the median sedimentation rate for the full core. For the high-resolution analysis (8 ka-6 ka), CHAR was resampled at a three-year resolution, close to the median sedimentation rate for that segment. For both analyses, background CHAR was estimated using loess regression with a 500-year window. A Gaussian mixture model was applied to distinguish peaks from "noise"; peak threshold was set at the 99th percentile of the noise distribution.

## Results

### Core description

Two parallel Livingstone sediment cores were collected from Gold Lake. The first core reached a depth of 13 m; further coring was not possible due to the stiffness of the sediment. The second core was obtained to provide overlapping segments for the post-Mazama section (8 m). No core loss or compression occurred during extrusion.

The core consists mainly of medium to dark brown biogenic sapropel except for a 50-cm section at the bottom of the core (1302-1252 cm) and three tephra layers (Figure S1). The first 1-cm tephra (831-832 cm depth) was identified as the Llao Rock tephra from Mt Mazama (Kathy Cashman, *personal communication*), which shortly predated the Mazama eruption and was previously aged to 7.833 ka (Mensing and Southon,1999) or 7.773 ka (Blinman et al.,1979). A second tephra (241-242 cm depth) was identified as the Rock Mesa tephra from the South Sister volcano (Table S1), previously aged to 2.5-2.74 ka (Skinner and Radosevich,1991). The 78-cm climactic Mazama tephra (732-810 cm depth) had a distinct reverse-graded stratigraphy (Figure S1; Table S2). From 78 to 74 cm, it was coarse sand and silt with mixed organic sediment. From 74 to 22 cm, it was coarse tephra (7 mm maximum diameter), and from 22 to 2 cm, much coarser tephra (up to 10 mm maximum diameter). The uppermost 2 cm was a coarse tephra lapillus (ca. 13-mm maximum diameter), which was followed by a 1.4 cm layer of mixed silt-sized ash and sediment. This mixed ash and sediment layer is graded into the laminated section of the core (Fig. 2.2).

Overall, LOI values ranged from 2-29% during the Late Glacial, 9-32% during the early Holocene, and 15-34% during the late Holocene. The core has sapropelic (biogenic) laminations (light and dark brown rhythmic banding) following the Mazama tephra (732-504 cm) and the 20 cm following the Llao Rock tephra to the Mazama tephra (830-810 cm). The laminated section post-Mazama eruption has a lower organic content (10-15%).

**Age-depth model**

Two radiocarbon ages were not retained in the analysis because of large age errors or because the age was out of stratigraphic order with the Mazama tephra. The remaining eleven radiocarbon dates occurred in stratigraphic order (Fig. 2.2; Table 2.1). The lowest radiocarbon date, 50 cm above the core base, is at a transition between silt and clay to sapropelic sediment, calibrated to 13.9 ka. Radiocarbon ages suggest a roughly constant sedimentation rate (0.071-0.11 cm/yr) up to 960 cm. Three radiocarbon dates strongly agree with the manually counted laminations and confirm them as annual events (Table 1). Varve counts suggest the Llao Rock tephra predates Mazama by 65 years. A total of 612 varves were counted over the 162 cm following the Mazama tephra, indicating a sedimentation rate 6-7 times greater (0.25 cm/yr) than

the remaining part of the core. The sedimentation rate decreased to 0.06-0.10 cm/yr during the late Holocene.

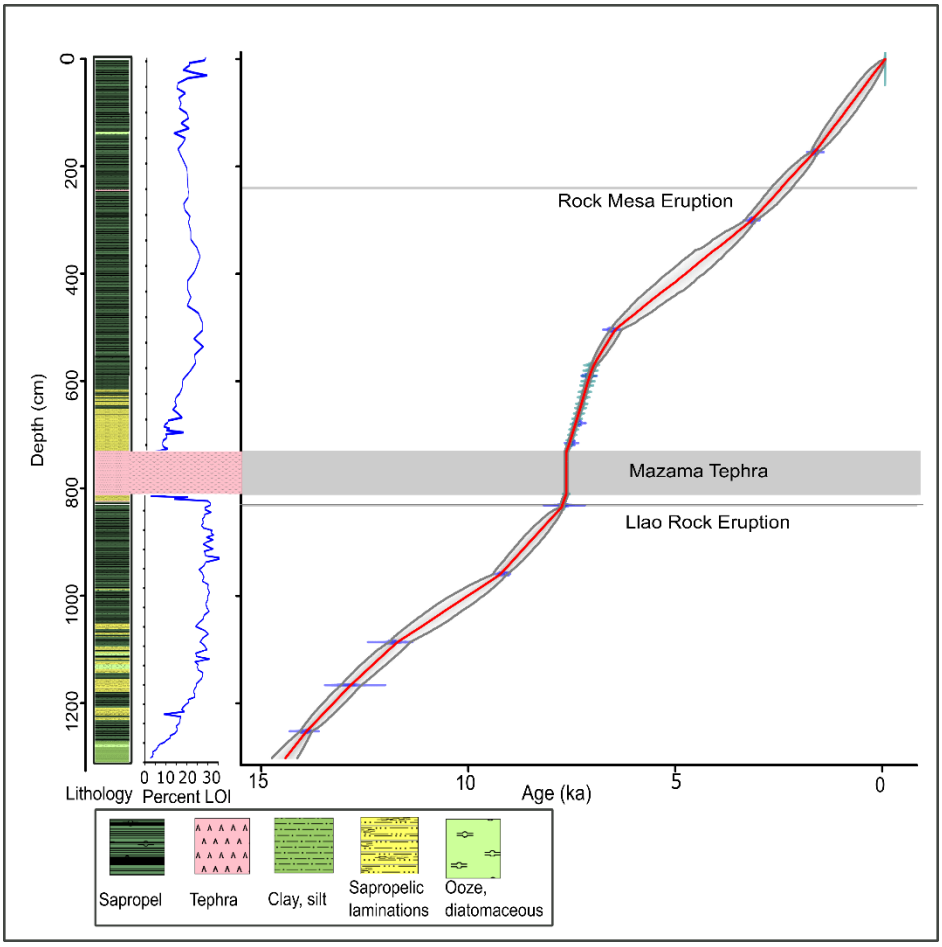


**Figure 2. 2 Bacon age-depth model for Gold Lake with LOI and lithology**. Horizontal bar lines represent three tephra layers found in the lake. Age estimates for a post-Mazama (732-570 cm) and post-Llao Rock (831-811 cm) tephras are based on radiocarbon dates and manually counted varves.

## Pollen

Pollen was very well preserved in all samples. For the coarse-resolution (50-cm sampling) data set, there were no statistically significant pollen zones identified, partly due to the small number of samples entering the analysis (n=26). Therefore, zones were created using major climatic and stratigraphic events: Late Glacial (14.4 ka-11.6 ka), Early Holocene-pre

Mazama (11.6 ka-7.6 ka), Middle Holocene-post Mazama (7.6-5 ka), and Middle/Late Holocene (5.0 ka-present; Fig. 2.3; Cohen et al., 2013).

High-resolution pollen analysis was made at 1-cm resolution pre- and post-Mazama eruption to analyze the effect of tephra on vegetation. The varve counts show that the samples span 60 years pre- and post-Mazama tephra. The stratigraphically constrained cluster analysis determined that the Mazama tephra was a statistically significant zone boundary, resulting in two pollen-assemblage zones (Fig. 2.4).

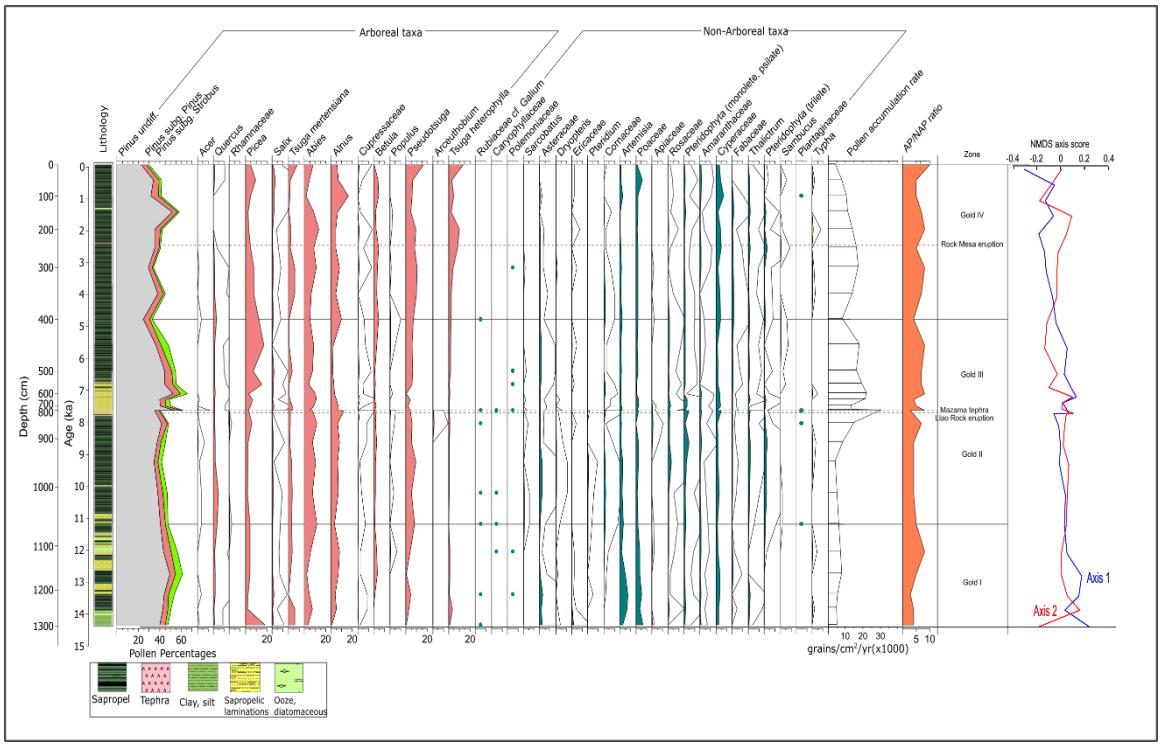


**Figure 2. 3 Pollen percentages, PAR, AP/NAP ratio (arboreal/non-arboreal), and NMDS axes from Gold Lake, Oregon.** Thin-line graphs of select pollen taxa indicate a 5x exaggeration of pollen percentage data. Horizontal dashed lines indicate the ages of tephra layers. Rare pollen types (Rubiaceae, Caryophyllaceae, *Sarcobatus*, and Plantaginaceae) are shown as a presence only. This diagram displays the coarse-resolution (50 cm interval: 26 samples) and two samples from a high-resolution (1-cm, ca. 4-year intervals) analysis pre-and post-Mazama tephra.

**Gold I-Post-Glacial period (1302-1110 cm; ca. 14.4-11.6 ka; 5 pollen samples)**

This zone is distinguished as having the highest percentage of *Picea* (2-19%) and *Pinus* (48-61%, with the highest observed subg. Strobus 3-7%). The remainder of arboreal taxa consists of *Abies* (3-7%), *Alnus* (1-7%), *Pseudotsuga* (0.7-4%), *Tsuga heterophylla* (0.4-4%), and *Tsuga mertensiana* (0.4-6.3%). Other minor components include *Salix* (0.4-1%), Cupressaceae (0.2-1%), *Quercus* (0.9-2%), and Aceraceae (0-0.4%). *Betula* (0.9-3%) was absent at the bottom of the core and appeared at 13 ka, while *Populus* (0-0.6%) appeared at 12 ka (only in the top sample of this zone).

The ratio of arboreal to non-arboreal pollen (AP/NAP) increased from 3 to 8 within this zone. Non-arboreal taxa were dominated by the highest percentage of Poaceae (3-7%), *Artemisia* (2-8%), Asteraceae (0.2-3%), and Ericaceae (0.2-2%) in the core. The remainder of non-arboreal taxa consists of Cyperaceae (1.7-4%), Pteridophytes-monolete (0.7-2%), Amaranthaceae (0.4-1%), Rosaceae (0-1.5%), *Thalictrum* (0-2%), Fabaceae (0-1%), Pteridophyte-trilete (0-0.2%), Dryopteris type (0-0.4%), Rubiaceae (0-0.5%), *Pteridium* (0-0.5%) and Cornaceae (0-0.4%) were absent in the last two samples and appeared by 13 ka). PAR varied between 4900 to 8000 grains/cm$^2$/yr with a sedimentation rate (0.071-0.11 cm/yr).

**Gold II-Early Holocene-Pre-Mazama (1060-860cm; ca. 11.6-7.7 ka; 5 pollen samples)**

This zone has the highest percentage of *Quercus* (1.4-5%). *Arceuthobium* (1.4%) appears only in the top sample of this zone in the whole core. The remainder of arboreal taxa consists of *Pinus* (42-48%), *Picea* (2-6%), *Alnus* (3-8%), *Abies* (8-12%), *Pseudotsuga* (4-9%), *Tsuga heterophylla* (0.2-1.4%), and *Tsuga mertensiana* (2-4%). Other minor components include *Salix* (0.2-1.2%), *Betula* (1-2%), Cupressaceae (0.2-0.8%), Aceraceae (0.2-0.7%), and *Populus* (0-0.4%). Rhamnaceae (0-0.2%) appears twice in this core section and in high-resolution pollen samples around Mazama eruption samples.

Most of the non-arboreal taxa are found in the highest percentage compared to the remainder of the core, with an AP/NAP ratio of 4-7. The most common non-arboreal pollen types are Rosaceae (0.9-3.3%), Cornaceae (0.2-2%), *Sarcobatus* (0-0.5%), Pteridophytes-monolete (0.9-5%), Pteridophytes-trilete (0.8-2.8%), Amaranthaceae (0.4-1.7%), *Thalictrum* (0-2.2%), *Dryopteris* type (0.4-1.1%), Apiaceae (0-0.7%), Rubiaceae (0-0.7%), *Pteridium* (0-0.9)

and Caryophyllaceae (0-0.2%) and Polygonaceae (0-0.2%). PAR varies between 4200 to 14,900 grains/cm$^2$/yr with a sedimentation rate (0.05-0.08 cm/yr).

**Gold III-Middle Holocene-Post-Mazama (700-450 cm; ca. 7.5-5 ka; 6 pollen samples)**

*Picea* (5-17%) reaches its highest percentage in the core at 5.5 ka. Other arboreal taxa include *Alnus* (1.7-7%), *Abies* (3.8-11%), *Pseudotsuga* (0.8-6.4%), *Tsuga heterophylla* (0.4-1.7%), *Tsuga mertensiana* (0.5-3.7%), *Betula* (1-3%), *Salix* (0-2%) and *Quercus* (1-1.8%).

The AP/NAP ratio varies from 4 to 8. Cyperaceae (1.4-4%) dominates the non-arboreal taxa, followed by Pteridophyte-monolete (1-3%), Poaceae (1-2.6%), and *Artemisia* (1-1.7%). Other minor components of non-arboreal taxa include Amaranthaceae (0-1.3%), Asteraceae (0.4-1.5%), *Thalictrum* (0.2-2%), Fabaceae (0.5-1%), Pteridophyte-trilete (0-2%), Cornaceae (0.2-1.3%), *Sarcobatus* (0-0.2%) and Polemoniaceae (0-0.3%). PAR varies between 13,200 to 22,100 grains/cm$^2$/yr with a sedimentation rate of 0.062-0.25 cm/yr.

**Gold IV-Middle/Late Holocene (400-0 cm; ca. 5 ka to present; 9 pollen samples)**

*Tsuga heterophylla* (2.4-14%) and *Abies* (2-13.5%) are the highest in this zone and reached their highest values at the core top and 1.9 ka, respectively. *Pinus* (30-58%) shows a decreasing trend compared to the previous zone, especially in the surface sample. *Picea* (2.6-12.6%) also decreased to 4.5% recently. *Tsuga mertensiana* (0.8-9%), and *Pseudotsuga* (5-16%) show no temporal pattern. *Alnus* (4-16%) and *Salix* (0.5-3%) increased to their highest percentage at 0.9 ka and then decreased to 5% and 1%, respectively, in the surface samples of this zone. *Betula* (0.6-4.7%) reached its highest percentage in this zone compared to the remaining core, which happened at 2.5 ka and decreased to 0.6% in the surface sample.

The AP/NAP ratio in this zone ranged between 4 to 10 and was highest in the top sample of this zone. The highest percentage of Cyperaceae (1-7%) and Fabaceae (0-2%) was found in this zone. Other non-arboreal taxa include *Artemisia* (0.4-3%), Poaceae (1.5-6%), Amaranthaceae (0-1.3%), Rosaceae (0-1%), Asteraceae (0-0.8%), *Thalictrum* (0.4-1.7%), Cornaceae (0-0.7%), Ericaceae (0-0.8%), Pteridophyte-monolete (0.6-4.7%), Pteridophyte-trilete (0-1.4%) appeared in few samples. PAR decreased at the onset of late Holocene to (8100 grains/cm$^2$/yr) followed by an increase up to 17,200 grains/cm$^2$/yr and later showing a decreasing

trend after 1.4 ka with a minimum accumulation rate of 4000 grains/cm$^2$/yr in the top sample. The sedimentation rate ranged between 0.062 and 0.11 cm/yr.

**High-resolution pollen analysis, Pre-Mazama eruption (822-811 cm; 7.69-7.63 ka; 12 pollen samples)**

*Pinus* decreases steadily from 61% to 41%, while *Alnus* increases from 3% to 13% over these 55 years (Fig. 2.4). Other arboreal taxa with less change are *Abies* (4-12%), *Pseudotsuga* (4-10%), *Picea* (2-6%) and *Tsuga mertensiana* (0.8-5%).

AP/NAP ratio decreases from 10 to 3 prior to Mazama due to increases of Cyperaceae (1 to 5.5%), Pteridophyte-monolete (0.8 to 4.6%), Poaceae (1 to 3%), *Artemisia* (0.4 to 2.5%), Rosaceae (0-2%), and *Thalictrum* (0 to 2%). Other minor components of non-arboreal taxa include *Dryopteris*-type (0.2-2.3%), Asteraceae (0.2-1.4%), *Sarcobatus* (0-0.6%), *Sambucus* (0-0.4%), Cornaceae (0.2-2%), Fabaceae (0-1%), Pteridophyte-trilete (0-1.5%), Apiaceae (0-0.4%), *Pteridium* (0-0.8%), and Caryophyllaceae (0-0.4%).

PAR is highest (30,700 grains/cm$^2$/yr) at the top sample directly preceding the Mazama tephra. The pre-Mazama section has a PAR varying between 9500 to 30,700 grains/cm$^2$/yr. This depth also has the highest PAR of non-arboreal pollen, 7800 grains/cm$^2$/yr. The sedimentation rate ranges between 0.17-0.33 cm/yr, which is six times higher than lower in the core. The high sedimentation rate contributed to the high PAR (30,700 grains/cm$^2$/yr) before the Mazama eruption.

**High-resolution pollen analysis, Post-Mazama eruption (731-720 cm; 7.63-7.5 ka; 12 pollen samples)**

Directly following the Mazama tephra, *Pinus* increases from 41 to 62% and remains near 64% for the next 52 years. *Pinus* subg. *Strobus* declines to trace levels after the tephra, then increases to 8% 52 years after the tephra. *Pseudotsuga* decreases after the tephra, then increases to 8% after 20 years, but after that, remains low. *Alnus* decreases from 12% to 6.6% but then increases to 10% within 11 years. Other arboreal taxa maintained their relative abundance through the Mazama tephra: *Picea* (0.9-4.8%), *Abies* (3-14%), *Tsuga mertensiana* (2-7.6%), *Quercus* (0.7-3%), and *Tsuga heterophylla* (0-2%) (Fig. 2.4).

AP/NAP ratio increases from 3 to 13 through the Mazama tephra, reaching its highest value at 25 years post-Mazama tephra. This happens due to a sudden decrease of non-arboreal taxa, including Cyperaceae (5 to 2%), Poaceae (2.6 to 0.5%), and Rosaceae (1.8 to 0.5%), while certain non-arboreal taxa disappear, including *Thalictrum* and *Arceuthobium*. Other non-arboreal taxa were dominated by *Artemisia* (0-2.4%), Pteridophyte-monolete (0.4-2.4%), and Asteraceae (0.4-1.7%).

Across the Mazama tephra, total PAR reduces from 30,000 to 13,300 grains/cm$^2$/yr. PAR (AP) declines from 23,500 to 12,200 grains/cm$^2$/yr, while PAR (NAP) reduces from 7100 to 1500 grains/cm$^2$/yr. PAR recovered quickly, to 22,000 grains/cm$^2$/yr, within nine varve-years after the tephra but eventually declined to 8000 to 9900 grains/cm$^2$/yr 50 years later. Right after the Mazama tephra, the sedimentation rate remained the same as the pre-eruption rate (0.33 cm/yr), which then decreased from 0.25 to 0.13 cm/yr from 7.6 to 7.58 ka.

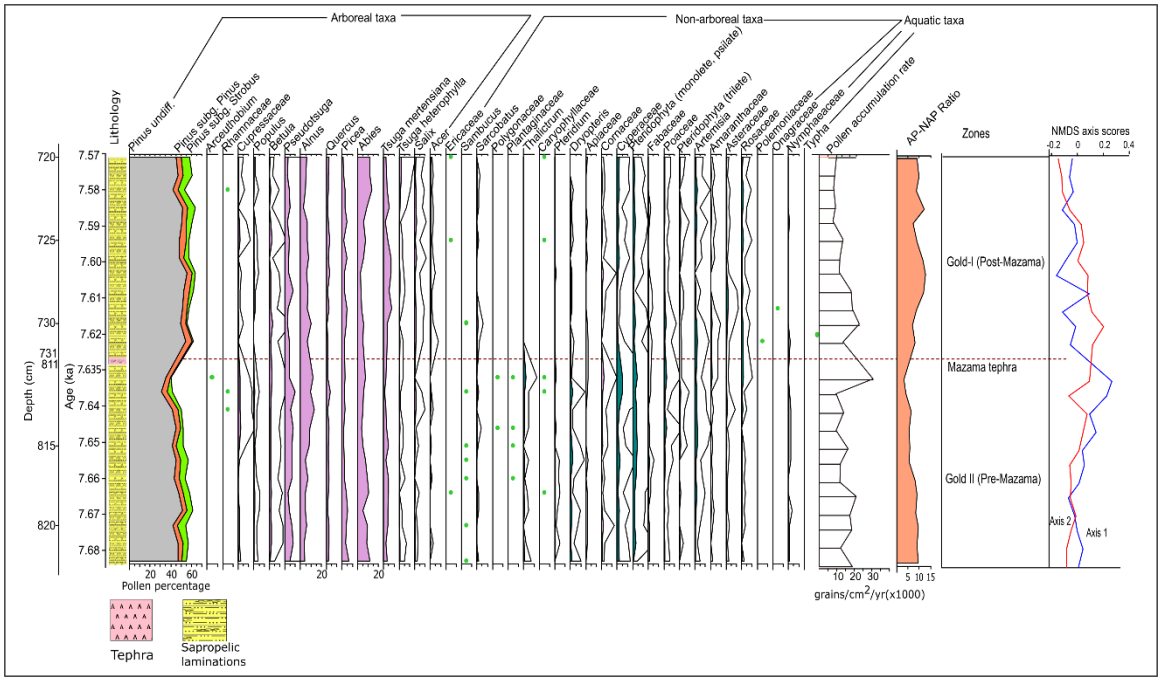


**Figure 2. 4 Pollen percentage, PAR, AP/NAP ratio, and NMDS axes from laminated sediments before and after the Mazama tephra at Gold Lake, Oregon**. Thin-line graphs of select pollen taxa indicate a 5x exaggeration of pollen percentage data. A horizontal dashed line indicates the age of the Mazama tephra layer. Rare pollen types (*Arceuthobium*, Rhamnaceae, Ericaceae, Caryophyllaceae, *Sarcobatus*, *Plantaginaceae*, Polygonaceae, Polemoniaceae, Onagraceae, *Typha*) are shown as a presence only. Arboreal and non-arboreal taxa are ordered by the NMDS Axis 1 scores (Fig. 2.5A & 2.5B).

**NMDS ordination of pollen assemblages**

Nonmetric multidimensional scaling produced two independent axes of gradients in the pollen data applied to the 50-cm resolution pollen record (Fig. 2.5A) and the high-resolution pollen across the Mazama tephra (Fig. 2.5B). Axis 1 is significantly positively correlated with *Pinus*, Asteraceae, *Pinus* subg. *Strobus* and *Artemisia* while negatively correlated with *Pseudotsuga*, *Tsuga heterophylla*, *Alnus*, and *Betula*. *Abies* and *Pinus* are positively correlated with axis 2, while it is significantly negatively correlated with *Picea* and *Betula*. NMDS applied to the full-core record has axis-1 scores that follow the transition from the Late Glacial period (*Picea*, Asteraceae, *Artemisia*, Poaceae, *Pinus*) to the dominance by *Abies*, *Alnus*, and *Pinus* in the early Holocene and followed by *Tsuga heterophylla*, *Betula*, and *Pseudotsuga* dominance in late Holocene. Axis 2 scores followed the taxa that were dominant during the Late Glacial and late Holocene (*Picea*, *Pinus*, *Pseudotsuga*, *Tsuga heterophylla*; Fig. 2.5A).

High-resolution pollen around the Mazama eruption shows that the first axis is positively correlated with *Thalictrum*, Cupressaceae, *Alnus*, and *Betula* while negatively correlated with *Tsuga mertensiana*, *Salix*, and *Tsuga heterophylla*. *Thalictrum* had peak abundance prior to the Mazama eruption, and soon after the Mazama eruption, it disappeared, resulting in bringing down axis 1 from values of 0.25 to -0.1, while *Pinus* had peak abundance after the Mazama eruption. Axis 2 is positively correlated with Asteraceae, *Alnus*, *Betula*, and *Pinus*, while it is negatively correlated with *Abies*, *Quercus*, *Populus*, and Cyperaceae. After the Mazama eruption, axis 1 decreased while axis 2 increased, and it returned to pre-Mazama pollen assemblage after almost 50 years (Fig. 2.5B).

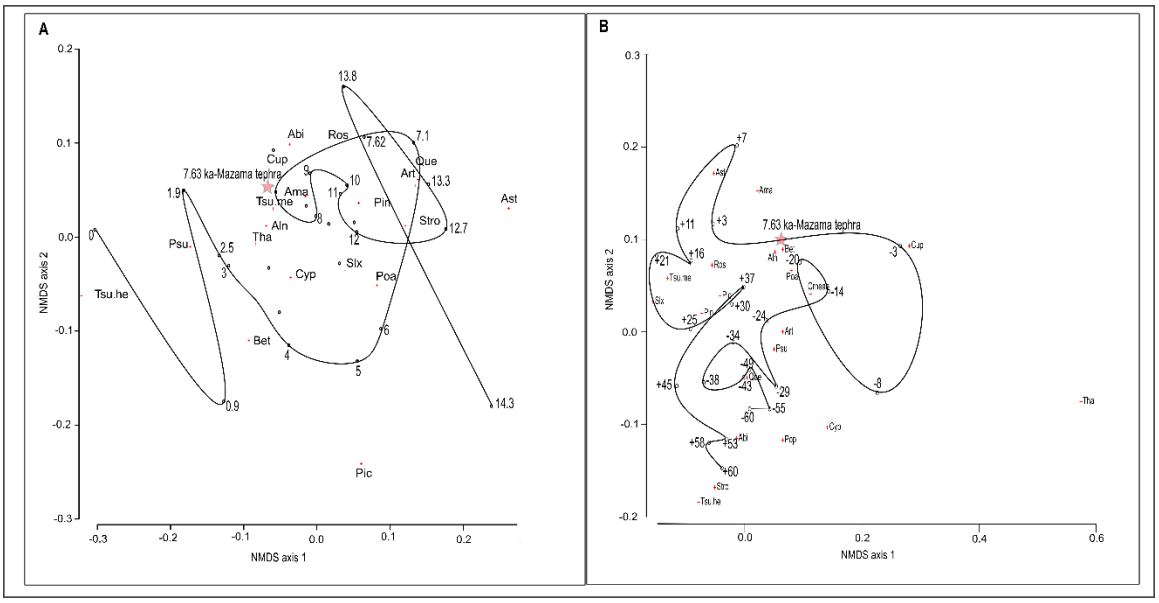


**Figure 2. 5 Nonmetric multidimensional scaling (NMDS) of the** (A) postglacial pollen assemblages and (B) fine-resolution pollen assemblage data pre- and post-Mazama tephra deposition from Gold Lake. In (A), a polyline connects samples spaced at ca. 1000 years except around the Mazama tephra and from 12 ka to 14.3 ka. In (B), a polyline connects all pollen samples, which are laveled with the number of varve years relative to the Mazama tephra. Star indicates the location of the Mazama tephra. Crosses indicate species scores: (Tsu.he: *Tsuga heterophylla*; Tsu.me: *Tsuga mertensiana*; Psu: *Pseudotsuga*; Bet: *Betula*; Tha: *Thalictrum*; Aln: *Alnus*; Poa: Poaceae; Stro: *Pinus* subg. Strobus; Pin: *Pinus* subg. Pinus; Cup: Cupressaceae; Slx: *Salix*; Abi: *Abies*; Ros: Rosaceae).

## Charcoal and fire history

The macrocharcoal record (1224 samples at 1 cm resolution) resulted in charcoal concentrations between 0 and 136 pieces/cm$^3$. The charcoal accumulation rate (CHAR) ranged from 0 to 6 pieces/cm$^2$/year (Fig. 2.6A). There was no charcoal found at some depths of the Late Glacial and early Holocene periods. Average CHAR generally increased throughout the record, from 0-1.96 pieces/cm$^2$/year in the Late Glacial to 0.05-5.2 pieces/cm$^2$/year in the late Holocene, but with the lowest values (0.1 to 2.8 pieces/cm$^2$/year) occurring in the early Holocene (11.6 to 9 ka) and higher CHAR during the period of higher sedimentation rate and varves preceding and following the Mazama (0 to 6.8 pieces/cm$^2$/year). CharAnalysis applied for peak identification resulted in a global signal-to-noise value of 3.95 (Fig. 2.7E), indicating charcoal peaks could be statistically distinguished from background variability (Kelly et al., 2011). However, the local

SNI (signal-to-noise) is <3 at some depths in the Late Glacial and early Holocene during periods of low CHAR. Apart from these depths, the local SNI is >3 with a maximum value of 7.64 (Fig. 2.7D), and only six peaks were removed due to low charcoal counts (i.e., the "minimum count test"; Higuera et al., 2010). Based on a threshold of 0.99 percentile of the modeled noise distribution in CharAnalysis, 81 fires were identified between 14.5 ka to the present (Fig. 2.6B).

The intervals between identified peaks (fire return intervals or FRI) varied throughout the record, with longer FRI during the early Holocene (10.8 ka to 7 ka) and shorter FRI during the Late Glacial, the middle Holocene after 7 ka, and the middle/late Holocene (Fig. 2.7B). The FRI were calculated for four time periods (Fig. 2.6C). Zone 1 (14.5 ka-11.6 ka) had the shortest mean FRI (121 years), with 20 fires identified. Zone 2 (Early Holocene-pre Mazama; 11.6 ka-7.63 ka) had the longest mean FRI (251 years) with 15 fires identified, with statistically longer fire intervals than in Zone 1. Zone 3 (Early Holocene-Post Mazama; 7.63-5 ka) had a shorter FRI compared to zone 2, with a mean FRI of 182 years and 14 fires identified. Fire activity increased in zone 4 (Late Holocene; 5 ka-2018 CE) with the second shortest mean FRI (155 years) with 32 fires. CHAR declined to the lowest levels of the late Holocene over the last 400 years.

**Fire history pre- and post-Mazama**

The full-core analysis with a ten years interpolation resulted in the loss of many peaks that could be identified in the high-sedimentation rate segment of the core. This period of high sedimentation rate (5-7 times higher than the remaining part of the core) spans from 7.75-6.5 ka; 834-506 cm or 110 years before Mazama to ca.1170 years after Mazama. In the 10-year interpolated data, this period often had a SNI < 3, indicating low variability and uncertain peak identification. However, using three-year interpolated data during this period, the mean SNI is > 4.25 and reaches values > 6, while it is < 3 only during periods with no peak identification.

The raw data during this period comprised 0-54 pieces/$cm^3$. CHAR ranged from 0-6 pieces/ $cm^2$/year (Fig. 2.8A). A total of 7 fires were identified during the pre-Mazama zone (8.1-7.63 ka), while 21 fires with a mean FRI of 52 years (Fig. 2.8B) were identified in the post-Mazama zone (7.63-6.5 ka). Very low CHAR and no peaks were detected in the post-Mazama

period for ca. 63 years until a major peak at ca. 7.57 ka. After this peak, there were ca. 500 years of high CHAR variability and a peak interval often less than 30 years (Fig. 2.8).

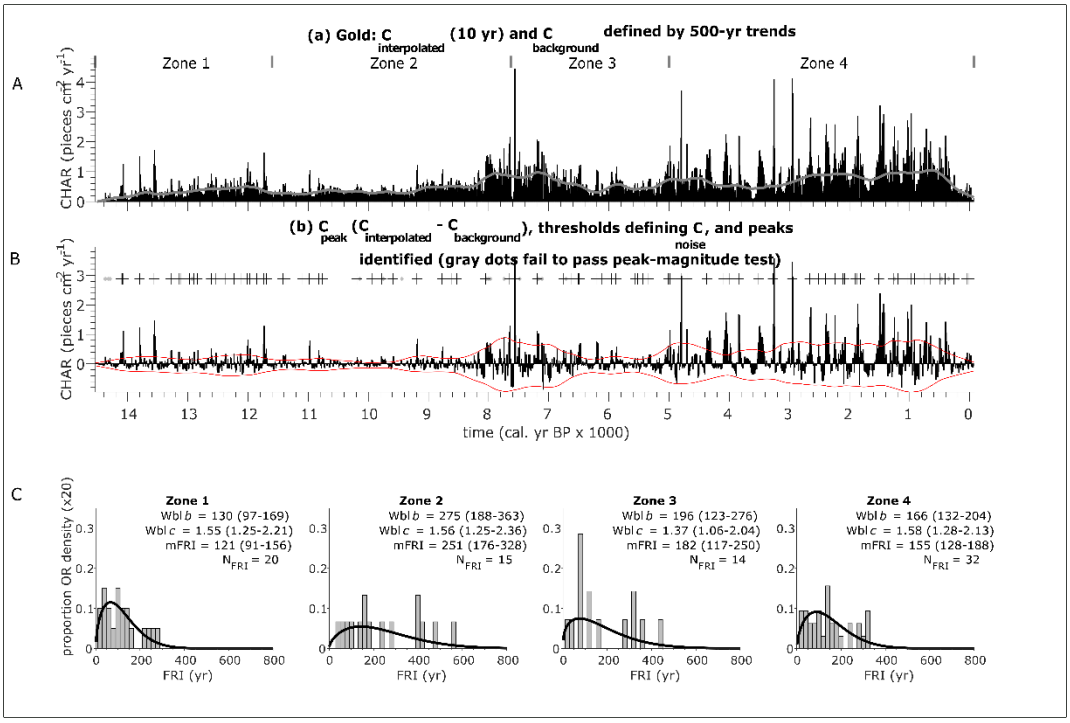


**Figure 2. 6 (A) Charcoal accumulation (CHAR**) pieces/cm$^2$/yr; the grey line represents background charcoal levels; (B) Peak identification with plus (+) symbols representing peaks/fire events and grey dots representing peaks that failed to pass the peak-magnitude test; (C) Mean fire return interval and confidence intervals for the four different pollen zones.

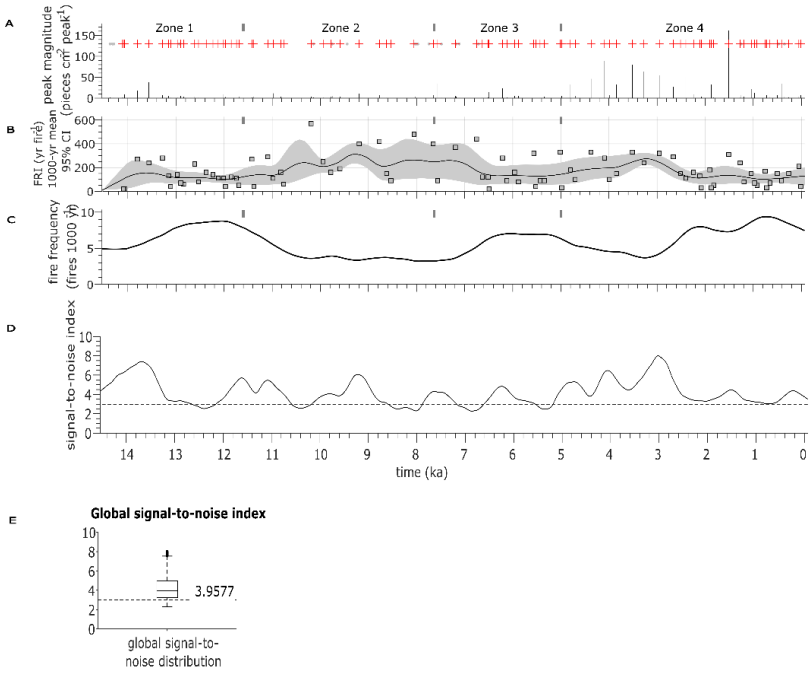


**Figure 2. 7 (A) Identified charcoal peaks represented by the red plus symbols and the peak magnitude in dark blue**; (B) Fire return interval with 95% confidence intervals; (C) Smoothed fire frequency (fires/1000 years); (D) Local signal to noise index throughout the record with global signal to noise index below; (E) Global signal-to-noise index.

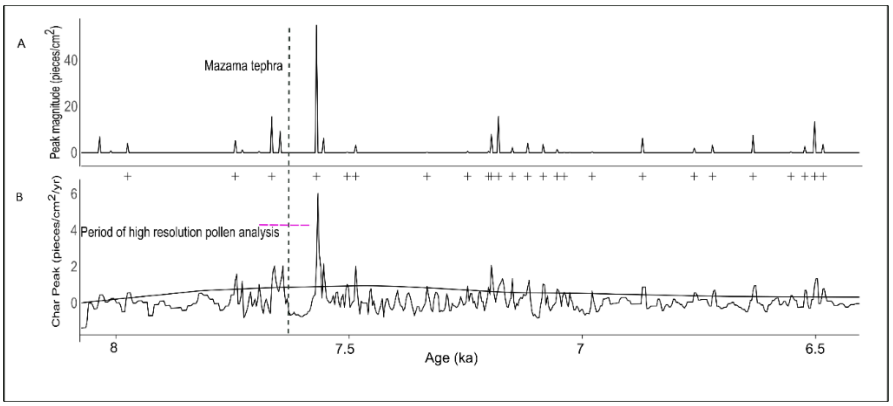


**Figure 2. 8 CharAnalysis peak identification applied to the segment of Gold Lake core with a high sedimentation rate and varved sediments**, interpolated to 3 years resolution (A) Peak magnitude (pieces/cm$^2$) (B) Charcoal accumulation (CHAR) pieces/cm$^2$/year; Peak identification with plus (+) symbols representing peaks/fire events. The time period of high-resolution pollen analysis is shown by a magenta line.

## Discussion

The Gold Lake core, spanning 14,400 years over 13 m, represents one of the highest-resolution postglacial sediment stratigraphies in the Pacific Northwest. This core has a strong chronology, anchored by 11 radiocarbon dates, and contains three tephras (Llao Rock, climactic Mazama, and Rock Mesa from the South Sister volcano). A 1.6 m laminated section of the core due to Si fertilization of the lake by Llao Rock and Mazama tephra is very well preserved and counted as annual varves. Radiocarbon dates verify that the laminated segment is annually varved, and they have been included as a part of the age-depth model.

The lamination count provides a new age estimate of the Llao Rock tephra at 75 years prior to the Mazama tephra. We counted 65 varves between the Mazama tephra and Llao Rock eruption. As there were no visible varves between 813 to 815 cm, we interpolated over this segment by adding 10 years because the varves at other depths between the tephras were very consistent in thickness. Llao Rock is a precursor event from Mt Mazama preceding its climactic eruption that resulted in a blanket of tephra that spread across the Pacific Northwest (Bacon, 1983). This event has been dated directly only a few times before. Mensing and Southon (1999) summarize prior age estimates of this tephra, which suggest an age <200 years preceding the Mazama tephra. Blinman et al. (1979) used pollen influx rates to estimate an age difference of ca. 140 years.

Despite having an age-depth model developed from radiocarbon-verified manual varves counts, the interpretation of the pollen and charcoal record presents some challenges. Greatly changing sedimentation rates make the charcoal record differ in its capacity to reconstruct short-interval fires through time. The lake catchment is large (48.4 $km^2$), and the lake surface is also large (38.9 hectares); thus, the airshed for the pollen source is also large. There are only minor changes in pollen percentages, which are typical for other montane lakes in the Oregon Cascade Range over the postglacial period (Long et al., 2011; Minckley and Long, 2016) but less dynamic than records from small lakes in the densely forested Oregon Coast Range (Long et al., 2007). This is due to Gold Lake being located near a pass in the High Cascades and receiving much regionally dispersed pollen from both east and west of the Cascade Range. From April to June, during pollen dispersal, wind speed ranges from 2-30 km/hr, with diurnal winds strong

from both the NW (*Tsuga heterophylla* forests) and SE (*Pinus contorta* forests). A previous study from Gold Lake Bog (Sea and Whitlock, 1995) also shows more changes in pollen assemblages over the Holocene, but that core site is closer to the forest edge and recorded a late Holocene increase in *Tsuga mertensiana* (mountain hemlock), while our lake site receives a larger component of regional pollen. Nevertheless, smaller changes in pollen (<5%) and changes in the arboreal/non-arboreal ratio likely represent changes in the watershed vegetation. In contrast, the macrocharcoal record shows a very dynamic disturbance regime. Large charcoal peaks likely represent fires in the watershed (Marlon et al., 2006; Rushton and Walsh, 2021) and a more local source than the pollen record.

**Gold I: Post-Glacial period (1302-1110 cm; ca. 14.4-11.6 ka)**

During the Late Glacial period, when glaciers were receding due to rising temperature, the Gold Lake core base consisted of silt and clay for 50 cm (14.4-13.8 ka). This section of the core has the highest magnetic susceptibility, which gradually reduced after 14 ka, increased briefly at the onset of Younger Dryas Chronozone (12.9 ka), and returned to lower values after this event (Fig. 2.9F). Organic content increased as magnetic susceptibility declined, increasing from < 5% to 25% prior to and during the Younger Dryas Chronozone (12.9-11.6 ka). The sedimentation rate was high (0.11 cm/yr) for 1,000 years, then slowed down to 0.08 cm/yr after 13.8 ka. It is likely little additional sediment exists below the deepest sediment reached, as the basal sediment has distinctly higher magnetic susceptibility and low organic matter, consistent with glacial sediments. In addition, no cirque lakes in the region date to > 14.5 ka, a time of montane glacial recession locally and globally (Gavin and Brubaker, 2015).

The changes in pollen assemblages at Gold Lake are similar to those found in other regional studies. Forest cover was established shortly after deglaciation, as inferred from the high proportion of arboreal pollen and increased soil stabilization inferred from declined magnetic susceptibility. PAR also showed little change from the Late Glacial to the early Holocene, consistent with the forest established at the time. Other pollen records from montane sites in the Cascade Range confirm the absence of the tundra period (Sea and Whitlock, 1995; Grigg and Whitlock, 1998; Minckley and Long, 2016). During this time, a subalpine forest of *Picea*, *Pinus*, *Abies*, and *Tsuga mertensiana* with non-arboreal taxa (Poaceae, *Artemisia*, and Asteraceae)

dominated around Gold Lake. The highest abundance of *Picea* was observed in this zone, showing it as an early colonizer in the Cascade Range during the Late Glacial period (Grigg and Whitlock, 1998; Minckley and Long, 2016) that decreased towards the top of this zone (19% to 4%) while *Pinus* increased from 48% to 61%. The high percentage of *Picea, Pinus, Tsuga mertensiana, Tsuga heterophylla*, Poaceae, and *Artemisia* show a similar pattern to pollen assemblages at Breitenbush Lake (Minckley and Long, 2016). *Pinus* expansion and decrease in *Tsuga heterophylla* from ca. 12.7 to 11.6 ka coincide with similar changes at Indian Prairie Fen from 12.5 to 11 ka (Sea and Whitlock, 1995), Gordon Lake, and Little Lake between 12.8 and 11 ka (Grigg and Whitlock, 1998), implying a regional climate change where summers were becoming warmer and drier during the Late Glacial (Grigg and Whitlock, 1998). At lower elevations, during the transition from the late Pleistocene to early Holocene (12-11 ka), a forested landscape dominated and replaced the open woodland and non-arboreal taxa (Whitlock, 1992; Walsh et al., 2008). At Gold Lake, a forest of *Picea* and *Pinus* was replaced by *Abies*, *Alnus*, and *Pseudotsuga* during the early Holocene, similar to the vegetation changes at Little Lake (Grigg and Whitlock, 1998) and other sites in the Oregon Cascade Range (Sea and Whitlock, 1995).

The AP/NAP ratio ranged from 3 to 8, representing the highest percentage of non-arboreal pollen compared to the remainder of the core. *Artemisia*, Poaceae, and other open-site indicators were often > 2% (Poaceae at 7% at the core base), indicating some openness in the vegetation and the presence of fuel to support frequent fire, as also suggested by Minckley et al. (2008) and Minckley and Whitlock (2000) at montane sites to the east of Gold Lake. The highest percentage of *Artemisia* and Poaceae suggests that the region's climate was drier than the present. These taxa decreased towards the end of this zone and have remained low in the remaining core. The decreasing pattern in *Artemisia* is consistent with increased tree density.

Increasing flammable fuels such as grass and sagebrush can increase fire frequency (Morris et al., 2013). The AP/NAP ratio has been interpreted as an indicator of fire severity (Minckley et al., 2012), in which higher NAP taxa suggest conditions that support frequent fires with less severity, such as during the Late Glacial period at Gold Lake. Fire episodes were more frequent from 13.2 to 11.8 ka (Gold-I; Fig. 2.7 A-C) with an average interval of 120 years but

did not produce abundant charcoal except at ~13.6 ka, which coincided with an increased abundance of *Pinus*. However, the size or intensity of the fire, as reflected by peak magnitude or overall charcoal accumulation rate, generally is higher during high AP/NAP (Fig. 2.9C), which is consistent with the notion of charcoal accumulation as an indicator of biomass burning (Marlon et al., 2008). For example, a review of several charcoal records shows that woody fuel abundance plays an important role in determining charcoal abundance, especially during the Late Glacial period (Marlon et al., 2006).

There are few paleoclimate records sensitive to summer hydroclimate from this region to compare the vegetation and fire history (Routson et al., 2021). A sea-surface temperature (SST) record from the northern California coast (ODP site 1019, Fig. 2.1; Barron et al., 2003) records a highly variable SST with a distinct Younger Dryas Chronozone (Fig. 2.9). The magnitude of the Younger Dryas inland, however, apparently was not sufficient to greatly transform the vegetation and fire regime, though pollen sampling resolution through this period was low.

**Gold II-Early/Middle Holocene-Pre-Mazama (ca. 11.6-8.1 ka)**

During the early Holocene, the record indicates increased productivity and open vegetation. Organic content remained high after its sudden increase after ~13.2 ka. LOI reached its highest value (37%) at ~9.2 ka and decreased after the Llao Rock tephra (14%). Magnetic susceptibility remained elevated until ca. 9.6 ka, indicating some terrigenous input to the lake. For the remainder of the core (except tephra events), magnetic susceptibility was very low due to the highly biogenic (i.e., diatom silica) sediment composition. PAR increased at the onset of Younger Dryas but showed a decreasing pattern until it reached its lowest value at 4185 grains/cm$^2$/yr at ~9.2 ka, with a sedimentation rate varying from 0.05 to 0.083 cm/yr. After 9.2 ka, pollen accumulation increased consistently and reached 14,900 grains/cm$^2$/yr. This section also has the second-highest NAP (22%). During the early Holocene, warm and dry summers resulting from increased summer insolation (Whitlock, 1992; Thompson et al., 1993) caused an increased abundance of *Pseudotsuga* and *Quercus*. These taxa were rare during the Late Glacial while today are abundant in the lower elevations of the *Tsuga heterophylla* zone, and today *Quercus* is limited to low-elevation south-facing exposures of the western Cascade Range (Minckley and Whitlock., 2000; Walsh et al., 2010). *Quercus* pollen at Gold Lake may reflect

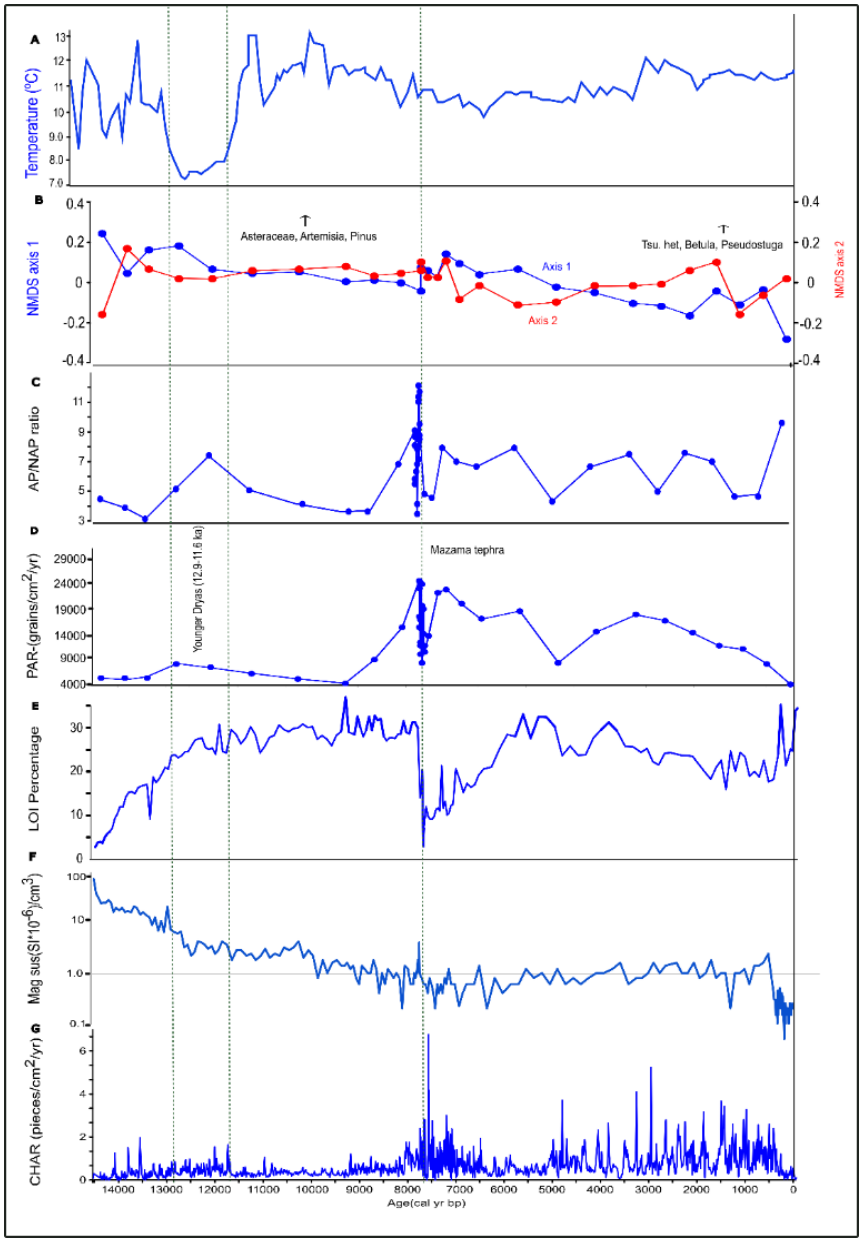


**Figure 2. 9 (A) Northeast Pacific sea surface temperature (SST) inferred from alkenone records from a core near northern California** (Barron et al., 2003) (B) NMDS axes from ordination of the pollen assemblages; (C) AP/NAP ratio; (D) PAR; (E) LOI percentage; (F) Magnetic susceptibility (High magnetic susceptibility values around three tephra layers are not shown; (G) Charcoal accumulation rate.

the establishment and long-distance pollen transport from large early Holocene populations at lower elevations. After ~9 ka, *Pseudotsuga* abundance decreases while most non-arboreal taxa (Poaceae, Pteridophyte-monolete, Pteridophyte-trilete, *Thalictrum*, *Dryopteris-type*, *Pteridium*) increase in abundance and remain high until the Mazama tephra.

The early Holocene increase in *Pseudotsuga*, *Alnus*, and *Pteridium* represents a change toward warmer and drier conditions (Agee, 1993). *Picea*, which had decreased at the end of the Late Glacial period, remained low in abundance during the early Holocene pre-Mazama period. *Alnus*, which had increased at the end of the Glacial period, reached 12% right before the Mazama tephra, possibly because of the Llao Rock tephra disturbance that facilitated its expansion. *Alnus* pollen also might contribute from the lower elevation *Alnus rubra*, which was not separated from other *Alnus* during pollen identification, where they are present in abundance (Whitlock, 1992). The increasing abundance of *Abies* and low percentage of *Tsuga mertensiana*, *Tsuga heterophylla*, and *Picea* resemble modern pollen assemblages of the *Abies amabilis* zone (Minckley and Whitlock, 2000). Gold Lake Bog had the same taxa composition with poor representation of *Picea* and *Tsuga mertensiana* during the early Holocene (Sea and Whitlock, 1995).

During the early Holocene, low peak magnitude (and low charcoal accumulation), low PAR, and high AP/NAP suggest high-frequency fires at lower severity such that few fires are represented in the core as distinct charcoal peaks. During the early Holocene, due to greater summer insolation, snowpack persistence was likely shortened, growing seasons had reduced moisture availability, and there was less biomass available for burning. The longer fire return intervals (210 years), as determined from peak-identification methods, are probably due to the time required for the fuel to accumulate to produce larger fires that produce more distinct charcoal peaks, while smaller fires remained undetected (Walsh et al., 2008a). Elevated magnetic susceptibility until 9.6 ka provides additional evidence of an open canopy and more frequent low-severity fires, as erosional inputs from the lake shore and inflowing streams suggest less protection of mineral soils by a thick organic horizon than later in the Holocene. Low-severity fires at Gold Lake during the early Holocene align with two studied lakes in the Sierra Nevada, California, with vegetation dominated by *Pinus* and montane chaparral shrubs (Hallett and

Anderson, 2010) that supports Anderson's (1990) conclusion that high-elevation pine forests were more open than today. At Long Lake in the eastern Cascade Range of Washington, Rushton and Walsh (2022) found very low CHAR before 6 ka and invoked limited fuel availability in *Pinus*/*Artemisia* vegetation. Very low CHAR was also found at nearby Tumalo Lake from 11 to 8.5 ka (Long et al., 2011), while CHAR was consistently lower in the early vs. late Holocene at Breitenbush Lake (Minckley and Long, 2016). Thus, fuel limitation may have been a regionally important factor affecting the fire regime of the High Cascade Range during the early Holocene.

**Gold III-Middle Holocene-Post-Mazama (ca. 7.5 to 5 ka)**

During this period, organic content increased from 10 to 33%, with magnetic susceptibility values of 0.2-1.7 $(SI*10^{-6})/cm^3$. The AP/NAP ratio values varied from 4 to 8. PAR varies between 13,200 to 22,100 grains/$cm^2$/yr with a sedimentation rate (0.062-0.25 cm/yr) that shows a decreasing trend after 5.5 ka, which started to increase again at 4.8 ka in the late Holocene. The sedimentation rate, which was 0.25-0.12 cm/yr until ~6.8 ka, decreases to 0.062 cm/yr at ~6.4 ka when laminations abruptly end, and the sediment becomes massive sapropel. Fire episode frequency shifted from an average of one fire every 121 years to 251 years in the early Holocene pre-Mazama to 182 years post-Mazama, returning to more frequent fires in the late Holocene with one fire every 155 years.

The high-resolution segment of the core, the 1200 years period from 7.6 to 6.4 ka, resulting from dramatically increased diatom production due to silica fertilization, permits an analysis of post-Mazama fire history as the forests developed on a new tephra parent material. In addition, climate changes occurred within the millennium following the tephra deposition. During the middle Holocene, summer insolation decreased, resulting in a cooler and wetter climate (Bartlein et al., 1998), and forests at lower elevations increased in density, thus affecting the fire regime (Walsh et al., 2008). On the crest of the Cascade Range, forest density also increased, as evidenced by the development of late-successional forest at Gold Lake (increase in *Abies, Picea,* and *Tsuga;* Fig. 2.3) and a large increase in the forest: understory ratio at Breitenbush Lake (Minckley and Long, 2016). The increase in forest density fostered a high-severity fire regime, while the non-arboreal taxa that were reduced following the tephra started to appear but in low abundance. *Thalictrum* that disappeared after the eruption appeared at ~7.5 ka

in almost the same abundance as before the eruption. Among non-arboreal taxa, Cyperaceae and Asteraceae increased, Poaceae and Rosaceae stabilized, and *Artemisia* decreased (Fig. 2.8 and Fig. 2.3).

**Gold IV-Middle/Late Holocene (ca. 5 ka to present)**

The transition into the middle/late Holocene starts with low PAR (8100 grains/cm$^2$/yr; Fig. 2.9D) at 4.8 ka, when AP/NAP also decreases (Fig. 2.9C), showing an increasing number of non-arboreal taxa. PAR shows an increasing trend after 4.5 ka, which reaches its maximum value of ~3.2 ka, but after that, it decreases until the recent time when it reaches the lowest value (4000 grains/cm$^2$/yr) that is close to that found at Gold Lake Bog (Sea and Whitlock, 1995) and closed montane forest (Fall, 1992). LOI fluctuates during this time with a decreasing trend during the transition to the late Holocene, increasing at 3.8 ka and then decreasing until it started increasing at ~ ca. 350 years (Fig. 2.9E). Magnetic susceptibility is constant (except when affected by tephra), suggesting fires were not resulting in measurable watershed erosion. The sedimentation rate is 0.062 cm/yr at the onset of the late Holocene, which increases to 0.11 cm/yr at ~ca. 900 years (Fig. 2.9F).

Arboreal taxa show a fluctuating pattern during the late Holocene. *Pinus* decreases during the middle Holocene, increases at ~1.4 ka, then decreases. *Pseudotsuga*, *Tsuga mertensiana*, and *Tsuga heterophylla* increase at the onset of the late Holocene and reach their highest abundance in the top part of the core. *Abies* and *Betula* increase in the late Holocene and reach maximum abundance at ~2.5 ka, while *Picea* has higher abundance at the onset of the late Holocene but then declines towards the core top. During the late Holocene, similar vegetational changes were recorded at Gold Lake Bog, where *Pinus* decreased while *Tsuga heterophylla*, *Tsuga mertensiana*, *Pseudotsuga*, *Picea*, and *Abies* increased (Sea and Whitlock, 1995). Among non-arboreal taxa, *Artemisia*, Poaceae, and Cyperaceae were present in higher abundance, with their maximum percentage ~ca. 0.9 ka.

The late Holocene continued to become more humid and cooler with decreasing summer radiation (Gavin et al., 2013). The increased moisture is reflected in increased lake levels through the late Holocene at downwind sites in Idaho (Parish et al., 2022). After 5 ka, pollen composition similar to the present-day forest started to establish at Gold Lake and resembles

pollen spectra of the High Cascade Range (Minckley et al., 2000). Expansion of *Tsuga heterophylla*, *Tsuga mertensiana*, *Pseudotsuga*, and *Abies* at Gold Lake and Gold Lake Bog (Sea and Whitlock, 1995) shows the development of late-successional forest (Agee, 1993). Fire activity increased after 5.5 ka, followed by a decreasing pattern, and then increased after 2 ka at multiple sites in PNW (Walsh et al., 2015), which is consistent with what we found at Gold Lake, having 32 fires identified with the second-lowest mFRI of 155 years in late Holocene. The gradual change in climate to cooler and more moisture resulted in closed forests and fuel build-up, which may explain larger fires and larger charcoal peaks observed regionally after 4 ka (Marlon et al., 2006, Walsh et al., 2015). At Gold Lake, fires were less frequent, but the peak magnitude was higher until 2.4 ka. After 2.4 ka, fires were more frequent with lower magnitude, with the exception of a single large peak at 1.5 ka (Fig. 2.7A-C).

Over the last 400 years, CHAR decreases to the lowest values of the middle and late Holocene, while NAP taxa reached their lowest levels. This recent period of low charcoal input is consistent with the predominance of old-growth forests with no above-ground evidence of fire surrounding Gold Lake today. It also encompasses the Little Ice Age and the period of greatest neoglacial advances in the Pacific Northwest. For example, most glaciers on the nearby Three Sisters volcanoes reached the maximum Holocene extent within the last 300 years (Marcott et al., 2009). The forest stands around Gold Lake are now becoming a refuge as large fires in 2020 CE and 2022 CE have burned through many other old *Tsuga mertensiana* forests in the region. The view from this single record is that the 21$^{st}$-century increase in fire is returning the fire regime to a late Holocene pattern of fire that was interrupted by an abnormally long fire-free period during the Little Ice Age.

**Impact and significance of Mazama tephra on vegetation and fire (Pre- and post-Mazama eruption-ca. 7.69 to 7.5 ka)**

The Mazama tephra deposit had a large impact on non-arboreal taxa, as seen in the AP/NAP ratio (Fig. 2.10C). Sixty years before the Mazama tephra, ca. 20 years after the Llao Rock tephra, the AP/NAP ratio was declining from 9 to more typical early Holocene value of ca. 3. After the Mazama tephra, the AP/NAP ratio increased from 3 (with the highest percentage of NAP in the core) to 13. Non-arboreal taxa reduced after the tephra as *Thalictrum* disappeared

and did not appear until ~7.4 ka and the remaining non-arboreal taxa reduced in number and occurrence with the lowest percentage (Fig. 2.10C). A similar pattern was observed at three lakes in the central Cascades (Breitenbush Lake, Three Creeks Lake, and Tumalo Lake), where it affected understory species more than arboreal taxa (Long et al., 2011, 2014), but it did not result in increased fire or changing vegetation composition. In addition, the shift to higher AP/NAP at these nearby sites was short-lived (Long et al., 2014), while at Gold Lake, AP/NAP remained high for centuries. This shift to higher arboreal taxa suggests that Mazama deposition affected the production of non-arboreal species due to their burial in 78 cm of tephra, lower rates of reproduction, low recovery, and limited seed dispersal (Antos and Zobel, 1986; Zobel and Antos, 1997). Studies from Mount Saint Helens 1980 eruption have shown that understory species are severely affected even with a low-intensity disturbance of 4.5 cm of tephra and that the topography and condition of the prior vegetation make the effects heterogenous (Antos and Zobel, 2005). The AP/NAP ratio returned to the pre-Mazama value by ca. 300 years later, indicating that non-arboreal taxa required a long time to recover from the catastrophic effect of the Mazama eruption (Fig. 2.8).

The PAR across the Mazama tephra does not reveal a clear impact on arboreal taxa (Fig. 2.10B). PAR was 30,700 grains/cm$^2$/yr just prior to the tephra, which might be an artifact of the mass of the tephra increasing the bulk density, and pollen concentration, of that sample. PAR was 13,300 grains/cm$^2$/yr immediately after the tephra, though the varve-measured sedimentation rate remained constant at 0.33 cm/yr. PAR increased to 22,000 grains/cm$^2$/yr within nine varve years after the Mazama tephra, after which it varies between 11,800-18,900 until 7.60 ka. At 30 years post-tephra, PAR starts declining and varies between 8000 to 9900 grains/cm$^2$/yr with a lower sedimentation rate (0.13-0.14 cm/yr). Given the lack of a clear pattern in PAR on the scale of tree lifespans, we conclude that trees were injured within the region but survived the tephra deposition, consistent with observations at Mount Saint Helens (Dale et al., 2005). Our results contrast with that from Foy Lake, Montana, where the Mazama eruption significantly affected vegetation, as seen by a decreased PAR decrease, requiring 200 years to return to the pre-Mazama depositional rate (Power et al., 2011). However, at Foy Lake, much more vegetation was non-arboreal and thus more susceptible to tephra.

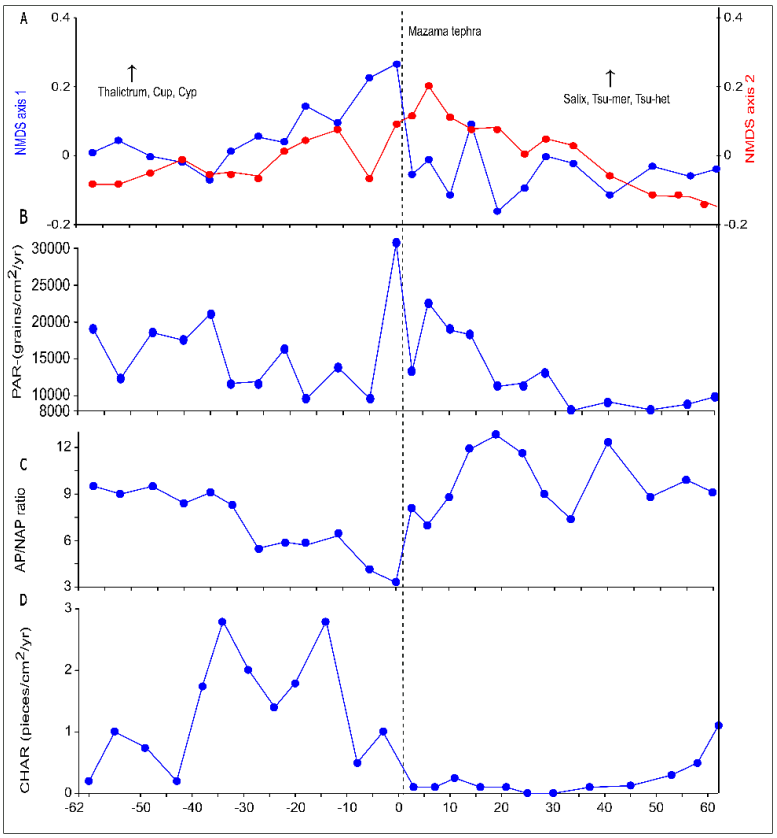


**Figure 2. 10 High-resolution pollen and charcoal data preceding and following the Mazama eruption** (A) NMDS axes; (B) PAR; (C) AP/NAP ratio; (D) CHAR (pieces/cm$^2$/yr).

Despite the lack of change in PAR, there were compositional changes in arboreal pollen as inferred from pollen percentages. Among arboreal taxa, *Pinus* increased from 40 to 62% (while *Pinus* subgenus *Strobus* decreased) and remained high until ~6 ka. *Pseudotsuga*, *Tsuga mertensiana*, and *Artemisia* percentages also increase directly following the tephra, while *Alnus*, *Picea*, *Abies*, *Tsuga heterophylla*, Dryopteris, and *Betula* decrease but then show an increasing pattern ten years after the eruption (Fig. 2.5A). These results are consistent with observed tree injury and growth reduction of *Abies* (but not *Pseudotsuga*) in the ashfall zone after the 1980 St. Helens eruption (Segura et al., 1994). It is possible that foliage traits are important predictors of decline, such that taxa that retain tephra in the foliage result in foliage death and limb breakage, as observed at St. Helens (Segura et al., 1994).

High-resolution charcoal data, which is interpolated to three-year intervals from 8 to 6.4 ka (Fig. 2.8), shows overall more frequent fire than after 4 ka when charcoal peaks are larger but less frequent. Although the temporal resolution is greater in the earlier period, the charcoal stratigraphy after 4 ka shows much autocorrelation and large distinct peaks, such that increasing temporal resolution during this period is unlikely to increase the number of peaks. Directly following the tephra deposition, charcoal declined for 60 years, indicating that tephra did not immediately contribute to fire (Long et al., 2014). However, the highest charcoal concentration (27 pieces/$cm^3$) occurred 63 years after the Mazama tephra, similar to the 20–40-year delay in fire reconstructed at Tumalo Lake (Long et al., 2014). Similarly, decreased fires were also recorded at Foy Lake, Montana, after the eruption, which shows that tephra suppressed wildfire (Power et al., 2011). At Gold Lake, the 78 cm of tephra would have buried surface fuels, requiring decades of plant establishment and limb fall to establish a surface fuel load sufficient for fire spread.

In contrast to these findings, other nearby sites (Three Creeks and Breitenbush lakes) show that fire increased after the Mazama eruption (Long et al., 2014), while at Lost Trail Pass Bog, the fire did not show a major response to the Mazama eruption except a decrease in *Pinus* percentage (Mehringer et al., 1977). However, these sites have a sedimentation rate that is <10% of that at Gold Lake and thus do not have the ability to detect the decadal-scale change (4-5 years per sample) available at Gold Lake.

## Conclusion

Our detailed pollen and charcoal analysis of Gold Lake provides information about vegetation and fire response to the major climatic events of the Late Glacial and Holocene and to volcanic eruptions. The Late Glacial period recorded high charcoal peaks that coincided with more open vegetation and warm temperatures that provided flammable fuel for a forest fire. Fewer fires in the early Holocene might result from less moisture availability, especially the climatic conditions that suppressed the herbaceous and shrub cover, which provides important surface fuel to support large fires. While other sites in the Pacific Northwest show increased fire during the early Holocene (e.g., Long et al., 1998; Gavin et al., 2013), the High Cascades Range may have been fuel-limited or supported a low-severity fire regime.

This study provides a high-resolution pollen analysis of pre and post-Mazama eruption in the high Cascades with 78 cm of tephra. It shows that the tephra affected both arboreal and non-arboreal taxa. Non-arboreal taxa were significantly affected, and their composition changed, while arboreal taxa recorded some changes in relative abundance. Furthermore, the tephra potentially promoted a low-severity fire regime for a millennium, as marked by frequent low-magnitude charcoal peaks and higher NAP abundance. Increased forest density during the late Holocene produced less frequent fires but of a greater magnitude, as inferred from larger charcoal peaks, suggesting more severe fires. The Little Ice Age period of low fire is anomalous in the context of the late Holocene at Gold Lake. More high-resolution studies are needed to explain tephra's spatial pattern and species-specific impacts on vegetation and fire.

In the next chapter, we will focus paleotemperature reconstruction based on chironomid head capsules from the Gold Lake sediment. This will be the first attempt to reconstruct paleotemperature in Oregon using IMW calibration dataset developed by Haskett and Porinchu (2014).

## References


Agee, J. K. (1996). *Fire ecology of Pacific Northwest forests*. Island Press.

Allen, J. R., & Huntley, B. (2018). Effects of tephra fall on vegetation: A Late-Quaternary record from southern Italy. *Journal of Ecology*, *106*(6), 2456-2472.

Anderson, R. S. (1990). Holocene forest development and paleoclimates within the central Sierra Nevada, California. *The Journal of Ecology*, 470-489.

Antos, J. A., & Zobel, D. B. (2005). Plant responses in forests of the tephra-fall zone. In *Ecological responses to the 1980 eruption of Mount Saint Helens* (pp. 47-58). Springer, New York, NY.

Antos, J. A., & Zobel, D. B. (1986). Recovery of forest understories buried by tephra from Mount Saint Helens. *Vegetatio*, *64*(2), 103-111.

Bacon, C. R. (1983). Eruptive history of Mount Mazama and Crater Lake caldera, Cascade Range, USA. *Journal of volcanology and Geothermal Research*, *18*(1-4), 57-115.

Bartlein, P. J., Anderson, K. H., Anderson, P. M., Edwards, M. E., Mock, C. J., Thompson, R. S., Webb, R. S., Webb, T., & Whitlock, C. (1998). Paleoclimate simulations for North America over the past 21,000 years:

Features of the simulated climate and comparisons with paleoenvironmental data. *Quaternary Science Reviews*, *17*(6-7), 549-585. https://doi.org/10.1016/S0277-3791(98)00012-2

Barron, J. A., Heusser, L., Herbert, T., & Lyle, M. (2003). High-resolution climatic evolution of coastal northern California during the past 16,000 years. *Paleoceanography*, 18(1). https://doi.org/10.1029/2002PA000768

Bassett, I., Crompton, C., & Parmelee, J. (1978). *An atlas of airborne pollen grains and common fungus spores of Canada*. Canadian Department of Agriculture Monograph 18.

Bennett, K. D. (1996). Determination of the number of zones in a biostratigraphical sequence. *New Phytol*, *132*(1), 155–170. https://doi.org/10.1111/j.1469-8137.1996.tb04521.x

Bennett, K. D., & Willis, K. J. (2001). 2001: Pollen. In Smol, JP, Birks, HJB and Last, WM, editors, Tracking environmental change using lake sediments. Volume 3: terrestrial, algal, and siliceous indicators, Kluwer Academic Publishers, 5-32.

Blaauw, M., & Christen, J. A. (2011). Flexible paleoclimate age-depth models using an autoregressive gamma process. *Bayesian analysis*, *6*(3), 457-474.

Birks, H. J. B., & Lotter, A. F. (1994). The impact of the Laacher See Volcano (11 000 yr BP) on terrestrial vegetation and diatoms. *Journal of Paleolimnology*, *11*(3), 313-322.

Blinman, E., Mehringer Jr, P. J., & Sheppard, J. C. (1979). Pollen influx and the deposition of Mazama and Glacier Peak tephra. In *Volcanic activity and human ecology* (pp. 393-425). Academic Press.

Brown, T. A., Nelson, D. E., Mathewes, R. W., Vogel, J. S., & Southon, J. R. (1989). Radiocarbon dating of pollen by accelerator mass spectrometry. *Quaternary Research*, *32*(2), 205–212. https://doi.org/10.1016/0033-5894(89)90076-8

Brubaker, L. B. (1975). Postglacial forest patterns associated with till and outwash in northcentral Upper Michigan. *Quaternary Research*, *5*(4), 499-527.

Buckland, H. M., Cashman, K. V., Engwell, S. L., & Rust, A. C. (2020). Sources of uncertainty in the Mazama isopachs and the implications for interpreting distal tephra deposits from large magnitude eruptions. Bulletin of Volcanology, 82(3), 1-17.

Chapin, F. S., & Shaver, G. R. (1985). Individualistic Growth Response of Tundra Plant Species to Environmental Manipulations in the Field. *Ecology*, *66*(2), 564–576. https://doi.org/10.2307/1940405

Cimarelli, C., Genareau, K., 2022. A review of volcanic electrification of the atmosphere and volcanic lightning. Journal of Volcanology and Geothermal Research 422, 107449. https://doi.org/10.1016/j.jvolgeores.2021.107449

Cohen, K. M., Finney, S. C., Gibbard, P. L., & Fan, J. X. (2013). The ICS International Chronostratigraphic Chart. *Episodes Journal of International Geoscience*, *36*(3), 199–204. https://doi.org/10.18814/EPIIUGS/2013/V36I3/002

Cohmap Members. (1988). Climatic changes of the last 18,000 years: observations and model simulations. Science, 241(4869), 1043-1052.

Crisafulli, C. M., Swanson, F. J., Halvorson, J. J., & Clarkson, B. D. (2015). Volcano ecology: disturbance characteristics and assembly of biological communities. In The encyclopedia of volcanoes (pp. 1265-1284). Academic Press.

Dale, V. H., & Crisafulli, C. M. (2018). Ecological responses to the 1980 eruption of Mount Saint Helens: key lessons and remaining questions. In *Ecological Responses at Mount Saint Helens: Revisited 35 years after the 1980 Eruption* (pp. 1-18). Springer, New York, NY.

Dean, W. E. (1974). Determination of carbonate and organic matter in calcareous sediments and sedimentary rocks by loss and ignition: comparison with other methods. *Journal of Sedimentary Petrology*, *44*(1), 242–248.

Egan, J., Fletcher, W. J., Allott, T. E., Lane, C. S., Blackford, J. J., & Clark, D. H. (2016). The impact and significance of tephra deposition on a Holocene forest environment in the North Cascades, Washington, USA. *Quaternary Science Reviews*, *137*, 135-155. https://doi.org/10.1016/j.quascirev.2016.02.013

Egan, J., Staff, R., & Blackford, J. (2015). A high-precision age estimate of the Holocene Plinian eruption of Mount Mazama, Oregon, USA. *Holocene*, *25*(7), 1054-1067. https://doi.org/10.1177/0959683615576230

Erdtman G. (1969). *Handbook of palynology: morphology taxonomy ecology; an introduction to the study of pollen grains and spores*. Hafner.

Faegri, K., Kaland, P. E., & Krzywinski, K. (1989). *Textbook of pollen analysis* (No. Ed. 4). John Wiley & Sons Ltd.

Fall, P. L. (1992). Pollen accumulation in a montane region of Colorado, USA: a comparison of moss polsters, atmospheric traps, and natural basins. *Review of Palaeobotany and Palynology*, *72*(3–4), 169–197.

Franklin, J.F., Dyrness, C.T., 1988. Natural Vegetation of Oregon and Washington. Oregon State University Press.

Gavin, D. G., & Brubaker, L. B. (2014). *Late Pleistocene and Holocene Environmental Change on the Olympic Peninsula, Washington* (Vol. 222). Springer.

Gavin, D. G., Brubaker, L. B., & Greenwald, D. N. (2013). Postglacial climate and fire-mediated vegetation change on the western Olympic Peninsula, Washington (USA). *Ecological Monographs*, *83*(4), 471–489. https://doi.org/10.1890/12-1742.1

Gavin, D. G., Henderson, A. C., Westover, K. S., Fritz, S. C., Walker, I. R., Leng, M. J., & Hu, F. S. (2011). Abrupt Holocene climate change and potential response to solar forcing in western Canada. *Quaternary Science Reviews*, *30*(9-10), 1243-1255.

Gedye, S. J., Jones, R. T., Tinner, W., Ammann, B., & Oldfield, F. (2000). The use of mineral magnetism in the reconstruction of fire history: a case study from Lago di Origlio, Swiss Alps. *Palaeogeography, Palaeoclimatology, Palaeoecology*, *164*(1–4), 101–110. https://doi.org/10.1016/S0031-0182(00)00178-4

Giles, T. M., Newnham, R. M., Lowe, D. J., & Munro, A. J. (1999). Impact of tephra fall and environmental change: a 1000 year record from Matakana Island, Bay of Plenty, North Island, New Zealand. *Geological Society, London, Special Publications*, *161*(1), 11–26. https://doi.org/10.1144/GSL.SP.1999.161.01.03

Grigg, L. D., & Whitlock, C. (1998). Late Glacial vegetation and climate change in western Oregon. *Quaternary Research*, *49*(3), 287–298. https://doi.org/10.1006/qres.1998.1966

Hallett, D.J., Hills, L.V., Clague, J.J., 1997. New accelerator mass spectrometry radiocarbon ages for the Mazama tephra layer from Kootenay National Park, British Columbia, Canada. Can. J. Earth Sci. 34, 1202–1209. https://doi.org/10.1139/e17-096

Hallett, D. J., & Anderson, R. S. (2010). Paleofire reconstruction for high-elevation forests in the Sierra Nevada, California, with implications for wildfire synchrony and climate variability in the late Holocene. *Quaternary Research*, *73*(2), 180–190. www.wrcc.dri.edu

Harris, J., & Van Couvering, J. (1995). Mock aridity and the paleoecology of volcanically influenced ecosystems. *Geology*, *23*(7), 593-596.

Herring, E., 2014. Late Quaternary and Holocene Paleoecology of Interior Mesic Forests of Northern Idaho (Ph.D. Disseration). University of Oregon, Eugene, OR.

Hickman, M., & Reasoner, M. A. (1994). Diatom responses to late Quaternary vegetation and climate change, and to deposition of two tephras in an alpine and a sub-alpine lake in Yoho National Park, British Columbia. *Journal of Paleolimnology*, *11*(2), 173-188.

Higuera, P. (2009). CharAnalysis 0.9: Diagnostic and analytical tools for sediment-charcoal analysis. *User's Guide, Montana State University, Bozeman, MT*.

Higuera, P. E., Gavin, D. G., Bartlein, P. J., & Hallett, D. J. (2010). Peak detection in sediment-charcoal records: Impacts of alternative data analysis methods on fire-history interpretations. *International Journal of Wildland Fire*, *19*(8), 996-1014. https://doi.org/10.1071/WF09134

Hotes, S., Poschlod, P., & Takahashi, H. (2006). Effects of volcanic activity on mire development: Case studies from Hokkaido, northern Japan. *Holocene*, *16*(4), 561-573. https://doi.org/10.1191/0959683606HL952RP

Johnson, D. M. (1985). *Atlas of Oregon Lakes*. Oregon State University Press.

Juggins, S. (2009). Package "rioja" - Analysis of Quaternary Science Data. *The Comprehensive R Archive Network*.

Kapp, R. O. (1969). Pollen and spores: Dubuque, William C. Brown Co.

Kelly, R. F., Higuera, P. E., Barrett, C. M., & Hu, F. S. (2011). A signal-to-noise index to quantify the potential for peak detection in sediment-charcoal records. *Quaternary Research*, *75*(1), 11–17. https://doi.org/10.1016/J.YQRES.2010.07.011

Kilian, R., Biester, H., Behrmann, J., Baeza, O., Fesq-Martin, M., Hohner, M., Schimpf, D., Friedmann, A., & Mangini, A. (2006). Millennium-scale volcanic impact on a superhumid and pristine ecosystem. *Geology*, *34*(8), 609–612. https://doi.org/10.1130/G22605.1

Kutzbach, J., Gallimore, R., Harrison, S., Behling, P., Selin, R., & Laarif, F. (1998). Climate and biome simulations for the past 21,000 years. *Quaternary Science Reviews*, *17*(6–7), 473–506. https://doi.org/10.1016/S0277-3791(98)00009-2

Long, C. J., Power, M. J., & Bartlein, P. J. (2011). The effects of fire and tephra deposition on forest vegetation in the Central Cascades, Oregon. *Quaternary Research*, *75*(1), 151–158. https://doi.org/10.1016/j.yqres.2010.08.010

Long, C. J., Power, M. J., Minckley, T. A., & Hass, A. L. (2014). The impact of Mt Mazama tephra deposition on forest vegetation in the Central Cascades, Oregon, USA. *Holocene*, *24*(4), 503–511. https://doi.org/10.1177/0959683613520258

Long, C. J., Whitlock, C., & Bartlein, P. J. (2007). Holocene vegetation and fire history of the Coast Range, western Oregon, USA. *Holocene*, *17*(7), 917–926. https://doi.org/10.1177/0959683607082408

Long, C. J., Whitlock, C., Bartlein, P. J., & Millspaugh, S. H. (1998). A 9000-year fire history from the Oregon Coast Range, based on a high-resolution charcoal study. *Can J For Res*, *28*, 774–787.

Lotter, A. F., Birks, H. J. B., & Zolitschka, B. (1995). Late-glacial pollen and diatom changes in response to two different environmental perturbations: volcanic eruption and Younger Dryas cooling. *Journal of Paleolimnology*, *14*(1), 23-47.

Mack, R. N. (1981). Initial Effects of Ashfall from Mount Saint Helens on Vegetation in Eastern Washington and Adjacent Idaho. *Science*, *213*(4507), 537–539. https://doi.org/10.1126/SCIENCE.213.4507.537

Mann, M. E., Zhang, Z., Rutherford, S., Bradley, R. S., Hughes, M. K., Shindell, D., Ammann, C., Faluvegi, G., & Ni, F. (2009). Global signatures and dynamical origins of the little ice age and medieval climate anomaly. *Science*, *326*(5957), 1256–1260.

Marcott, S.A., Fountain, A.G., O'Connor, J.E., Sniffen, P.J., & Dethier, D.P. (2009). A latest Pleistocene and Holocene glacial history and paleoclimate reconstruction at Three Sisters and Broken Top Volcanoes, Oregon, USA. *Quaternary Research*, 71, 181–189. https://doi.org/10.1016/j.yqres.2008.09.002

Marlon, J., Bartlein, P. J., & Whitlock, C. (2006). Fire-fuel-climate linkages in the northwestern USA during the Holocene. *Holocene*, *16*(8), 1059–1071. https://doi.org/10.1177/0959683606069396

Marlon, J. R., Bartlein, P. J., Carcaillet, C., Gavin, D. G., Harrison, S. P., Higuera, P. E., Joos, F., Power, M. J., & Prentice, I. C. (2008). Climate and human influences on global biomass burning over the past two millennia. *Nature Geoscience*, *1*(10), 697–702. https://doi.org/10.1038/ngeo313

Mathewes, R. W., Heusser, L. E., & Patterson, R. T. (1993). Evidence for a Younger Dryas-like cooling event on the British Columbia coast. *Geology*, *21*(2), 101–104.

McDaniel, P. A., Wilson, M. A., Burt, R., Lammers, D., Thorson, T. D., McGrath, C. L., & Peterson, N. (2005). Andic soils of the Inland Pacific Northwest, USA: Properties and ecological significance. *Soil Science*, *170*(4), 300-311. https://doi.org/10.1097/00010694-200504000-00007

Mehringer, P. J., Blinman, E., & Petersen, K. L. (1977). Pollen Influx and Volcanic Ash: The pollen content of Mazama and Glacier Peak ashes reveals details of their depositional chronologies. *Science*, *198*(4314), 257–261.

Mensing, S. A., & Southon, J. R. (1999). A simple method to separate pollen for AMS radiocarbon dating and its application to lacustrine and marine sediments. *Radiocarbon*, *41*(1), 1–8. https://doi.org/10.1017/S0033822200019287

Millar, C. I., King, J. C., Westfall, R. D., Alden, H. A., & Delany, D. L. (2006). Late Holocene forest dynamics, volcanism, and climate change at Whitewing Mountain and San Joaquin Ridge, Mono County, Sierra Nevada, CA, USA. *Quaternary Research*, *66*(2), 273–287. www.elsevier.com/locate/yqres

Minckley, T. A., Whitlock, C., & Bartlein, P. J. (2007). Vegetation, fire, and climate history of the northwestern Great Basin during the last 14,000 years. *Quaternary Science Reviews*, *26*(17-18), 2167-2184.

Minckley, T. A., Bartlein, P. J., Whitlock, C., Shuman, B. N., Williams, J. W., & Davis, O. K. (2008). Associations among modern pollen, vegetation, and climate in western North America. *Quaternary Science Reviews*, *27*(21–22), 1962–1991. https://doi.org/10.1016/j.quascirev.2008.07.006

Minckley, T. A., Shriver, R. K., & Shuman, B. (2012). Resilience and regime change in a southern Rocky Mountain ecosystem during the past 17 000 years. *Ecological Monographs*, *82*(1), 49–68. https://doi.org/10.1890/11-0283.1

Minckley, T., & Whitlock, C. (2000). Spatial variation of modern pollen in Oregon and southern Washington, USA. *Review of Palaeobotany and Palynology*, *112*, 97–123. www.elsevier.nl/locate/revpalbo

Minckley, T. A., & Long, C. J. (2016). Paleofire severity and vegetation change in the Cascade Range, Oregon, USA. *Quaternary Research*, *85*(2), 211-217.

Moore, P. D., Webb, J. A., & Collison, M. E. (1991). *Pollen analysis*. Blackwell scientific publications.

Morris, J. L., Brunelle, A., Munson, A. S., Spencer, J., & Power, M. J. (2013). Holocene vegetation and fire reconstructions from the Aquarius Plateau, Utah, USA. *Quaternary International*, *310*, 111–123. https://doi.org/10.1016/j.quaint.2012.10.055

Oetelaar, G. A., & Beaudoin, A. B. (2005). Darkened Skies and sparkling grasses: the potential impact of the Mazama Ash fall on the northwestern plains. *Plains Anthropologist*, *50*(195), 285-305.

Parish, M.C., Wolf, K.D., Higuera, P.E., Shuman, B.N., 2022. Holocene water levels of Silver Lake, Montana, and the hydroclimate history of the Inland Northwest. Quat. Res. 110, 54–66. https://doi.org/10.1017/qua.2022.17

Power, M. J., Whitlock, C., & Bartlein, P. J. (2011). Postglacial fire, vegetation, and climate history across an elevational gradient in the Northern Rocky Mountains, USA and Canada. *Quaternary Science Reviews*, *30*(19-20), 2520-2533. https://doi.org/10.1016/J.QUASCIREV.2011.04.012

Prentice, I. C. (1980). Multidimensional scaling as a research tool in quaternary palynology: A review of theory and methods. *Review of Palaeobotany and Palynology*, *31*, 71-104. https://doi.org/10.1016/0034-6667(80)90023-8

Reimer, P. J., Baillie, M. G. L., Bard, E., Bayliss, A., Beck, J. W., Blackwell, P. G., Ramsey, C. B., Buck, C. E., Burr, G. S., Edwards, R. L., Friedrich, M., Grootes, P. M., Guilderson, T. P., Hajdas, I., Heaton, T. J., Hogg, A. G., Hughen, K. A., Kaiser, K. F., Kromer, B., … Weyhenmeyer, C. E. (2009). IntCal09 and Marine09 radiocarbon age calibration curves, 0-50,000 years CAL BP. *Radiocarbon*, *51*(4), 1111–1150. https://doi.org/10.1017/S0033822200034202

Reimer, Paula J., Austin, W. E. N., Bard, E., Bayliss, A., Blackwell, P. G., Bronk Ramsey, C., Butzin, M., Cheng, H., Edwards, R. L., Friedrich, M., Grootes, P. M., Guilderson, T. P., Hajdas, I., Heaton, T. J., Hogg, A. G., Hughen, K. A., Kromer, B., Manning, S. W., Muscheler, R., … Talamo, S. (2020). The IntCal20 Northern Hemisphere Radiocarbon Age Calibration Curve (0–55 cal kBP). *Radiocarbon*, *62*(4), 725–757. https://doi.org/10.1017/RDC.2020.41

Rollins, M.G., 2009. LANDFIRE: a nationally consistent vegetation, wildland fire, and fuel assessment. *Int. J. Wildland Fire*,18, 235–249. https://doi.org/10.1071/WF08088

Routson, C. C., Kaufman, D. S., McKay, N. P., Erb, M. P., Arcusa, S. H., Brown, K. J., ...& Cumming, B. F. (2021). A multiproxy database of western North American Holocene paleoclimate records. *Earth System Science Data*, *13*(4), 1613-1632.

Rushton, Z. A., & Walsh, M. K. (2021). Holocene fire history reconstruction of a mid-elevation mixed-conifer forest in the Eastern Cascades, Washington, USA. *The Holocene*, *31*(5), 778-790.

Schnurrenberger, D., Russell, J., & Kelts, K. (2003). Classification of lacustrine sediments based on sedimentary components. *Journal of Paleolimnology*, *29*(2), 141–154. https://doi.org/10.1023/A:1023270324800

Sea, D. S., & Whitlock, C. (1995). Postglacial vegetation and climate of the Cascade Range, central Oregon. *Quaternary Research*, 43(3), 370-381.

Segura, G., Brubaker, L. B., Franklin, J. F., Hickley, T. M., Maguire, D. A., & Wright, G. (1994). Recent mortality and decline in mature Abiesamabilis: the interaction between site factors and tephra deposition from Mount Saint Helens. *Can J For Res*, *24*(6), 1112–1122. https://doi.org/10.1139/X94-148

Segura, G., Hinckley, T. M., & Brubaker, L. B. (1994). Variations in radial growth of declining old-growth stands of *Abies amabilis* after tephra deposition from Mount Saint Helens. *Can J For Res*, *25*(9), 1484-1492. https://doi.org/10.1139/X95-161

Skinner, C.E., Radosevich, S.C. (1991). Holocene volcanic tephra in the Willamette National Forest, western Oregon: distribution, geochemical characterization, and geoarchaeological evaluation. Final Report to the Willamette National Forest, Eugene, Oregon for Contract 53-04R4-0-2780 (217 pp.).

Steinman, B. A., Nelson, D. B., Abbott, M. B., Stansell, N. D., Finkenbinder, M. S., & Finney, B. P. (2019). Lake sediment records of Holocene hydroclimate and impacts of the Mount Mazama eruption, north-central Washington, USA. *Quaternary Science Reviews*, *204*, 17-36.

Telford, R. J., Barker, P., Metcalfe, S., & Newton, A. (2004). Lacustrine responses to tephra deposition: examples from Mexico. *Quaternary Science Reviews*, *23*(23-24), 2337-2353.

Thorarinsson, S. (1979). On the damage caused by volcanic eruptions with special reference to tephra and gases. In *Volcanica activity and human ecology* (pp. 125-59).

Tweiten, M. A., Calcote, R. R., Lynch, E. A., Hotchkiss, S. C., & Schuurman, G. W. (2015). Geophysical features influence the climate change sensitivity of northern Wisconsin pine and oak forests. *Ecological Applications*, *25*(7), 1984–1996. https://doi.org/10.1890/14-2015.1

Walsh, M. K., Marlon, J. R., Goring, S. J., Brown, K. J., & Gavin, D. G. (2015). A Regional Perspective on Holocene Fire–Climate–Human Interactions in the Pacific Northwest of North America. *Annals of the Association of American Geographers*, *105*(6), 1135–1157. https://doi.org/10.1080/00045608.2015.1064457

Walsh, M. K., Whitlock, C., & Bartlein, P. J. (2008). A 14,300-year-long record of fire-vegetation-climate linkages at Battle Ground Lake, southwestern Washington. *Quaternary Research*, *70*(2), 251–264. https://doi.org/10.1016/j.yqres.2008.05.002

Walsh, M. K., Whitlock, C., & Bartlein, P. J. (2010). 1200 years of fire and vegetation history in the Willamette Valley, Oregon and Washington, reconstructed using high-resolution macroscopic charcoal and pollen analysis. *Palaeogeography, Palaeoclimatology, Palaeoecology*, *297*(2), 273–289. https://doi.org/10.1016/j.palaeo.2010.08.007

Webb, T. (1986). Is vegetation in equilibrium with climate? How to interpret late-Quaternary pollen data. *Vegetatio*, *67*(2), 75-91.

Whitlock, C. (1992). Vegetational and climatic history of the Pacific Northwest during the last 20000 years: implications for understanding present-day biodiversity. *Northwest Environmental Journal*, *8*(1), 5–28.

Whitlock, C., & Larsen, C. (2002). Charcoal as a fire proxy. In *Tracking environmental change using lake sediments* (pp. 75-97). Springer, Dordrecht.

Whitlock, C., McWethy, D. B., Tepley, A. J., Veblen, T. T., Holz, A., McGlone, M. S., ... & Wood, S. W. (2015). Past and present vulnerability of closed-canopy temperate forests to altered fire regimes: a comparison of the Pacific Northwest, New Zealand, and Patagonia. *BioScience*, *65*(2), 151-163.

Zobel, D. B., & Antos, J. A. (1997). A Decade of Recovery of Understory Vegetation Buried by Volcanic Tephra From Mount Saint Helens. *Ecological Monographs*, *67*(3), 317. https://doi.org/10.2307/2963458

# III. CHIRONOMID-INFERRED POSTGLACIAL TEMPERATURE RECONSTRUCTION FROM GOLD LAKE, OREGON, USA

**Manuscript in preparation for Journal of Quaternary Science**

Jamila Baig, Dan Gavin, Ian Walker, David Porinchu, and Patrick Bartlein

JB and DGG conceptualized the study, devised the methodology, and conducted the field investigation. JB acquired the funding and curated, analyzed, and visualized the data. IW and DP helped in chironomid identification and classification. JB wrote the original manuscript, and DGG reviewed, edited, and contributed to the final manuscript. IW, DP, and PB contributed to editing and finalizing the manuscript.

## Introduction

Natural archives, including lake sediments, accumulate biological material, such as chironomid head capsules, that are vital to understanding millennial-scale climate change because they serve as a proxy for temperature (Smol et al., 2001a, 2001b; Dolman et al., 2018). Subfossil Chironomidae (midges), particularly the fossilized head capsule, preserve well in quaternary lake sediments and remain identifiable, typically to genus, species-group, or morphotype level (Brooks et al., 2007). When identified in Late Glacial and Holocene lake sediments, because of their taxon-specific temperature thresholds, they have the capacity to reveal changes in summer temperature (Walker & Cwynar, 2006). Thus, they provide an important function as an indicator of past climate independent of other paleoclimate proxies, such as pollen and charcoal (Williams et al., 2002). Even though there is limited data available on lake water temperature, which is used in some cases to calibrate the chironomid transfer function, the reliability of the chironomid proxy has been demonstrated in multiple studies (Brooks & Birks, 2001; Larocque et al., 2001; Gouw-Bouman et al., 2019).

Reconstruction of paleotemperature from fossilized chironomids was motivated by observations that the abundance of cold-adapted chironomid taxa declined after deglaciation, suggesting that lake-water temperature increased (Walker & Mathewes, 1989). This well-dated

established proxy-based inference model has been further corroborated by a new study that calibrated chironomid community shifts shaped by the rate and magnitude of climate change, including temperature (Mayfield et al., 2021). Paleotemperature can be reconstructed using chironomid taxa because they have taxa-specific temperature thresholds to complete different life cycle stages, including larval, pupal, and adult stages that affect their abundance and distribution (Walker & Cwynar, 2006). Water temperature has a direct and immediate effect on chironomid larval stages compared to air temperature, which can reduce reproductive success by affecting the emergence of adults (Armitage et al., 2012).

Livingstone and Lotter (1998) found a strong association between water and air temperatures, although air temperature is a more relevant variable than water temperature since it is simpler to comprehend what it signifies in climatic terms. For paleoclimate studies, water temperature affects the larval stages of chironomids, but air temperature is important in affecting the dispersion of the winged adult stage and the reproduction of chironomids (Isabelle Larocque & Hall, 2003). Mean July air temperature provides more reliable temperature data for each lake compared to spot measurements of surface-water temperature used in prior models (Olander et al., 1997; Walker et al., 1991). Chironomid training data sets, developed from surface sediments of a network of sites, have confirmed that the primary control of the distribution of Chironomidae larvae is summer air and lake water temperature (Brooks & Birks, 2001; Porinchu & MacDonald, 2003; Walker et al., 1997). Therefore, palaeoecological analysis of fossil chironomid assemblages can be used to reconstruct past changes in the chironomid fauna of lakes and, indirectly, to provide information about past temperature changes (Cwynar & Levesque, 1995; Porinchu et al., 2003b).

Ecosystems at high elevation areas are very sensitive to climate change (Battarbee et al., 2002). Increasing temperature, for example, may extirpate temperature-sensitive species from lakes (Schindler et al., 1990). Using sub-fossil midges from lake sediment to understand the temporal and spatial patterns by applying air and water inference models (Porinchu et al., 2007, 2010) has improved our understanding of regional climatic changes during the Pleistocene and Holocene in the Western USA (Porinchu et al., 2003; Potito et al., 2006; Reinemann et al., 2009; Reinemann et al., 2014). These same high-elevation ecosystems in the western USA are

experiencing increased wildfire due to earlier snow melt and a longer fire season (Alizadeh et al., 2021); thus, understanding Holocene climatic variability is important to place modern dynamics in context.

In this paper, I document changes in chironomid assemblages that are interpreted as resulting from changes in climate to reconstruct the paleotemperature for the last 14.5 ka at a high-elevation lake in the central Oregon Cascade Range. This study is the first attempt to develop a midge-based quantitative temperature reconstruction in Oregon, USA. I use a robust midge-based training data set developed by (Haskett and Porinchu, 2014) from the inter-mountain west (hereafter referred to as the IMW training set). I developed an inference model for mean July air temperature (MJAT) using improved elevation-adjusted temperature estimates. I compare the Gold Lake MJAT reconstruction with previous paleoclimate work in the region to assess controls of high-elevation climate during the late Quaternary.

## Materials and Methods

### Study Site Description

Gold Lake is located at 1465 m a.s.l in the Willamette National Forest in the Cascade Range (43° 37' 57"N, 122° 02' 36" W). It is a 38.9-hectare lake with a 48.4 $km^2$ watershed (Fig. 3.1). Water enters Gold Lake from Salt Creek after passing through Gold Lake Bog and from lake-shore springs. Gold Lake is classified as a mesotrophic lake. It is more productive than other lakes in the Cascade Range due to particulate and organic matter that enters the lake via Gold Lake Bog (Fig. 3.1; Johnson et al., 1985). In the Cascade Range, temperature and precipitation vary with elevation, leading to unique plant zonation (Franklin & Dyrness, 1988). Mean annual precipitation in the Gold Lake region is 1600 mm, while mean January and July temperature is -2.5°C and 12.5 °C, respectively, from 1991 to 2020 (PRISM Climate Group, 2020). In April, snowpack peaks are 76 cm at Gold Lake, with the snowpack completely melting by the end of May (USDA, Natural Resource Conservation Services, 2022).

A previous study of postglacial vegetation and fire (Baig & Gavin, 2023) from Gold Lake found that pollen spectra change little from the Late Glacial to the Younger Dryas. The early Holocene is marked by a sudden increase in Pseudotsuga, indicating warmer conditions, while the late Holocene is marked by an increase in *Tsuga heterophylla* (Western hemlock) and *Tsuga*

*mertensiana* (Mountain hemlock), indicating the onset of moist conditions in the region during late Holocene (Baig & Gavin, 2023).

### Field Collection

Sediment coring was described in Baig & Gavin (2023). In 2018, two parallel cores were obtained using a square-rod piston corer. Each core drive (1 meter) was measured and briefly described after being extruded from the deepest point of Gold Lake. Each core was covered in plastic wrap within PVC pipe halves and was labeled. A surface core was collected in a clear polycarbonate tube fitted with a piston. The surface core was sectioned at 1cm intervals. All sediment cores were transferred to the laboratory at the University of Oregon and kept at 4°C in the refrigerator until further processing (baig & Gavin, 2023).

## Laboratory Analysis

### Core Processing and Loss-on-ignition

Baig and Gavin (2023) described Gold Lake core processing in detail. All core drives were split longitudinally into the archive and working core halves. Uninterpreted stratigraphy was developed using tie points between parallel cores except for the lower 5-meter core drives for which a parallel core did not exist. Magnetic susceptibility using a Sapphire cup meter was used to locate tie points between the uppermost piston core drive and surface core from 0 to 50 cm at a 1 cm resolution. To determine the organic matter, one hundred seventy-eight samples were analyzed at 5 cm and 10 cm intervals from pre- and post-Mazama sections, respectively. One $cm^3$ sub-samples were dried at 80 °C and combusted at 550 °C for two hours. Lake sediment was classified with the help of visual observations and organic matter analysis based on Schnurrenberger et al. (2003).

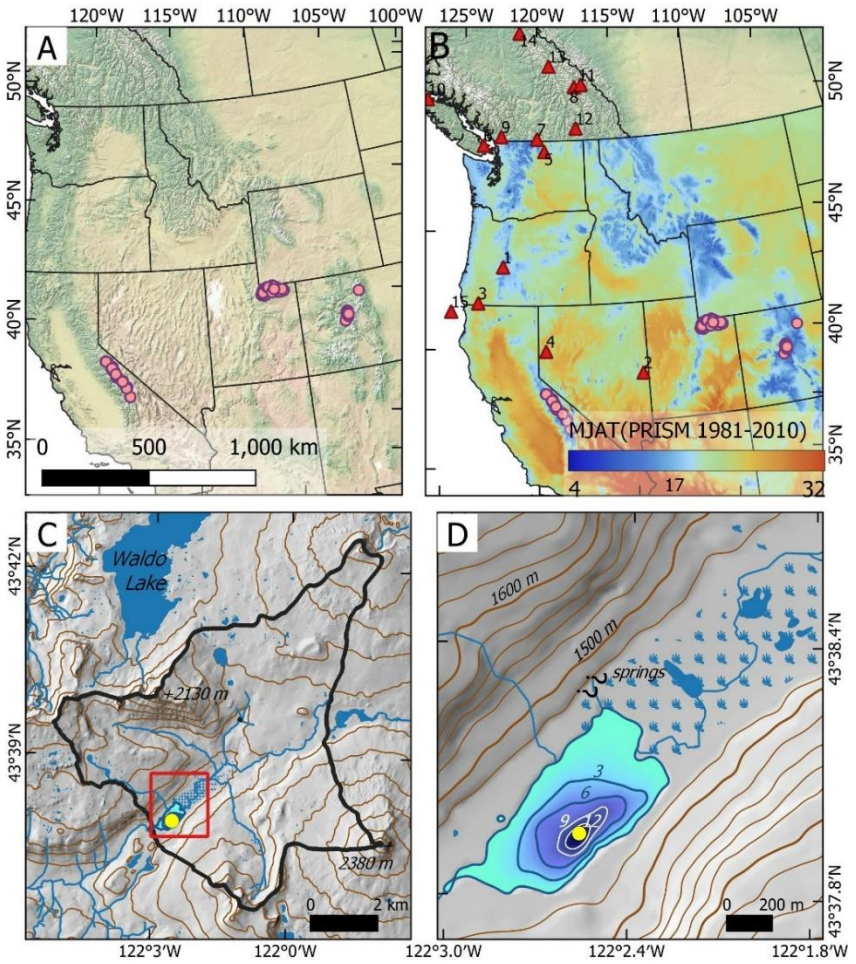


**Figure 3. 1 (A) Map showing the location of the IMW calibration data set of chironomids in California, Utah, and Colorado and the study site (Gold Lake) in Oregon**. (B) Distribution of IMW training set lakes, study sites, Oregon caves, and other records discussed in the paper (MJAT-1981-2010). a: Gold Lake,1: Gordon Lake (Grigg and Whitlock, 1998), 2: Stella Lake (Reinemann et al., 2009), 3: Oregon Caves Caves (Ersek et al., 2012) ,4: Pyramid Lake (Benson et al., 2002), 5: Castor Lake (Nelson et al., 2011), 6: Stowell Lake (Lemmen & Lacourse, 2018), 7: North Crater Lake (Palmer et al., 2002), 8: Marrion Lake (Walker & Cwynar, 2006), 9: Mike Lake (Walker & Mathewes, 1989), 10: Misty Lake (Walker & Mathewes, 1989), 11: Cabin Lake (Smith et al., 1998), 12: Windy Lake (Chase et al., 2008), 13: Thunder Lake (Chase et al., 2008), 14: Redmountain Lake (Chase et al., 2008), 15: ODP-1091 (Barron et al., 2003). (C) Shaded relief map with a 100-m contour interval, showing the 48.4 $km^2$ Gold Lake watershed (black line) and 100-m contour interval. The red box indicates the extent of map D. (D) Bathymetric map of Gold Lake (3 m contour interval; Johnson et al., 1985), core location (yellow circle), and the location of the Gold Lake Bog wetland studied by Sea and Whitlock (1995). Springs on the north side of the lake are indicated.

**Age depth model and Radiocarbon dating**

The preparation of samples for radiocarbon dating was described in Baig & Gavin (2023). Thirteen samples for radiocarbon dating consisting of charcoal, identifiable plant material, pollen isolates, and bulk sediment were analyzed (Table 2.1: Chapter II). Three tephra layers were identified, including the Mazama tephra (78 cm thick) and two thinner tephra layers (1cm thick each), which were identified using an electron microprobe at the University of Oregon and Washington State University.

Following the Mazama tephra, a portion of the core was coarsely laminated. These laminations were counted by visual inspection by JB and DGG. Ages at 10-cm intervals were estimated and were added to the age-depth model as a calendar year using the Mazama eruption (7633±25 cal yr BP; Egan et al., 2015) as a baseline. To accommodate the increasing uncertainty along the varve sequence, the 25-year error was incremented by two years per 10 cm (ca. 5% error). Varves were counted from 732 to 504cm, but due to the difference in counting between two researchers from 570 to 504 cm, these varves were not used during age-depth model development. Laminations counted post-Llao eruption are also part of the age-depth model. To confirm the accuracy of the counted laminations, three radiocarbon dates were obtained between 732 to 570 cm (Baig & Gavin, 2023). An age model was developed with 11 radiocarbon ages, 17 varve-age estimates (at 10 cm intervals), and the age of the Mazama tephra. The age-depth model was built using Bacon for R (Blaauw & Christen, 2011), a Bayesian statistical software. Three tephra layers were modeled as intervals of instantaneous deposition. The program applied the INTCAL20 calibration curve (Reimer et al., 2020).

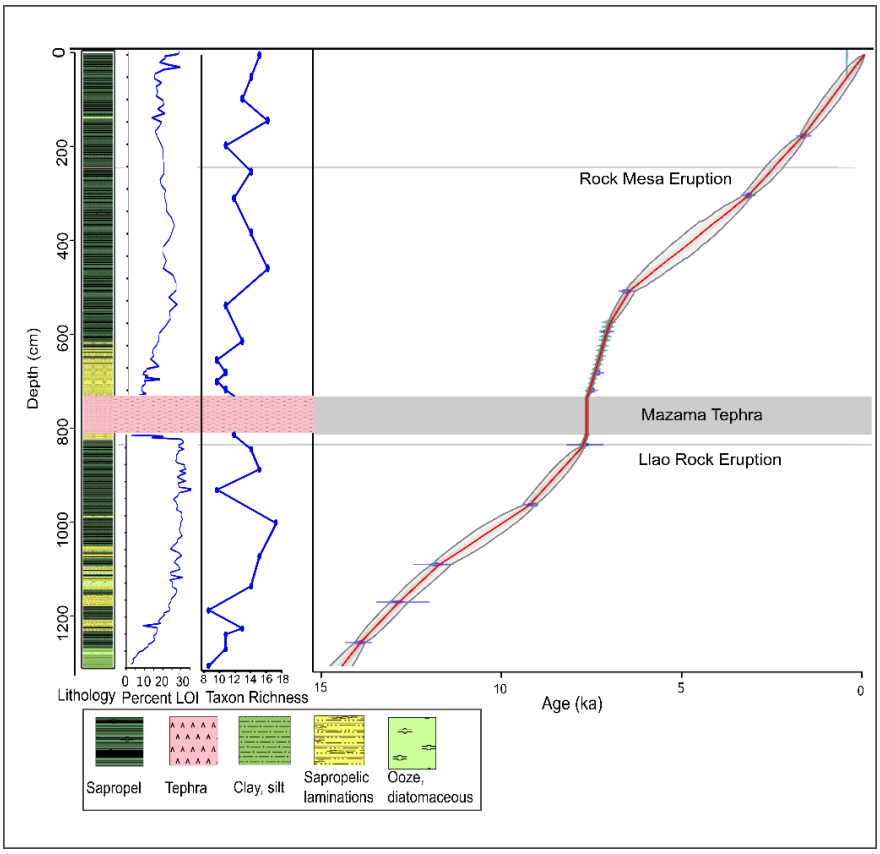


**Figure 3. 2 Bacon age-depth model for Gold Lake with lithology, LOI, and taxon richness. Horizontal bar lines represent three tephra layers found in the lake**. Age estimates for a post-Mazama (732-570 cm) and post-Llao Rock (831-811 cm) tephras are based on radiocarbon dates and manually counted varves.

## Chironomid analysis

Chironomid head capsules were processed by following the standard protocols outlined by (Walker, 2001). Samples ranging in volume between 1 and 1.25 ml were taken at 50-cm intervals. Samples were treated with 10% KOH at 30°C for 30 minutes, washed with distilled water through a 90 μm mesh, backwashed into vials, and stored at low temperature. Using a Bogorov counting tray, samples were examined under a stereomicroscope at 40-50x magnification. Chironomid head capsules were handpicked with the help of fine tweezers, placed on a cover slip in a drop of distilled water, and upon drying, were mounted on a glass slide using Entellan®. A minimum of 50 chironomid head capsules (Heiri & Lotter, 2001; Quinlan & Smol, 2001) were picked and identified from each sample, with the exception of the sample directly above the Mazama tephra, where only 34 head capsules could be found in 1.25 ml of sediment.

Broken head capsules having more than half of a mentum were counted as one head capsule. Each chironomid head capsule was photographed multiple times using a camera mounted to a stereoscope. Identifications were made in consultation with Prof. Walker (University of British Columbia), Prof. David Porinchu (University of Georgia), and available taxonomic keys (Brooks et al., 2007; Walker, 2007). The taxonomy was harmonized with that used in the IMW training data set. Specifically, Tanytarsus, which were not identified to species level in the IMW, were grouped together as Tanytarsus (undifferentiated).

**Numerical analysis, plotting, and temperature reconstruction**

The relative abundance of all chironomid taxa was plotted in a percentage diagram using TILIA (https://www.neotomadb.org), with taxa arranged according to their temperature optima (decreasing optima from left to right in Fig. 3.4), determined from the IMW chironomid-based inference model (Haskett & Porinchu, 2014). Zones were created using major climatic and stratigraphic events: Late-Glacial (14.4 ka-11.6 ka), early Holocene-pre Mazama (11.6-7.6 ka), middle Holocene-post Mazama (7.6-5 ka), and Middle/late Holocene (5.0 ka-present) (Cohen et al., 2013).

Correspondence analysis (CA) was used to plot subfossil chironomid assemblage from Gold Lake passively within an ordination of the IMW training set lakes to determine the representation of the Gold Lake sub-fossil assemblages in the IMW training set (Fig. 3.3). To maximize the 'signal to noise' ratio (Prentice, 1980), relative abundance data were square-root transformed before ordination analyses. CA was performed using the vegan package in R (Oksanen, 2008), while program C2 (Juggins, 2003) was used to develop the WA-PLS inference models and to estimate sample-specific errors. Prior to building the WA-PLS model, we updated estimates of MJAT at each of the 91 lakes in the IMW data set. The previous inference model of this data set (Haskett & Porinchu, 2014) was based upon MJAT estimates obtained from the PRISM Climate Group (PRISM Climate Group, 2020), which is at a 2.5 arc minute (ca. 4 km) resolution. In the mountainous terrain surrounding the IMW sites, temperatures vary greatly with elevation, such that the grid-cell temperature estimate may differ greatly from that at any specific elevation. Therefore, we used lapse-rate adjusted estimates of MJAT using ClimateWNA software (Wang et al., 2016).

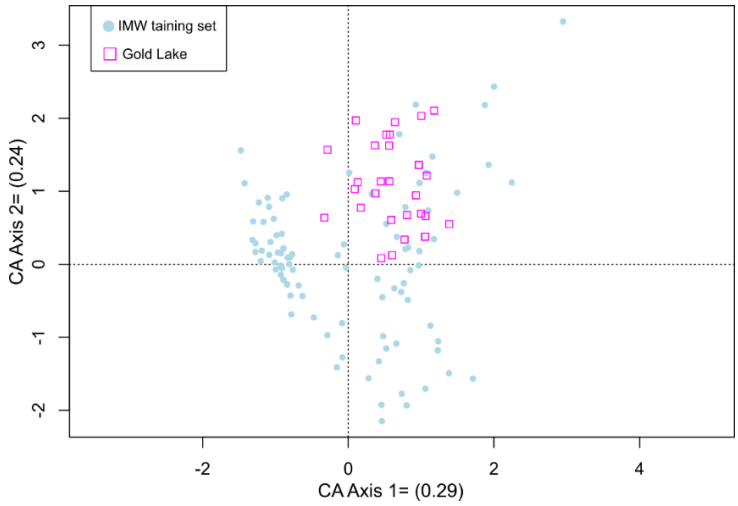


**Figure 3. 3 Correspondence analysis (CA)** passively plotting Gold Lake midge assemblages with chironomid assemblages of IMW (CA Axis 1) (λ=0.29) and CA Axis 2(λ=0.24)

This software uses the same PRISM climate grids with the coarse-resolution elevation data underlying the PRISM data to develop a local temperature lapse rate and, thus, elevation-specific estimates of MJAT. Prior to running ClimateWNA, we verified the published name, size, elevation, and coordinates of the IMW lakes with maps from the USGS and Google Earth. We obtained lapse-rate corrected estimates of MJAT (1981-2010). Locations could not be verified for four lakes in the IMW database, and thus, the originally published temperatures were used.

To assess the reliability of the chironomid-inferred MJAT reconstruction at Gold Lake, several criteria were considered. First, according to (Heiri & Lotter, 2001), a minimum of 50 head capsules should be present in each fossil sample, and having >95% of sub-fossil assemblages present in the calibration dataset makes the quantitative environmental reconstruction highly reliable. Second, the proportion of rare taxa present in the down-core fossil samples was also used to evaluate the reliability of inference model estimates (Birks, 1998). A taxon is classified as rare if its Hill's N2 or the effective number of occurrences $\leq$5 (Hill, 1973), so reliable estimates of temperature optima can be obtained with taxa having Hills N2 values >5 in the training set (Brooks & Birks, 2001). Third, we used the test of Telford and Birks (2011) to determine if the training data set significantly explains the reconstruction. A reconstruction is

statistically significant if it explains greater than 95% of the variance in the fossil data relative to that explained by reconstructions based on 999 transfer functions derived from random environmental data.

## Results

### Chronology and sediment stratigraphy

Bayesian modeling in Bacon was used to develop an age-depth model (Blaauw & Christen, 2011), where two radiocarbon ages were removed from the age-depth model because of a large age error, and an additional date was not incorporated in the age model because it was out of stratigraphic order with the Mazama eruption age. Eleven radiocarbon dates that occurred in stratigraphic order (Fig. 3.2; Table 2.1: Chapter II) are part of the age-depth model. A constant sedimentation rate was recorded from the base up to 960 cm (0.071-0.11 cm/yr). There is a transition from silt and clay to sapropelic sediment at 50 cm above the core base ~ ca. 13.9 ka. Manually counted laminations were verified by three radiocarbon dates between 732-570 cm, confirming them as annual layers in the lake sediments (612 varves-732-570 cm-post-Mazama; 65 varves-831-810 cm-post-Llao to pre-Mazama). The sedimentation rate is 6-7 times higher than the remainder of the core in the post-Mazama section up to 570 cm, after which it decreases and remains low through the late Holocene (0.06-0.10 cm/yr) (Baig & Gavin, 2023).
With the exception of the three tephra layers and a 50-cm segment at the bottom of the core (1302-1252 cm), the core is primarily composed of medium- to dark-brown biogenic sapropel (Figure S1; Table S2). The core features sapropelic (biogenic) laminations (732-504 cm after the Mazama tephra and 20 cm from the Llao Rock tephra to the Mazama tephra), which are rhythmically banded in light and dark brown (830-810 cm). Silt and clay made up the base sediment, which has a relatively low loss-on-ignition (LOI) of 2-10%. The LOI values during the Late Glacial were between 2- 29%; during the early Holocene, 9-32%; and during the Late Holocene, 15-34%. Around three of the detected tephra layers, LOI remained around 5%, while laminated sections formed after the Mazama eruption have lower LOI (10–15%) (Baig & Gavin, 2023).

## Gold Lake chironomid diversity and community change

Chironomid head capsules were very well preserved in the Gold Lake sediment. Thirty-one midge taxa were identified in 28 samples spanning the last 14,400 yr. Taxon richness varies throughout the core, ranging between 8 and 16 extant taxa, with the highest richness occurring at ca.10 ka. *Chironomus* (14%), *Corynocera near ambigua* (19%), *Corynocera oliveri* type (7%), and *Glyptotendipes* (5%) were the most abundant taxa found (Fig. 3.4).

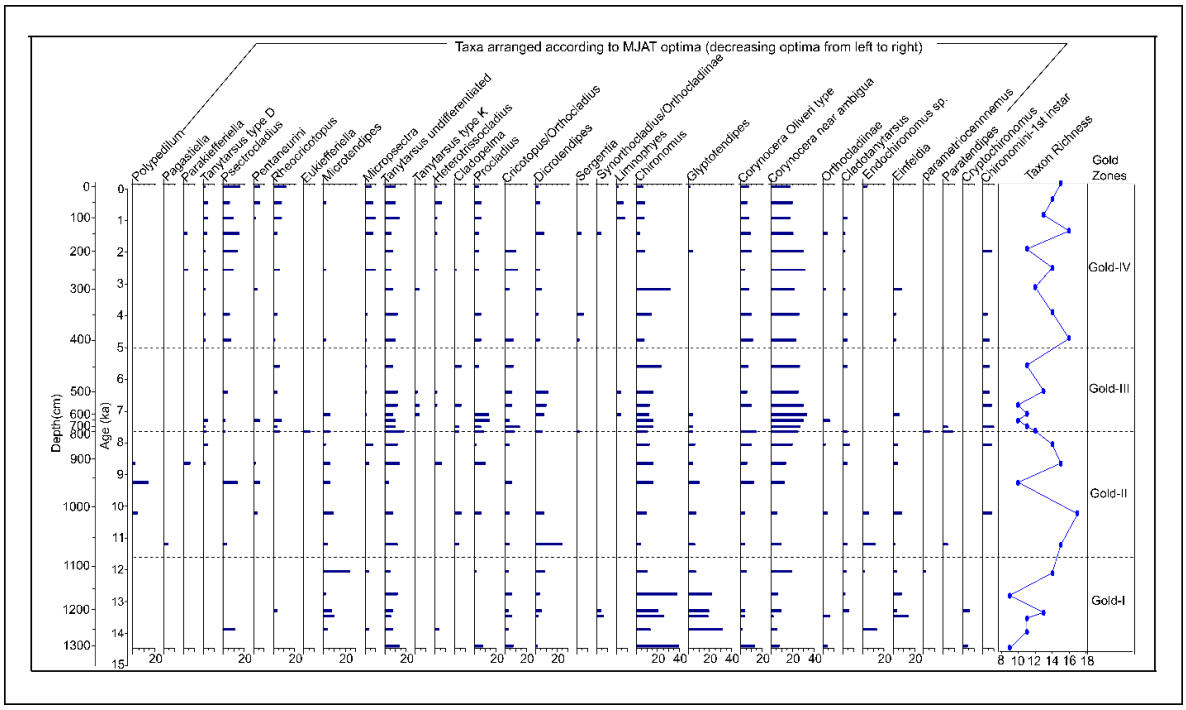


**Figure 3. 4 Relative abundance of chironomid taxa and taxon richness at Gold Lake** with zonation based on major climatic events. Taxa are arranged according to their MJAT optima inferred from the chironomid inference model with decreasing optima from left to right.

### Gold-I: Late Glacial period (1302-1110 cm; ca. 14.4-11.6 ka, 6 samples)

The midge community present in the postglacial period is dominated by *Chironomus* (11-40%), *Glyptotendipes (*0-32%), *Microtendipes* (0-25%), *Corynocera* near *ambigua* (2-19%), *Einfeldia* (14%) and *Tanytarsini* (5-14%) followed by *Corynocera oliveri* type (0-14%), *Dicrotendipes* (0-9%), *Cricotopus/Orthocladius* (4-8%). *Cryptochironomus* (4-7%), *Synorthocladius* (4-6%), and *Procladius* (2-8%) appeared only in two samples, while

*Psectrocladius* (11%) *and Heterotrissocladius* (4%) appeared only in one sample respectively. Taxon richness varies between 8 and 14, with minimum richness at the bottom and highest at the top of the zone. *Chironomus* reaches its highest value in the core, ~ 39%, at the bottom of the core, which eventually decreases to 10% at the zone top, while *Microtendipes* (24%) reach their highest core maximum at the zone top. Other taxa that also reach the highest percentages in the core are *Cladotanytarsus* (6%), *Einfeldia* (14%), *Endochironomus* (14%), *Glyptotendipes* (32%), and *Synorthocladius* (6%).

**Gold II-Early Holocene-Pre-Mazama (1060-810cm; ca. 11.6-7.6 ka, 6 samples)**

This zone is characterized by a diverse midge assemblage with taxon richness values between 10 and 17. The relative abundance of *Corynocera* near *ambigua* remains high, increasing up to 24% (6-24%) at the top of this zone, followed by *Chironomus* (4-16%), which decreases to ~40% at the transition to this zone. Other taxa dominating this zone are *Tanytarsus* undifferentiated (4-14%) *Corynocera oliveri* type (4-14%). *Glyptotendipes* (4-10%) and *Microtendipes* (2-10%) decrease in relative abundance compared to the previous zone. Other taxa that are present in minor percentages are *Endochironomus*, *Cricotopus/Orthocladius Cladotanytarsus*, *Heterotrissocladius*, *Microspectra*, *Procladius*, and *Psectrocladius*. *Cladopelma, Polypedilum, Pagastiella*, *Paratendipes*, *Pentaneurini, Tanytarsus* type-*D, Chironomini*-1st instar, *Parakiefferiella*, and *Eukiefferiella* appear for the first time. Some of these taxa reach their highest core maximum in this zone, e.g., *Dicrotendipes* increase up to 25%, *Cladopelma* (6%), and *Parakiefferiella* (6%) while *Pagastiella* (4%), and *Polypedilum* (14%) appear only in this zone (Fig. 3.4).

**Gold III-Early Holocene-Post-Mazama (732-450 cm; ca. 7.6 to 5 ka, 7 samples)**

Taxon richness in this zone decreases with values ranging between 10 and 13. This zone is still dominated by *Corynocera* near *ambigua*, which reaches its core maximum of 33% at ~7.1 ka, followed by *Chironomus,* which increases up to 23% at ~5.5 ka after being low in abundance in the pre-Mazama zone. Other major taxa include *Procladius* and Tanytarsini (indeterminate), followed by *Dicrotendipes* (0-12%), *Microtendipes* (0-6%), *Psectrocladius* (0-4%), and

*Rheocricotopus* (0-6%). This zone has a sample following the Mazama eruption, where 1.25 ml of sediment yielded only 37 head capsules.

Some of the other taxa that reach a core maximum include *Corynocera oliveri*-type (15%), Cricotopus /Orthocladius (14%), Chironomi-1$^{st}$ instar (10%), and *Procladius* (14%). Other taxa like *Parametriocennnemus* (6%), *Eukiefferiella* (6%), and *Paratendipes* (9%) reached a core maximum and did not appear in the remainder of the core. A number of other taxa did not appear after the Mazama eruption for ~300 cal yr, including *Dicrotendipes*, *Einfeldia*, *Heterotrissocladius*, and *Pentaneurini*, while *Cladotanytarsus* re-appeared at ~5.5 ka. Some taxa appear for the first time, including *Limnophyes*, *Sergentia*, and *Tanytarsus* type-K (Fig. 3.4).

**Gold IV-Late Holocene (450-0 cm; ca. 5 ka to present, 9 samples)**

The midge community in this zone is dominated by *Corynocera* near *ambigua* (18-31%), *Corynocera oliveri* type (8-12%), followed by *Chironomus*, which fluctuates between 0 and 8% and reaches 31% at ~3.1 ka. The relative abundance of *Tanytarsus* type *D* (2-4%) and Tanytarsus indeterminate (6-14%) increase during this interval.

Other taxa dominating the late Holocene include *Psectrocladius* (0-16%), *Rheocricotopus* (0-12%), *Sergentia* (0-6%), *Microspectra* (0-10%), and *Pentaneurini* (0-6%) which reaches a core maximum in this zone. *Limnophyes* appear at ~900 cal yr bp with a maximum abundance of 8%. Taxa such as *Dicrotendipes* (2-8%) remain low in this zone, while *Cricotopus Orthocladius* (4-12%) are not present after ~1.9 ka. *Einfeldia* was absent in the remainder of the core after ~3.9 ka; *Heterotrissocladius* reappeared at ~2.5 ka with a higher relative abundance than the previous zone. Some taxa that re-appeared in one or two samples with a low abundance include *Cladopelma* (2% at ~2.5 ka), *Glyptotendipes* (2-4%; ~2.5 ka and surface sample), *Parakiefferiella* (4% at ~2.4 and 1.4 ka), *Synorthocladius* (4% at ~1.4 ka), and *Tanytarsus* type-K (4% at ~3.1 ka). Taxon richness increased compared to the previous zone and varied between 12 and 16. The surface sample is dominated by *Corynocera* near *ambigua*, *Corynocera oliveri* type, *Psectrocladius*, and *Rheocricotopus* (Fig. 3.4).

**Inference model using lapse-rate adjusted MJAT**

The (lapse-rate adjusted) MJAT estimates for 91 lakes in the IMW data set varied substantially from the prior grid-cell estimates (Haskett & Porinchu, 2014). The difference in

MJAT was large (>1.0°C) for 18% of the lakes and >0.25°C for 70% of the lakes. When comparing the two estimates, there was a mean and maximum absolute deviation of 0.8°C and 5.7°C, respectively, and a root-mean-square error of 1.3°C.

The adjusted MJAT estimates for the IMW data set improved the fit of the inference models. Using a two-component weighted averaging-partial least squares (WA-PLS), including all taxa, resulted in a $r^2_{jack}$ of 0.71, root mean square error of prediction (RMSEP) of 1.09°C, and maximum bias of 0.85°C. In contrast, the prior model resulted in a $r^2_{jack}$ (a coefficient of determination) of 0.61, RMSEP of 0.97°C, and maximum bias of 2.22°C (Haskett & Porinchu, 2014). Excluding rare taxa (i.e., taxa present in <5% of training set lakes) during the development of the inference model resulted in $r^2_{jack}$=0.67, RMSEP=1.09°C, and a maximum bias of 0.89°C. We chose to use the inference model with all taxa included to reconstruct Gold Lake temperature due to its higher $r^2_{jack}$ and low maximum bias (Fig. 3.5).

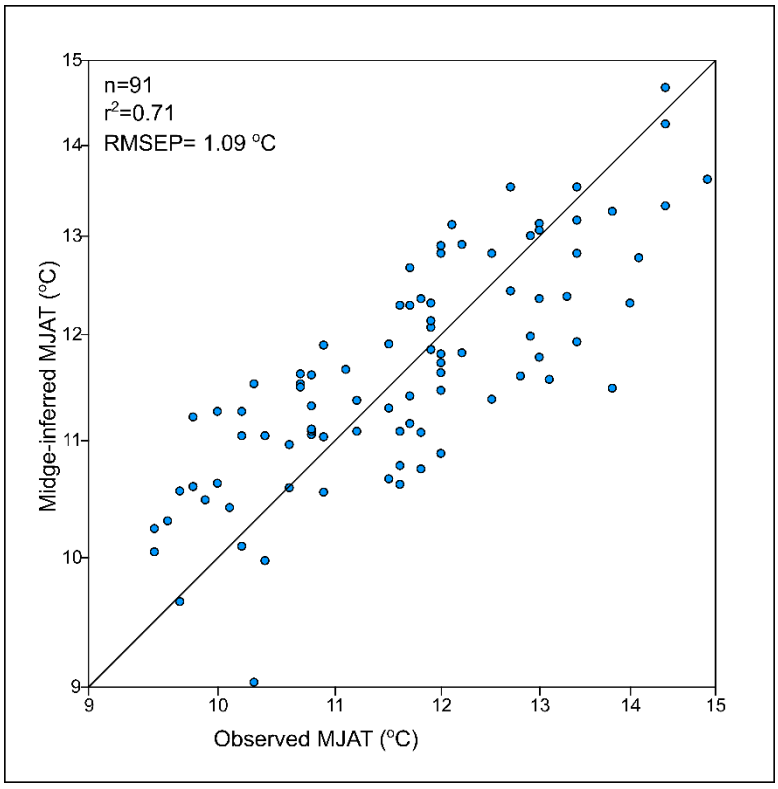


**Figure 3. 5 Relationship between mean July air temperature derived using PRISM for the IMW calibration dataset** and the midge-inferred mean July air temperature (The solid line represents a 1:1 relationship)

**Gold Lake midge-based MJAT**

The Gold Lake chironomid assemblages and the IMW training set assemblages were similar. A total of 32 chironomid taxa were identified in Gold Lake. Only four taxa (3% of identified head capsules) were not present in the IMW training set lakes, including *Chironomini*-1$^{st}$instar (2.2%), *Cryptochironomus* (0.35%), *Paratendipes* (0.5%), and *Parametriocennnemus* (0.21%). In addition, the midge assemblages of Gold Lake, plotted passively against the IMW training set using CA, show that the Gold Lake midges are located within the ordination space captured by the IMW training set. The sample-specific error estimates associated with Gold Lake midge-based MJAT estimates vary between 1.0°C and 2.0°C. The taxa present in Gold Lake are well represented in the IMW calibration set with Hills N2 diversity index (Hill, 1973) ranging between 9 and 57 for 22 taxa. Although six taxa have Hill's N2 value below 4, the proportion of rare taxa is low as they are present in < 7 samples and do not dominate the assemblages except *Glyptotendipes* and *Einfeldia*. The MJAT midge-based reconstruction also passed the significance test of (Telford & Birks, 2011) with a value of p=0.025 (Fig. 3.6). Overall, the Gold Lake midge-based MJAT reconstruction can be considered reliable based on the above tests (Birks, 1998).

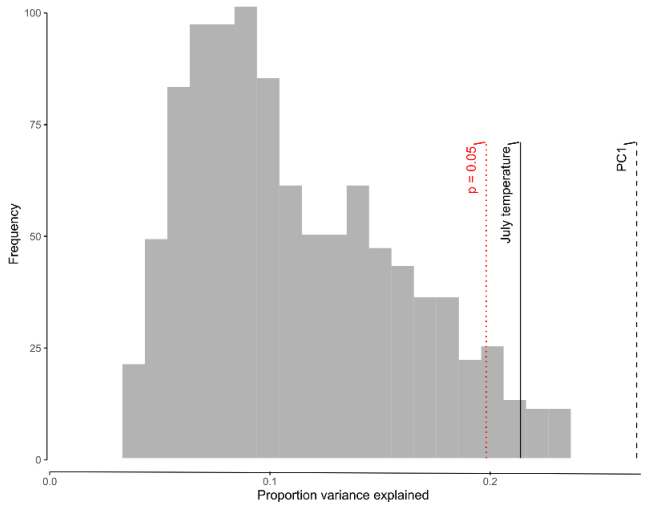


**Figure 3. 6 The results of Telford and Birks (2011) significance test.** The proportion of variance in the Gold Lake fossil site is represented by a histogram that is explained by the 999-transfer function trained on random data. The July temperature line shows the proportion of variance in the fossil data that is explained by each reconstruction (n= 999, p=0.021), and the black dash line shows the proportion explained by the first axis of a PCA.

### Temperature reconstruction

The average midge-inferred MJAT for Gold Lake for the last 14.5 ka is 11.3 °C (Fig. 3.7E). During the Late Glacial (14.4 ka-11.6 ka), the MJAT remained low, ranging between 9.3 and 10.8°C), or 0.5 to 2.0 °C below the long-term average. The lowest temperature (9.0 °C) occurred within the Younger Dryas at ca. 12.7 ka.

MJAT increased by 1.0 °C at 9.2 ka during the early Holocene but remained below the long-term average. The Holocene-pre Mazama period (11.6 ka-7.6 ka; 10.9- 12.0°C) is marked by a sudden increase in temperature of 0.8°C (10.2-11.0°C) that reaches 12.0°C at 9.2 ka and remains high until 8 ka when it decreased to 10.9°C immediately before the Mazama eruption. The transition into the middle Holocene post-Mazama (7.6-5 ka;10.8-12.6°C) is marked by a sudden increase in midge-inferred MJAT (10.9 to 12.0°C) MJAT remained high until 7.3 ka after which time it drops to 10.7°C at 7.1 ka and then increases to 11.1 °C in the adjacent sample at ca. 6.8 ka. MJAT decreases towards the end of the middle Holocene and reaches 10.8°C at ca. 5.6 ka. During the late Holocene, midge-inferred MJAT increases to the highest recorded temperature of ~13.1°C at 2.5 ka and then decreases to 11.6°C at 1.9 ka. MJAT remains high during the last ~2 ka, fluctuating between 12.2 and 12.6°C.

## Discussion

### Gold-I: Late Glacial period (1302-1110 cm; ca. 14.4-11.6 ka, 6 samples)

The Gold Lake midge stratigraphy reveals large changes in the community structure and inferred temperature since deglaciation. The Late Glacial period, especially ca. 14.4 to 13 ka, is dominated by *Chironomus*, *Dicrotendipes*, *Glyptotendipes*, *Einfeldia*, and *Corynocera* near *ambigua*, taxa that are found today in eutrophic to mesotrophic lakes (Brodersen et al., 2001; Brooks et al., 2007). These taxa decreased during the Younger Dryas period and remained low during the transition into the early Holocene with the exception of *Microtendipes*, which reached a core maximum at ca. 12 ka, and *Corynocera* near *ambigua* which increased to 19%. *Corynocera oliveri*-type, commonly associated with cold water (Brooks et al., 2007), was present consistently, with its maximum abundance occurring in the bottom sample of the Late-Glacial period.

During the Late Glacial period, the midge community is marked by early colonizing taxa typical of hypoxic, low pH, and cold water. *Chironomus*, considered an early colonizer of lakes (Brooks et al., 1997) and commonly confined to the deeper part of lakes in hypoxic to anoxic conditions (Brooks et al., 2007), was present in maximum abundance at the bottom sample of the Late Glacial period. *Glyptotendipes* appear at ca. 13.8 ka, reaching a maximum abundance (32%) before decreasing to almost 20% for the rest of this zone. The appearance of *Cladotanytarsus* for the first time with its maximum abundance (6%) at 13.2 ka may reflect decreasing pH (Henrikson et al., 1982). A higher abundance of *Glyptotendipes* during this time further supports the inference of low pH as it is an acidophilic taxon (Brodin, 1986). The occurrence of *Dicrotendipes*, *Cladotanytarsus*, and *Einfeldia* at ~ 13.4 ka suggests the potential establishment of aquatic macrophytes in the littoral zone (Brodersen et al., 2001; Langdon et al., 2006). *Cricotopus /Orthocladius* was consistently present during the Late Glacial period and is commonly associated with standing and flowing waters (Brooks et al., 2007) and aquatic vegetation (Brodin, 1986).

The Gold Lake midge-inferred temperature matches well with the northern hemisphere pattern of sudden warming at ca. 14.7 ka, followed by a cold reversal (Younger Dryas) at ca. 12.7 ka, which persists until the start of the Holocene (Lotter et al., 1992). The high percentages of *Chironomus* and *Glyptotendipes* contributed to the elevated midge-inferred MJAT of 10.9-9.8°C between 14.3 to 13.2 ka. The decline in MJAT to 9.4°C during the Younger Dryas period at ca. 12 ka was driven by the increase in *Einfeldia, Synorthocladius,* and *Corynocera* near *ambigua* and the presence of the cold-adapted taxa *Corynocera oliveri* type. The Gold Lake record suggests that the Late Glacial period (10.6°C), ca.14.3 ka, was characterized by a MJAT that was 1.6 °C lower than the inferred modern temperature. This pattern agrees with the inferred temperature at Stowell Lake (Lemmen & Lacourse, 2018) and Windy Lake, British Columbia (Chase et al., 2008).

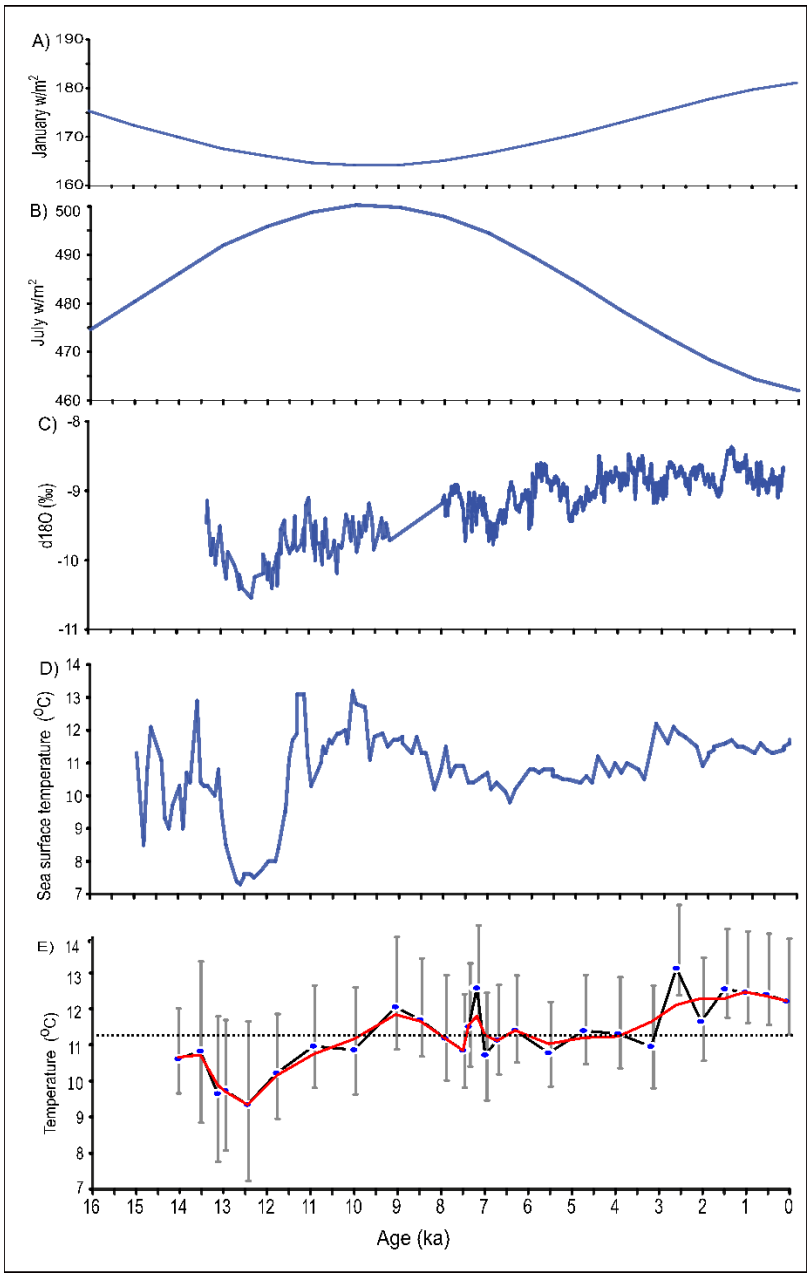


**Figure 3. 7** January (A) and July (B) insolation at 40°N. C) the δ18O at Oregon Caves (Ersek et al., 2012). D) Northeast Pacific sea surface temperature (SST) inferred from alkenone records from cores near northern California (Barron et al., 2003) E) Chironomid-based mean July air temperature (MJAT: Black line) reconstruction for Gold Lake spanning with a LOWESS smoother (span=0.18: red line), Horizontal dashed black line represents the mean reconstructed MJAT.

During the Younger Dryas, Gold Lake MJAT reaches its minimum at 9.4 °C, which is 2.8 °C lower than modern, and it coincides with many other proxy-based temperatures showing a decline in temperature during Younger Dryas (MacDonald et al., 2008; Barron et al., 2003; Lacourse, 2005; Mathewes, 1993). Gavin et al. (2013) also suggested, based on the midge inferred paleotemperature from southern British Columbia, that MJAT was 2.5 °C lower than present during the Younger Dryas.

**Gold II-Early Holocene-Pre-Mazama (1060-810cm; ca. 11.6-7.6 ka, 6 samples)**

During the early Holocene, there was an increase in the abundance and diversity of warm-adapted taxa at Gold Lake. *Dicrotendipes* increased to 25%, and *Polypedilum* appeared for the first time, reaching its maximum abundance (14%). These taxa drive an increased in MJAT to 11°C from 10.2°C, reflecting an elevated temperature (Brodersen et al., 2001). Increased abundance of *Dicrotendipes* in the Intermountain West region has been associated with increased temperature during the late 20$^{th}$ century (Porinchu et al., 2007; Reinemann et al., 2014) and has been identified as a thermophilic taxon in the IMW dataset (Haskett & Porinchu, 2014). *Paratendipes, Cladopelma,* and *Pagastiella* appear for the first time at ca. 11.1 ka, followed by *Polypedilum* and *Pentaneurini,* which maximum abundance in the core at ~10.2 ka supporting the inference of increased temperature during this interval (Cranston et al., 1983). The occurrence of *Polypedilum*, *Paratendipes*, and *Psectrocladius* between 10.2 to 8.6 ka may reflect the presence of aquatic macrophytes in the lake's littoral zone, elevated temperature (Brodin, 1986) and possibly a lowering of the lake level (Cranston et al., 1983). Taxa, such as *Pagastiella*, *Pentaneurini*, and *Polypedilum,* have high MJAT optima in the Intermountain West training set (Haskett & Porinchu, 2014).

The presence of these species suggests that Gold Lake was warmer and more productive during the early Holocene. Gold Lake MJAT deviates between -0.3 to 1.3°C from the long-term average, compared to –1.9 to -0.4 °C for the Late-Glacial period. Notably, at 9.2 ka, the temperature reaches 12.0°C and remains high until 8 ka with a MJAT of 10.9 °C right prior to Mazama eruption ca. 7.63 ka. The elevated temperature at Gold Lake during this interval coincides with the maximum summer insolation in the Pacific Northwest with dry summers

(Bartlein et al., 1998; Heusser et al., 1985; Walker & Pellatt, 2003); however, it did not exceed the modern recorded temperature.

Before the Mazama eruption, some thermophilous taxa decreased, e.g., *Chironomus*, *Glyptotendipes*, and *Microtendipes.* At the same time, cold-adapted taxa such as *Corynocera* near *ambigua*, *Corynocera oliveri*-type, and *Heterotrissocladius* increased (Walker & Mathewes, 1988). Evidence of cooling prior to the Mazama eruption has also been inferred from a pollen-climate transfer function for Coastal British Columbia (Mathewes & Heusser, 1981). During this zone (8-7.63 ka), the MJAT remained low, approximately -0.1 to -0.4°C below the 14.5 ka average, was 11.3 °C while it remained above 0.4 to 0.7 °C during 9.2 to 8.6 ka (Fig. 3.7).

**Gold III-Early Holocene-Post-Mazama (732-450 cm; ca. 7.6 to 5 ka, 7 samples)**

After the Mazama tephra deposition at ~7.5 ka, MJAT increases to 11.5°C and reaches a maximum of approximately 12.6°C at ~7.2 ka, 1.3°C above the long-term average for the last 14.5 ka. Following this interval of elevated temperature, MJAT decreases and remains low relative to the early Holocene. This pattern agrees with evidence of Northern Hemisphere cooling during the middle Holocene (Marcott et al., 2013) and cooler summers along the North Pacific coast (Barron et al., 2003; Praetorius et al., 2015) likely driven by decreasing summer insolation (Bartlein et al., 1998). Transition to lower temperatures at Gold Lake started at ca. 7 ka, while at Windy Lake and Thunder Lake, British Columbia, it occurred at 6 ka and 4.5 ka, respectively (Chase et al., 2008).

During the early Holocene at Gold Lake, peak warmth occurred at 7.2 ka shortly following the tephra deposition. An increase in *Pentaneurini* and *Tanytarsus* type-*D*, which have MJAT optima of 12.4 and 14.6 °C, respectively, coincide with increase temperature reconstruction at Gold Lake (Haskett & Porinchu, 2014). This inferred warming may partly be caused by the "aridification" effect of the tephra, reducing the leaf area of the surrounding vegetation and reducing latent heat flux, thus increasing the sensible heat (Harris & Van Couvering, 1995). Peak warmth at sites further to the south occurred later in the Holocene: at Stella Lake, Great Basin, the temperature peaked at 5.4 ka at 11.0 °C (Reinemann et al., 2009a), while at Pyramid Lake, Nevada, δ18O record shows the warmest interval during the Holocene was at ~6.8 ka (Benson et

al., 2002). A site in eastern Nevada provides evidence for peak Holocene warmth at 6.5 ka (Potito et al., 2006), while at a site to the north (in southern British Columbia), peak warmth occurred earlier in the Holocene, closer to 9 ka (Chase et al., 2008). Following the short-lived period of post-Mazama warmth, cold-adapted and thermophilous taxa varied in relative abundance, resulting in fluctuating MJAT.

**Gold IV-Late Holocene (450-0 cm; ca. 5 ka to present, 9 samples)**

During the late Holocene, midge inferred MJAT reaches a maximum of 13.7ºC at 2.5 ka, after which time it decreases to 11.7ºC at 1.9 ka and then fluctuates between 12.2 and 12.6°C for the remainder of the record. MJAT inferred temperature increases from 10.8 to 11.4 °C at the bottom of this zone, which is 0.09°C above the long-term average, and remained high for the rest of the core, fluctuating between 0.04 to 1.8 °C except at 3.1 ka, where it was 0.3 °C below the long-term average MJAT.

During the late Holocene, taxa associated with warmer, more productive conditions increased, e.g., *Dicrotendipes*, *Microtendipes*, and *Tanytarsus* type-*D* (Brodersen et al., 2001; Brooks et al., 2007; Porinchu et al., 2007) and taxa associated with cooler, less productive conditions decreased, e.g., *Chironomus* and *Corynocera* near *ambigua.* At 2.5 ka when MJAT reaches its maximum (13.7 °C) a taxon associated with eutrophic lakes, *Cladopelma,* appears for the first time (Cranston et al., 1983) along with *Parakiefferiella bathophila*-type, *Dicrotendipes*, *Microtendipes*, and *Procladius* (Brooks et al., 2007; Haskett & Porinchu, 2014; Walker et al., 1991; Wiederholm, 1983). Between 4.5 and 3.5 ka, ENSO activities were intensified, resulting in Indo-Pacific warming (Donders et al., 2008). Proxy data from Castor Lake in Washington also suggests a basin-scale change during 4-5 ka in the Pacific Ocean with variability in drought conditions (Nelson et al., 2011).

During the Medieval Climate Anomaly (MCA), MJAT at Gold Lake is 1.2 °C above the long-term average for the last 14.5 ka. This warming episode preceded the MCA, starting at 1.4 ka when MJAT was 1.28 °C above the long-term average. A similar pattern was recorded at Stella Lake, where MJAT was 0.4 °C above the late-Holocene average during the MCA (Reinemann et al., 2014). During the Little Ice Age (LIA), MJAT at Gold Lake was 0.09 °C below the mean MCA temperature but was 1.10 °C above the long-term average. At Stella Lake, MJAT was ~1.0

°C below the 2000-yr mean temperature (Reinemann et al., 2014), with MJAT 1.5 °C below peak Holocene warmth (Reinemann et al., 2009a). After the LIA, the temperature declines, reaching 12.3 °C in the uppermost sediment. This temperature is slightly below the MJAT inferred during the MCA. Maximum temperature (13.2 °C) during late Holocene at ~2.5 ka at Gold Lake agrees with the Northeast Pacific sea surface temperature that recorded a permanent increase up to 1.0 °C in alkenone SST at ca. 3.2 ka, which reflects an increasing wintertime insolation in northern California (Barron et al., 2003). There might be a general link between SST and high elevation temperature, possibly via affecting lapse rate. Increased late Holocene precipitation, widely documented in the Pacific Northwest, could have resulted in more latent heat transfer and decreased lapse rates, contributing to the reconstructed increase in late Holocene temperature at Gold Lake.

The timing of the increased temperature at Gold Lake corresponds well to the warming events in North America reconstructed based on pollen (Ahmed et al., 2013), midge-inferred reconstruction at Stella Lake, Central Great Basin, Nevada (Reinemann et al., 2014), and other reconstructions done in Northern Hemisphere (Mann et al., 2009; Moberg et al., 2005). At Gold Lake, we observed the recorded high temperature at ~2.5 ka, but it seems like, based on the above-recorded data, it might start earlier, and it could be confirmed if decadal-based chironomid inferred MJAT is used in the future to fill this gap.

## Conclusion

This is the first study of chironomids and paleotemperature reconstruction in the Pacific Northwest from the Late Glacial period to the present. Quantitative reconstructions based on chironomids are still rare and developing in the USA. Gold Lake midge-inferred MJAT suggests a cool late Glacial period with ~10.6 °C, which is 1.6 °C cooler than the modern temperature. Younger Dryas event was clearly recorded with a minimum temperature of 9.4 °C followed by an increasing trend of temperature in transition into the early Holocene. The temperature increased during the early Holocene to ca. 12.0 °C  at 9.2 ka with increased abundance of the thermophilous taxa. The middle Holocene was overall cooler compared to the early Holocene. The highest temperature was recorded during the late Holocene at ~2.5 ka, which generally

coincides with the Northeast Pacific sea surface temperature, which recorded a permanent increase up to 1.0 °C in alkenone SST at ca. 3.2 ka (Barron et al., 2003). Overall, the late Holocene appears to be the warmest period compared to the Holocene period and has clear evidence of increased temperature during MCA, though sample resolution was insufficient to address the MCA and LIA in detail. This chironomid MJAT history, although coarsely-sampled (multi-centennial intervals), produced new findings of the impact of Mazama tephra on temperature and a previously unrecognized late Holocene temperature trend. This suggests that further studies, including multiple lakes from the Pacific Northwest and increased temporal resolution, are crucial to placing the projected climatic changes into a long-term context. In addition, while the IMW training data set was statistically appropriate for the Gold Lake history, expanding this calibration data set into the Pacific Northwest will increase its application to temperature reconstruction from lakes in the Pacific Northwest.

In the next chapter, we will develop the paleolimnological history of Gold Lake using geochemical signatures of organic matter. This study will add more to the aquatic environmental conditions and paleo productivity of Gold Lake at high resolution for the last 14 500 years.

## References


Ahmed, M., Anchukaitis, K. J., Asrat, A., Borgaonkar, H. P., Braida, M., Buckley, B. M., Büntgen, U., Chase, B. M., Christie, D. A., Cook, E. R., Curran, M. A. J., Diaz, H. F., Esper, J., Fan, Z. X., Gaire, N. P., Ge, Q., Gergis, J., González-Rouco, J. F., Goosse, H., … Zorita, E. (2013). Continental-scale temperature variability during the past two millennia. *Nature Geoscience*, *6*(5), 339–346. https://doi.org/10.1038/ngeo1797

Alizadeh, M. R., Abatzoglou, J. T., Luce, C. H., Adamowski, J. F., Farid, A., & Sadegh, M. (2021). Warming enabled upslope advance in western US forest fires. *Proceedings of the National Academy of Sciences of the United States of America*, *118*(22).

Armitage, P., D., Pinder, L. C., & Cranston, P. S. (2012). *The Chironomidae: biology and ecology of non-biting midges (Eds.)*. Springer Science & Business Media.

Baig, J., & Gavin, D. G. (2023). Postglacial vegetation and fire history with a high-resolution analysis of tephra impacts, high Cascade Range, Oregon, USA. *Quaternary Science Reviews*, *303*, 107970. https://doi.org/10.1016/j.quascirev.2023.107970

Barron, J. A., Heusser, L., Herbert, T., & Lyle, M. (2003a). High-resolution climatic evolution of coastal northern California during the past 16,000 years. *Paleoceanography*, *18*(1). https://doi.org/10.1029/2002PA000768

Barron, J. A., Heusser, L., Herbert, T., & Lyle, M. (2003b). High-resolution climatic evolution of coastal northern California during the past 16,000 years. *Paleoceanography*, *18*(1), 1020. https://doi.org/10.1029/2002PA000768

Bartlein, P. J., Anderson, K. H., Anderson, P. M., Edwards, M. E., Mock, C. J., Thompson, R. S., Webb, R. S., Webb, T., & Whitlock, C. (1998). Paleoclimate simulations for North America over the past 21,000 years: Features of the simulated climate and comparisons with paleoenvironmental data. *Quaternary Science Reviews*, *17*(6–7), 549–585. https://doi.org/10.1016/S0277-3791(98)00012-2

Battarbee, R. W., Thompson, R., Catalan, J., Grytnes, J. A., & Birks, H. J. B. (2002). Climate variability and ecosystem dynamics of remote alpine arctic lakes: the MOLAR project. *J Paleolimnol*, *28*(1), 1–6. https://doi.org/10.1023/a:1020342316326

Benson, L., Kashgarian, M., Rye, R., Lund, S., Paillet, F., Smoot, J., Kester, C., Mensing, S., Meko, D., & Lindström, S. (2002). Holocene multidecadal and multicentennial droughts affecting Northern California and Nevada. *Quaternary Science Reviews*, *21*(4–6), 659–682. https://doi.org/10.1016/s0277-3791(01)00048-8

Birks, H. J. B. (1998). Numerical tools in palaeolimnology-Progress, potentialities, and problems. In *Journal of Paleolimnology* (Vol. 20). https://link.springer.com/content/pdf/10.1023%2FA%3A1008038808690.pdf

Blaauw, M., & Christen, J. A. (2011). *Bacon manual*. 15. http://chrono.qub.ac.uk/blaauw/bacon.html

Brodersen, K. P., Odgaard, B. V., Vestergaard, O., & John Anderson, N. (2001). Chironomid stratigraphy in the shallow and eutrophic Lake Søbygaard, Denmark: chironomid–macrophyte co-occurrence. *Freshwater Biology*, *46*(2), 253–267. https://doi.org/10.1046/J.1365-2427.2001.00652.X

Brodin, Y. W. (1986a). The Postglacial History of Lake Flarken, Southern Sweden, Interpreted from Subfossil Insect Remains. *Internationale Revue Der Gesamten Hydrobiologie Und Hydrographie*, *71*(3), 371–432. https://doi.org/10.1002/iroh.19860710313

Brodin, Y. W. (1986b). The Postglacial History of Lake Flarken, Southern Sweden, Interpreted from Subfossil Insect Remains. *Internationale Revue Der Gesamten Hydrobiologie Und Hydrographie*, *71*(3), 371–432. https://doi.org/10.1002/IROH.19860710313

Brooks, S. J., Langdon, P. G., & Heiri, O. (2007a). *The identification and use of Palaearctic Chironomidae larvae in palaeoecology. QRA Technical Guide No. 10*. Quaternary Research Association.

Brooks, S. J., Langdon, P. G., & Heiri, O. (2007b). *The identification and use of palaearctic chironomidae larvae in palaeoecology (Technical guide / quaternary research association, no. 10)*. Quaternary Research Association.

Brooks, S.J., Mayle, F. E., & Lowe, J. J. (1997). Chironomid-based Lateglacial climatic reconstruction for southeast Scotland. *Journal of Quaternary Science*, *12*(2), 161–167.

Brooks, Stephen J., & Birks, H. J. B. (2001a). Chironomid-inferred air temperatures from Lateglacial and Holocene sites in north-west Europe: Progress and problems. *Quaternary Science Reviews*, *20*(16–17), 1723–1741. https://doi.org/10.1016/S0277-3791(01)00038-5

Brooks, Stephen J., & Birks, H. J. B. (2001b). Chironomid-inferred air temperatures from Lateglacial and Holocene sites in north-west Europe: progress and problems. *Quaternary Science Reviews*, *20*(16–17), 1723–1741. https://doi.org/10.1016/S0277-3791(01)00038-5

Brooks, Stephen J, & Birks, H. J. B. (2001). Chironomid-inferred air temperatures from Lateglacial and Holocene sites in north-west Europe: Progress and problems. *Quaternary Science Reviews*, *20*(16–17), 1723–1741. https://doi.org/10.1016/S0277-3791(01)00038-5

Chase, M., Bleskie, C., Walker, I. R., Gavin, D. G., & Hu, F. S. (2008). Midge-inferred Holocene summer temperatures in Southeastern British Columbia, Canada. *Palaeogeography, Palaeoclimatology, Palaeoecology*, *257*(1–2), 244–259. https://doi.org/10.1016/j.palaeo.2007.10.020

Cohen, K. M., Finney, S. C., Gibbard, P. L., & Fan, J. X. (2013). The ICS International Chronostratigraphic Chart. *Episodes Journal of International Geoscience*, *36*(3), 199–204.

Cranston, P. S., Oliver, D. R., & Sæther, O. A. (1983). *The larvae of the Orthocladiinae (Diptera: Chironomidae) of the Holarctic region: keys and diagnoses. In: Wiederholm, T. (Ed.), Chironomidae of the Holarctic Region. Keys and Diagnoses. Part 1-Larvae.* Entomologica Scandinavica Supplement 19.

Cwynar, L. C., & Levesque, A. J. (1995). Chironomid evidence for late-glacial climatic reversals in maine. *Quaternary Research*, *43*(3), 405–413. https://doi.org/10.1006/qres.1995.1046

Donders, T. H., Wagner-Cremer, F., & Visscher, H. (2008). Integration of proxy data and model scenarios for the mid-Holocene onset of modern ENSO variability. *Quaternary Science Reviews*, *27*(5–6), 571–579. https://doi.org/10.1016/j.quascirev.2007.11.010

Dolman, A. M., & Laepple, T. (2018). Sedproxy: a forward model for sediment-archived climate proxies. Climate of the Past, 14(12), 1851-1868.

Ersek, V., Clark, P. U., Mix, A. C., Cheng, H., & Lawrence Edwards, & R. (2012). ARTICLE Holocene winter climate variability in mid-latitude western North America. *Nature Communications*. https://doi.org/10.1038/ncomms2222

Franklin, J. ., & Dyrness, C. . (1988). *Natural Vegetation of Oregon and Washington*. Oregon State University Press.

Gavin, D. G., Brubaker, L. B., & Greenwald, D. N. (2013). Postglacial climate and fire-mediated vegetation change on the western Olympic Peninsula, Washington (USA). *Ecological Monographs*, *83*(4), 471–489. https://doi.org/10.1890/12-1742.1

Gouw-Bouman, M. T. I. J., Van Asch, N., Engels, S., & Hoek, W. Z. (2019). Late Holocene ecological shifts and chironomid-inferred summer temperature changes reconstructed from Lake Uddelermeer, the Netherlands. Palaeogeography, Palaeoclimatology, Palaeoecology, 535, 109366.

Harris, J., & Van Couvering, J. (1995). Mock aridity and the paleoecology of volcanically influenced ecosystems. *Geology*, *23*(7), 593–596.

Haskett, D. R., & Porinchu, D. F. (2014a). A quantitative midge-based reconstruction of mean July air temperature from a high-elevation site in central Colorado, USA, for MIS 6 and 5. *Quaternary Research*, *82*(3), 580–591. https://doi.org/10.1016/j.yqres.2014.05.002

Haskett, D. R., & Porinchu, D. F. (2014b). A quantitative midge-based reconstruction of mean July air temperature from a high-elevation site in central Colorado, USA, for MIS 6 and 5. *Quaternary Research*, *82*(3), 580–591. https://doi.org/10.1016/J.YQRES.2014.05.002

Heiri, O., & Lotter, A. F. (2001). Effect of low count sums on quantitative environmental reconstructions: An example using subfossil chironomids. *Journal of Paleolimnology*, *26*(3), 343–350. https://doi.org/10.1023/A:1017568913302

Henrikson, L., Olofsson, J. B., & Oscarson, H. G. (1982). The impact of acidification on Chironomidae (Diptera) as indicated by subfossil stratification. *Hydrobiologia 1982 86:3*, *86*(3), 223–229. https://doi.org/10.1007/BF00006140

Heusser, C. J., Heusser, L. E., & Peteet, D. M. (1985). Late-Quaternary climatic change on the American North Pacific Coast. *Nature*, *315*(6019), 485–487. https://doi.org/10.1038/315485a0

Hill, M. O. (1973). Diversity and Evenness: A Unifying Notation and Its Consequences. *Ecology*, *54*(2), 427–432. https://doi.org/10.2307/1934352

Juggins, S. (2003). C2 user guide: Software for ecological and palaeoecological data analysis and visualization. *University of Newcastle, Newcastle upon Tyne, UK*, 1–73.

Lacourse, T. (2005). Late Quaternary dynamics of forest vegetation on northern Vancouver Island, British Columbia, Canada. *Quat Sci Rev*, *24*(1–2), 105–121. https://doi.org/10.1016/j.quascirev.2004.05.008

Langdon, P. G., Ruiz, Z., Brodersen, K. P., & Foster, I. D. L. (2006). Assessing lake eutrophication using chironomids: Understanding the nature of community response in different lake types. *Freshwater Biology*, *51*(3), 562–577. https://doi.org/10.1111/J.1365-2427.2005.01500.X

Larocque, I, Hall, R. I., & Grahn, E. (2001). Chironomids as indicators of climate change: a 100-lake training set from a subarctic region of northern Sweden (Lapland). In *Journal of Paleolimnology* (Vol. 26).

Larocque, Isabelle, & Hall, R. I. (2003). Chironomids as quantitative indicators of mean July air temperature: validation by comparison with century-long meteorological records from northern Sweden. In *Journal of Paleolimnology* (Vol. 29). https://link.springer.com/content/pdf/10.1023/A:1024423813384.pdf

Lemmen, J., & Lacourse, T. (2018). Fossil chironomid assemblages and inferred summer temperatures for the past 14,000 years from a low-elevation lake in Pacific Canada. *Journal of Paleolimnology*, *59*(4), 427–442. https://doi.org/10.1007/s10933-017-9998-3

Livingstone, D. M., & Lotter, A. F. (1998). The relationship between air and water temperatures in lakes of the Swiss Plateau: A case study with palaeolimnological implications. *Journal of Paleolimnology*, *19*(2), 181–198. https://doi.org/10.1023/A:1007904817619

Lotter, A. F., Eicher, U., Siegenthaler, U., & Birks, H. J. B. (1992). Late-glacial climatic oscillations as recorded in Swiss lake sediments. *Journal of Quaternary Science*, *7*(3), 187–204. https://doi.org/10.1002/JQS.3390070302

MacDonald, G. M., Moser, K. A., Bloom, A. M., Porinchu, D. F., Potito, A. P., Wolfe, B. B., Edwards, T. W. D., Petel, A., Orme, A. R., & Orme, A. J. (2008). Evidence of temperature depression and hydrological variations in the eastern Sierra Nevada during the Younger Dryas stade. *Quaternary Research*, *70*(2), 131–140. https://doi.org/10.1016/J.YQRES.2008.04.005

Mann, M. E., Zhang, Z., Rutherford, S., Bradley, R. S., Hughes, M. K., Shindell, D., Ammann, C., Faluvegi, G., & Ni, F. (2009). Global signatures and dynamical origins of the little ice age and medieval climate anomaly. *Science*, *326*(5957), 1256–1260.

Marcott, S. A., Shakun, J. D., Clark, P. U., & Mix, A. C. (2013). A reconstruction of regional and global temperature for the past 11,300 years. *Science*, *339*(6124), 1198–1201. https://doi.org/10.1126/science.1228026

Mathewes, R. W., & Heusser, L. E. (1981). A 12 000 year palynological record of temperature and precipitation trends in southwestern British Columbia ( Marion Lake). *Canadian Journal of Botany*, *59*(5), 707–710. https://doi.org/10.1139/b81-100

Mathewes, Rolf W. (1993). Evidence for Younger Dryas-age cooling on the north Pacific coast of America. *Quat Sci Rev*, *12*(5), 321–331. https://doi.org/10.1016/0277-3791(93)90040-s

Mayfield, R. J., Langdon, P. G., Doncaster, C. P., Dearing, J. A., Wang, R., Velle, G., ... & Brooks, S. J. (2021). Late Quaternary chironomid community structure shaped by rate and magnitude of climate change. Journal of Quaternary Science, 36(3), 360-376

Moberg, A., Sonechkin, D. M., Holmgren, K., Datsenko, M. H., & Karlén, W. (2005). Highly variable Northern Hemisphere temperatures reconstructed from low- and high-resolution proxy data. *Nature*, *433*(7026), 613–617. https://doi.org/10.1038/nature03265

Nelson, D. B., Abbott, M. B., Steinman, B., Polissar, P. J., Stansell, N. D., Ortiz, J. D., Rosenmeier, M. F., Finney, B. P., & Riedel, J. (2011). Drought variability in the Pacific Northwest from a 6,000-yr lake sediment record. *Proceedings of the National Academy of Sciences of the United States of America*, *108*(10), 3870–3875. https://doi.org/10.1073/pnas.1009194108

Oksanen, J. (2008). Vegan: an introduction to ordination.

Olander, H., Korhola, A., & Blom, T. (1997). Surface sediment chironomidae (Insecta: Diptera) distributions along an ecotonal transect in subarctic fennoscandia: Developing a tool for palaeotemperature reconstructions. *Journal of Paleolimnology*. https://doi.org/10.1023/A:1007906609155

Palmer, S., Walker, I., Heinrichs, M., Hebda, R., & Scudder, G. (2002). Postglacial midge community change and Holocene palaeotemperature reconstructions near treeline, southern British Columbia (Canada). *Journal of Paleolimnology*, *28*(4), 469–490. https://doi.org/10.1023/A:1021644122727

Porinchu, D. F., & MacDonald, G. M. (2003). The use and application of freshwater midges (Chironomidae: Insecta: Diptera) in geographical research. *Progress in Physical Geography*, *27*(3), 378–422. https://doi.org/10.1191/0309133303767888491

Porinchu, D. F., MacDonald, G. M., Bloom, A. M., & Moser, K. A. (2003a). Late Pleistocene and early Holocene climate and limnological changes in the Sierra Nevada, California, USA inferred from midges (Insecta: Diptera: Chironomidae). *Palaeogeography, Palaeoclimatology, Palaeoecology*, *198*(3–4), 403–422. https://doi.org/10.1016/S0031-0182(03)00481-4

Porinchu, D. F., MacDonald, G. M., Bloom, A. M., & Moser, K. A. (2003b). Late Pleistocene and early Holocene climate and limnological changes in the Sierra Nevada, California, USA inferred from midges (Insecta: Diptera: Chironomidae). *Palaeogeography, Palaeoclimatology, Palaeoecology*, *198*(3–4), 403–422. https://doi.org/10.1016/S0031-0182(03)00481-4

Porinchu, D. F., Potito, A. P., MacDonald, G. M., & Bloom, A. M. (2007). Subfossil chironomids as indicators of recent climate change in Sierra Nevada, California, lakes. *Arctic, Antarctic, and Alpine Research*, *39*(2), 286–296.

Porinchu, D. F., Reinemann, S., Mark, B. G., Box, J. E., & Rolland, N. (2010). Application of a midge-based inference model for air temperature reveals evidence of late-20th century warming in sub-alpine lakes in the central Great Basin, United States. *Quaternary International*, *215*(1–2), 15–26. https://doi.org/10.1016/j.quaint.2009.07.021

Potito, A. P., Porinchu, D. F., MacDonald, G. M., & Moser, K. A. (2006). A late Quaternary chironomid-inferred temperature record from the Sierra Nevada, California, with connections to northeast Pacific sea surface temperatures. *Quaternary Research*, *66*(2), 356–363. https://doi.org/10.1016/j.yqres.2006.05.005

Praetorius, S. K., Mix, A. C., Walczak, M. H., Wolhowe, M. D., Addison, J. A., & Prahl, F. G. (2015). North Pacific deglacial hypoxic events linked to abrupt ocean warming. *Nature*, *527*(7578), 362–366. https://doi.org/10.1038/nature15753

Prentice, I. C. (1980). Multidimensional scaling as a research tool in quaternary palynology: A review of theory and methods. *Review of Palaeobotany and Palynology*, *31*, 71–104.

PRISM Climate Group. (2020). *PRISM Climate Group*. Oregon State University. http://www.prism.oregonstate.edu/

Quinlan, R., & Smol, J. P. (2001). Setting minimum head capsule abundance and taxa deletion criteria in chironomid-based inference models. *Journal of Paleolimnology*, *26*(3), 327–342.

Reimer, P. J., Austin, W. E. N., Bard, E., Bayliss, A., Blackwell, P. G., Bronk Ramsey, C., Butzin, M., Cheng, H., Edwards, R. L., Friedrich, M., Grootes, P. M., Guilderson, T. P., Hajdas, I., Heaton, T. J., Hogg, A. G., Hughen, K. A., Kromer, B., Manning, S. W., Muscheler, R., … Talamo, S. (2020). The IntCal20 Northern Hemisphere Radiocarbon Age Calibration Curve (0–55 cal kBP). *Radiocarbon*, *62*(4), 725–757. https://doi.org/10.1017/RDC.2020.41

Reinemann, S. A., Porinchu, D. F., Bloom, A. M., Mark, B. G., & Box, J. E. (2009a). A multi-proxy paleolimnological reconstruction of Holocene climate conditions in the Great Basin, United States. *Quaternary Research*, *72*(3), 347–358. https://doi.org/10.1016/j.yqres.2009.06.003

Reinemann, S. A., Porinchu, D. F., Bloom, A. M., Mark, B. G., & Box, J. E. (2009b). A multi-proxy paleolimnological reconstruction of Holocene climate conditions in the Great Basin, United States. *Quaternary Research*, *72*, 347–358. https://doi.org/10.1016/j.yqres.2009.06.003

Reinemann, S. A., Porinchu, D. F., MacDonald, G. M., Mark, B. G., & DeGrand, J. Q. (2014). A 2000-yr reconstruction of air temperature in the Great Basin of the United States with specific reference to the Medieval Climatic Anomaly. *Quaternary Research (United States)*, *82*(2), 309–317. https://doi.org/10.1016/j.yqres.2014.06.002

Reinemann, S. A., Porinchu, D. F., & Mark, B. G. (2014). Regional climate change evidenced by recent shifts in chironomid community composition in subalpine and alpine lakes in the Great Basin of the United States. *Arctic, Antarctic, and Alpine Research*, *46*(3), 600–615. https://doi.org/10.1657/1938-4246-46.3.600

S. E. Wilson, I. R. W. R. J. M. J. P. S. (1993). Climatic and limnological changes associated with the Younger Dryas in Atlantic Canada. *Clim. Dyn.*, *8*, 177–187.

Schindler, D. W., Beaty, K. G., Fee, E. J., Cruikshank, D. R., DeBruyn, E. R., Findlay, D. L., Linsey, G. A., Shearer, J. A., Stainton, M. P., & Turner, M. A. (1990). Effects of climatic warming on lakes of the central boreal forest. *Science*, *250*(4983), 967–971.

Schnurrenberger, D., Russell, J., & Kelts, K. (2003). Classification of lacustrine sediments based on sedimentary components. *Journal of Paleolimnology*, *29*(2), 141–154. https://doi.org/10.1023/A:1023270324800

Smith, M. J., Pellatt, M. G., Walker, I. R., & Mathewes, R. W. (1998). Postglacial changes in chironomid communities and inferred climate near treeline at Mount Stoyoma, Cascade Mountains, southwestern British Columbia, Canada. *Journal of Paleolimnology*, *20*(3), 277–293. https://doi.org/10.1023/A:1007904917419

Smol, J. P., Birks, H. J. B., & Last, W. M. (Eds.). (2001a). *Tracking Environmental Change Using Lake Sediments* (Vol. 4). Springer Netherlands. https://doi.org/10.1007/0-306-47671-1

Smol, J. P., Birks, H. J. B., & Last, W. M. (2001b). *Zoological Indicators in Lake Sediments: An Introduction* (pp. 1–4). https://doi.org/10.1007/0-306-47671-1_1

Telford, R. J., & Birks, H. J. B. (2011). A novel method for assessing the statistical significance of quantitative reconstructions inferred from biotic assemblages. *Quaternary Science Reviews*, *30*(9–10), 1272–1278.

Walker, I. R., & Mathewes, R. W. (1989). Chironomidae (Diptera) remains in surficial lake sediments from the Canadian Cordillera: analysis of the fauna across an altitudinal gradient. Journal of Paleolimnology, 2, 61-80.

Walker, I. (2001). *Midges: Chironomidae and related Diptera* (pp. 43–66). Kluwer Academic Publishers.

Walker, I. R. (2007). *The WWW field guide to fossil midges*. http://www.paleolab.ca/wwwguide/

Walker, I. R., Smol, J. P., Engstrom, D. R., & Birks, H. J. B. (1991). An assessment of Chironomidae as quantitative indicators of past climatic change. *Canadian Journal of Fisheries and Aquatic Sciences*, *48*(6), 975–987. https://doi.org/10.1139/f91-114

Walker, I R., & Mathewes, R. W. (1988). Late-Quaternary fossil Chironomidae (Diptera) from Hippa Lake, Queen Charlotte Islands, British Columbia, with special reference to Corynocera Zett. *Can Entomol*, *120*, 739–751.

Walker, Ian R., & Cwynar, L. C. (2006). Midges and palaeotemperature reconstruction-the North American experience. *Quaternary Science Reviews*, *25*(15–16), 1911–1925. https://doi.org/10.1016/j.quascirev.2006.01.014

Walker, Ian R., & Mathewes, R. W. (1989). Early postglacial chironomid succession in southwestern British Columbia, Canada, and its paleoenvironmental significance. *Journal of Paleolimnology*, *2*(1), 1–14. https://doi.org/10.1007/BF00156979

Walker, Ian R, Levesque, A. J., Cwynar, L. C., & Lotter, A. F. (1997). An expanded surface-water palaeotemperature inference model for use with fossil midges from eastern Canada. In *Journal of Paleolimnology* (Vol. 18). Kluwer Academic Publishers.

Walker, Ian R, & Pellatt, M. G. (2003). Climate Change in Coastal British Columbia — A Paleoenvironmental Perspective. *Canadian Water Resources Journal*, *531*(4).

Wang, T., Hamann, A., Spittlehouse, D., & Carroll, C. (2016). Locally downscaled and spatially customizable climate data for historical and future periods for North America. PloS one, 11(6), e0156720.

Wiederholm, T. (1983). *Chironomidae of the Holarctic Region: Keys and Diagnoses*.

Williams, J. W., Post, D. M., Cwynar, L. C., Lotter, A. F., & Levesque, A. J. (2002). Rapid and widespread vegetation responses to past climate change in the North Atlantic region. *Geology*, *30*(11), 971–974.

Zhang, Y. C., Slomp, C. P., Broers, H. P., Bostick, B., Passier, H. F., Böttcher, M. E., Omoregie, E. O., Lloyd, J. R., Polya, D. A., & Van Cappellen, P. (2012). Isotopic and microbiological signatures of pyrite-driven denitrification in a sandy aquifer. *Chemical Geology*, *300–301*, 123–132.

# IV. PALEOLIMNOLOGICAL HISTORY OF GOLD LAKE USING GEOCHEMICAL SIGNATURES OF ORGANIC MATTER, OREGON, USA

**Manuscript in preparation for Journal of Quaternary Science**

Jamila Baig and Dan Gavin

JB and DGG conceptualized the study, devised the methodology, and conducted the field investigation. JB acquired the funding and curated, analyzed, and visualized the data. JB wrote the original manuscript, and DGG reviewed, edited, and contributed to the final manuscript.

## Introduction

Lakes respond rapidly to shifting environmental circumstances due to the rapid production of lacustrine algae (Adrian et al., 1995). Organic matter in lakes is a key indicator of lake productivity, a representation of the terrestrial vegetation around lakes, and a climate change indicator. Lake sediment organic matter might be a minor sediment component, but it has high paleolimnological value because it contains various proxies that provide paleoenvironmental information about the lake and its surroundings (Meyers, 2003). Relative to ocean sediments, lakes' high primary productivity and sedimentation rate make them well-suited to understanding the many processes that affect organic matter in the palaeoecological record. Some proxies of lake primary production and sedimentation rate include organic carbon concentration and accumulation rate (Hodell & Schelske, 1998; Jellison et al., 1996), C/N (carbon to nitrogen ratio) ratio indicating the proportion of algal and terrestrial organic matter (Meyers, 1994), $\delta^{13}C$ indicating algal production rate (Hodell & Schelske, 1998; Talbot & Johannessen, 1992), and $\delta^{15}N$ affected by several processes including N cycling and the proportion of land plants and algal organic matter (Hodell & Schelske, 1998; McLauchlan et al., 2007; Peterson & Howard, 1987; Teranes & Bernasconi, 2000).

Many factors complicate the interpretation of organic matter proxies in lake sediment. For example, clastic sediment particles and diatom productivity can dilute TOC (total organic carbon), while the dissolution of carbonate minerals can concentrate it (Dean, 1999). TOC concentrations can also be affected and show an increased pattern in the deeper lake sediment

with larger grain sizes (Meyers, 2003). To minimize these effects, accumulation rates may be calculated on well-dated sediment cores. For example, the carbon accumulation rate (CMAR) may indicate the delivery rate and preservation of organic matter, which, along with diatom (biogenic silica), reflects the lake's primary production. As the C/N ratio represents the terrestrial vs. aquatic source of organic matter, its fluctuation can be the result of changes in their accumulation rates (Meyers, 2003). For example, the basal sediment from Lake Ontario, which originated from glacial material, had low concentrations of TOC and a low C/N ratio, indicating aquatic productivity dominated by algal production (Meyers, 2003; Silliman et al., 1996). TOC and C/N gradually increased, indicating terrestrial input increased, consistent with increased vegetation and soil carbon in the watershed (Meyers, 2003; Silliman et al., 1996).

A stable carbon isotope of bulk organic matter may also indicate high lake productivity, especially in regions where C4 vegetation (with a much higher d13C) is not likely to have occurred in the past. Aquatic plants selectively use 12C during photosynthesis, leaving the DIC pool enriched at $^{13}C$. If the photosynthesis rate exceeds the rate at which $CO_2$ is dissolved into lake water, higher rates of productivity will result in increased positive $\delta^{13}C$ (Meyers & Lallier-Vergès, 1999). However, organic matter cycling into the DIC pool can reduce $\delta^{13}C$. The C/N ratio and its correlation with $\delta^{13}C$, help to determine whether $\delta^{13}C$ primarily reflects phytoplankton productivity or the source of organic matter (Meyers, 1994b, 2003).

Nutrient availability is a primary control of aquatic productivity, especially for diatoms (Battarbee et al., 2002; Mackay et al., 2003). For example, tephra deposition from volcanic activity adds silica into the water column (Barker et al., 2000), which may expedite the growth of silicious organisms (Hickman & Reasoner, 1994). Silica fertilization of diatom production by volcanic tephra is sometimes recorded as dramatically increased diatom content of lacustrine sediment (Zolitschka et al., 2015). Similar to tephra effects, increased clastic flux to the lake from glacial sediments deposited during regional deglaciation, when glaciers still covered the watershed, might be responsible for transporting mineral nutrients to the lake (Karlén, 1981).

Nitrogen inputs may also increase aquatic productivity. Nitrogen input from the watershed may increase after the fire (Dunnette et al., 2014), from increased populations of nitrogen-fixing plant species (Hu et al., 2001), and from glacial meltwater (Larsen et al., 2016).

Glacial sediments deposited during regional deglaciation, when glaciers still covered the watershed, and meltwater and sub-glacial erosion might be responsible for transporting sediment to lakes (Karlén, 1981). $\delta^{15}N$ may fluctuate due to changes in rates of N cycling within the lake or watershed, resulting in enriching 15N in inorganic N (Talbot, 2001) or due to increased nitrogen-fixing from cyanobacteria (Gu et al., 1996). In addition, glacial meltwater has been noted to have higher dissolved inorganic nitrogen and a higher $\delta^{15}N$ (Larsen et al., 2016). Interpretation of $\delta^{15}N$ becomes complicated due to these several co-occurring factors, in addition to early diagenesis in surface sediments, but despite this, it improves understanding of paleolimnological reconstruction (Meyers, 2003).

Gold Lake, one of the most productive lakes in the High Cascade Range of central Oregon, with a sediment record that extends back to 14.5 ka with multiple tephra layers and a two-meter section of laminations (Baig & Gavin, 2023), is well-suited to investigate the response of lake sediment to multiple environmental factors. This paper aims to develop a high-resolution record of lake productivity using multiple proxies in lacustrine lake sediment with multiple factors affecting its concentration since the Late Glacial period.

## Materials and Methods

### Study Site Description

Gold Lake is located in the Willamette National Forest at 1465 m a.s.l. on the crest of the Cascade Range in Oregon. It is in a glacially carved depression of basaltic andesite in the Cascade Range (43° 37' 57"N, 122° 02' 36" W), with a lake area of 38.9 ha and a watershed area of 48.4 $km^2$. Gold Lake receives water from nearby springs and Salt Creek, which flows through Gold Lake Bog on its northeast side (Fig. 4.1). The basin is oval in shape, with the deepest area (12 m) on the southeastern edge. Particulate and dissolved organic matter enter the lake after passing through Gold Lake Bog, supporting higher productivity than most other lakes in the Cascade Range. Johnson et al. (1985) classified the lake as mesotrophic due to the levels of phosphorus (0.047 mg/l).

## Field Collection

Baig & Gavin (2023) described sediment coring. In 2018, a square-rod piston corer was used to produce two parallel cores. Each 1-meter core drive was measured and briefly described after being extruded onto the raft anchored above Gold Lake's deepest point. Using a polycarbonate tube fitted with a piston corer, a 42 cm deep surface core was collected, sectioned into 1 cm intervals, and stored in polythene bags. Inside PVC pipe halves, each core was wrapped in plastic and labeled. The sediment cores were transported to the University of Oregon and stored in a refrigerator at 4°C. A depth profile of physicochemical properties (temperature, conductivity, and dissolved oxygen) was measured with a YSI meter during the fieldwork (Table S 4.1).

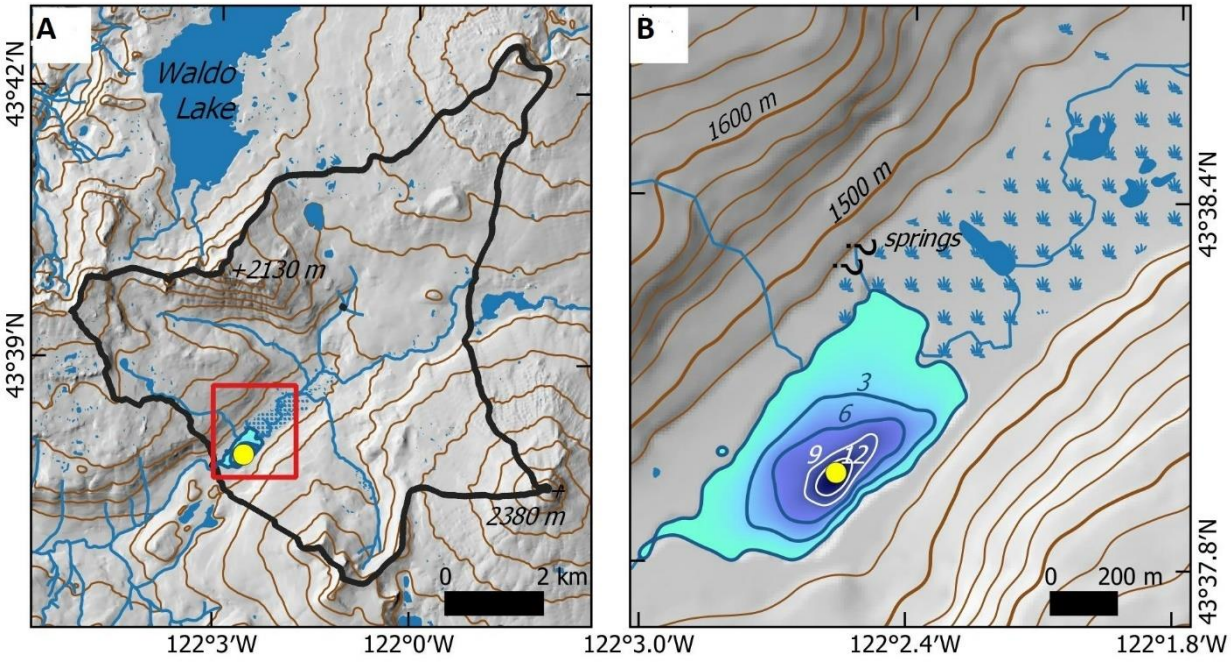


Figure 4. 1 (A) Shaded relief map with a 100-m contour interval, showing the 48.4 km$^2$ Gold Lake watershed (black line) and 100-m contour interval. The red box indicates the extent of map D. (B) Bathymetric map of Gold Lake (3 m contour interval; (Johnson et al., 1985), core location (yellow circle), and the location of the Gold Lake Bog wetland studied by (Sea & Whitlock, 1995).

## Laboratory Analysis

### Core Processing, Loss-on-ignition, and RGB values

Baig & Gavin (2023) thoroughly described the Gold Lake core processing. Every core drive was divided longitudinally into working core and archive core halves, except for the bottom 5-meter core drives, for which no parallel core, an uninterpreted stratigraphy was built utilizing tie points between parallel cores. Using a Sapphire Instruments magnetic susceptibility cup meter, tie points were identified between the uppermost piston core drive and the surface core. To evaluate the amount of organic matter in lake sediment, 178 samples were taken from pre- and post-Mazama sections at 5 cm and 10 cm intervals, respectively. These sub-samples of 1 $cm^3$ were placed in crucibles, dried at 80 °C, and burned at 550 °C for two hours. Lake sediment was categorized using terms described by Schnurrenberger et al. (2003) with the help of visual observations and organic matter analyses.

### Aquatic Taxa

Fifty sediment samples were prepared for pollen analysis using standard methods (Faegri et al. (1989) as reported in Baig & Gavin (2023). These samples spanned the entire core at ca. 500-yr resolution and 24 samples at 1-cm (ca. 4-6 yrs) resolution before and after a 78-cm thick Mazama tephra. Pediastrum colony fragments, Isoëtes microspores, and *Equisetum* spores were counted to the first 30 exotic spikes. Counts were scaled to the final exotic spike counted and expressed as percentages of total terrestrial pollen. These algae and aquatic taxa were not reported in Baig & Gavin (2023).

### Chronology

Baig & Gavin (2023) provided a description of radiocarbon dates and age models. Charcoal, recognizable plant material, pollen isolates, and bulk sediment were submitted in 13 samples for radiocarbon dating (Table S 4.1). Using electron microprobe analysis at the University of Oregon and Washington State University, two tephra layers (1 cm each) in addition to the 78-cm Mazama tephra were identified. A portion of the core is coarsely laminated after the Mazama tephra. JB and DGG visually counted the laminations independently. Using the Mazama eruption as a reference point (7633±25 cal yr BP; Egan et al., 2015), ages at 10-cm intervals were determined and incorporated into the age-depth model as a calendar year. The 25-

year error was incremented by two years per 10 cm (about 5% error) to account for the growing uncertainty along the varve sequence. Laminations were counted from 732 to 504 cm; however, discrepancies in counting from 570 to 504 cm between the two researchers were not included in developing an age-depth model. Laminations were also counted for the 245cm segment above the Llao Rock tephra and the Mazama tephra. Three radiocarbon dates between 732-570 cm were utilized to verify the precision of the counted laminations (Baig & Gavin, 2023). 11 radiocarbon dates, 17 varve-age estimations (at 10 cm intervals), and the age of the Mazama tephra were used to create an age model where three tephra layers were modeled as intervals of instantaneous deposition. Bayesian model Bacon for R was used to create the age-depth model (Blaauw & Christen, 2011) with the INTCAL20 calibration curve (Reimer et al., 2020).

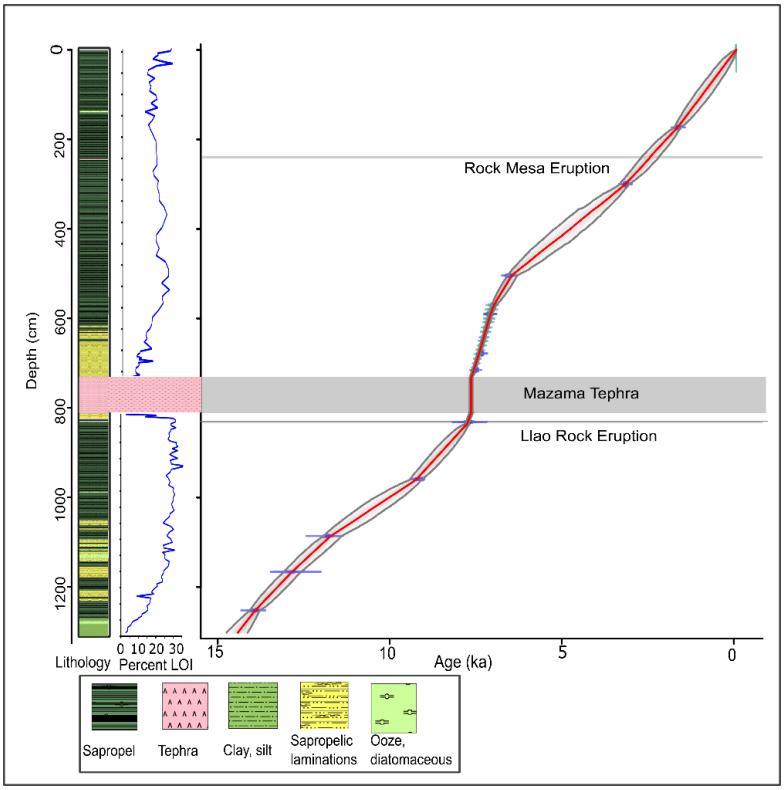


Figure 4. 2 Bacon age-depth model for Gold Lake with LOI and lithology. Horizontal bar lines represent three tephra layers found in the lake. Age estimates for post-Mazama (732-570 cm) and post-Llao Rock (831-811 cm) tephras are based on radiocarbon dates and manually counted varves (Baig & Gavin, 2023).

**Sediment color analysis**

Split sediment cores were imaged using a line scan camera on a GEOTEK XZ system at Oregon State University. ImageJ software (http://rsbweb.nih.gov/ij) extracted RGB values from core images along ca. 1 cm wide transects. Depth values were assigned along the transect precisely using core markers placed within the core. Color values were transformed from RGB values into CIELAB color space to obtain b* values that distinguish yellow from blue. We focused on b* because it has been shown to be effective at reflecting diatom content in organic-rich sediment cores (Debret et al., 2006). Color values were binned at 1 mm intervals for plotting or 1 cm intervals for comparison with geochemical data.

**Geochemical Analysis**

A total of 171 samples were analyzed for % carbon, % nitrogen, $\delta^{13}C$ (‰ vs. Vienna Pee Dee Belemnite), and $\delta^{15}N$ (‰ vs. air). Samples were at every 10 cm resolution pre-Mazama eruption (1302-810 cm) and every 5 cm resolution post-Mazama eruption (732 -0 cm). Samples were acid-rinsed to remove any potential for carbonates. Each sample (1.25 ml) was placed in a 15 ml centrifuge tube, and ~10 ml of 0.5% HCl was added. After 30 minutes, it was centrifuged for 5 minutes and decanted. 10 ml of DDI water (distilled de-ionized) was added, centrifuged, and decanted at least 3-4 times. Samples were then placed in a crucible and dried at 70°C in the oven for 12-24 hours. Later, they were grounded in a mortar and pestle until they had a fine powder consistency. Samples (2 to 5 mg) were weighed on a microbalance, folded into tin capsules, and analyzed at the University of California Stable Isotope Facility. The mean absolute accuracy for both $\delta^{13}C_{org}$ and $\delta^{15}N$ was reported to be 0.05‰. The mass accumulation rate for organic carbon was calculated from the product of the sedimentation rate (from the age-depth model), the bulk density (from the loss-on-ignition analysis), and the percentage of organic carbon. Inorganic mass accumulation was similarly calculated from loss-on-ignition.

## Results

### Sediment description and age-depth model

The core mostly comprises medium- to dark-brown biogenic sapropel, except for the three tephra layers and a 50-cm segment at the bottom (1302-1252 cm) (Figure S1; Table S2). Sapropelic (biogenic) laminations, rhythmically banded in light and dark brown, are seen in the core after the Mazama tephra (732-504 cm) and in the 20 cm between the Llao Rock tephra and the Mazama tephra (831-810 cm). The basal sediment, which has a 2-10% LOI, is mainly composed of silt and clay. LOI levels were typically between 2- 29% during the Late Glacial, 9-32% during the early Holocene (), and 15-34% during the late Holocene, while the laminated portion following the Mazama eruption had 10–15% LOI (Baig & Gavin, 2023).

Two radiocarbon dates were eliminated due to substantial measurement error (600 years age error) or occurring out of stratigraphic order with the age of the Mazama eruption (carbon date taken after Mazama tephra was younger than the age of Mazama eruption date). The age-depth model includes eleven radiocarbon dates in stratigraphic order (Fig. 4.2; Table 2.1: Chapter II). From the base up to 960 cm, a consistent sedimentation rate (0.07-0.11 cm/yr) was observed. About 50 cm above the core base, or around 13.9 ka, there is a change in sediment type from silt and clay to biogenic sapropelic. Three radiocarbon dates between 732-570 cm validated the manually counted laminations as yearly layers in the lake sediments (612 varves; 732-570 cm-post-Mazama, 65 varves; 831-810 cm-post-Llao to pre-Mazama). In the post-Mazama region, the sedimentation rate was 6-7 times greater than the rest of the core. After that, it falls and persists low (0.06-0.10 cm/yr) until the late Holocene (Baig & Gavin, 2023).

### Geochemical Analysis

Gold Lake, TOC (total organic carbon), and TN (total nitrogen) concentrations vary from 0.8% to 17.7% and 0.11% to 2.03%, respectively, yielding a C/N ratio ranging from 6.7 to 13.6. Sediment color (b*) is strongly correlated with TOC. $\delta^{13}C_{org}$ values range from -32.85‰ to -22.66‰, and $\delta^{15}N$ values from -1.71‰ to 1.65‰. Geochemical data has been organized into four major climatic and stratigraphic periods that are consistent with our two other research articles done on the Gold Lake: Late Glacial (14.4 ka-11.6 ka), Early Holocene-pre Mazama (11.6 ka-7.6

ka), Middle Holocene-post Mazama (7.6-5 ka), and Middle/Late Holocene (5.0 ka-present; Fig. 4.3; Cohen et al., 2013) which are described below.

**Gold I-Post-Glacial period (1302-1085 cm; ca. 14.4-11.6 ka)**

At the beginning of the Late Glacial period, the lowest TOC, TN, CMAR, and C/N ratio with the highest $\delta^{13}C_{org}$ and $\delta^{15}N$ values were recorded compared to the remainder of the core. TOC and TN gradually increase from 0.84% to 13.8% and from 0.13% to 1.27%, respectively, at 11.8 ka while $\delta^{13}C_{org}$ and $\delta^{15}N$ gradually decrease towards the top of this zone with values ranging from -22.66‰ to -29.18‰ and 1.6‰ to -0.56‰ respectively. The C/N ratio also increases from 6.6 to 12.5 at 12.6 ka and remains high for the remainder of this zone. The carbon mass accumulation rate (CMAR) was lowest at the bottom of the core (0.2 mg/cm$^2$/yr), gradually increasing and reaching 2.4 mg/cm$^2$/yr at 12.8 ka. The zone's sedimentation rate peaked early on (0.11 cm/year), then steadily decreased until it reached its lowest point (0.07 cm/year) near the zone top, which is mirrored by the trend in IMAR (Fig. 4.3).

**Gold II-Early Holocene-Pre-Mazama (1060-860 cm; ca. 11.6-7.7 ka)**

During this period, TOC, TN, and C/N were higher than in the Late Glacial period and were generally stable, reaching their highest values around 8.9 to 8.5 ka. Just after the Llao Rock tephra and prior to the Mazama tephra, when values reached the zone's lowest values: TOC 17% to 1.27%; TN 1.41% to 0.15%; C/N 12.3 to 8.46 (Fig. 4.3). $\delta^{13}C_{org}$ fluctuates between -31.35 to -27.4 over this zone, while $\delta^{15}N$ was highest at the zone base between 11.2 ka to 10.8 ka and a top sample with values ranging between 0.18‰ to 0.35‰, and generally declined over the zone to minimum values (-0.77 ‰ and -0.93‰) at ~8.9 ka and 7.7 ka, respectively.

CMAR values were at the second-highest levels throughout the studied stages. In the first half of the zone, CMAR ranged from 1.05 to 1.6 mg/cm$^2$/yr during a period of the lowest sedimentation rate in the core (0.04 cm/yr). After 9.1 ka, CMAR fluctuated between 1.7 and 3.0 mg/cm$^2$/yr as overall sedimentation increased following the Llao Rock tephra, up to 0.33 cm/yr, with a value ranging from 2.8 to 3.0 mg/cm$^2$/yr prior to Mazama eruption while the zone bottom recorded the lowest sedimentation rate (0.04 cm/yr) (Baig & Gavin, 2023). IMAR had no long-

term trend through this zone, varying between 6 and 30 mg/cm$^2$/yr with sample pre-Mazama eruption with a 230 mg/cm2/yr value due to tephra impact.

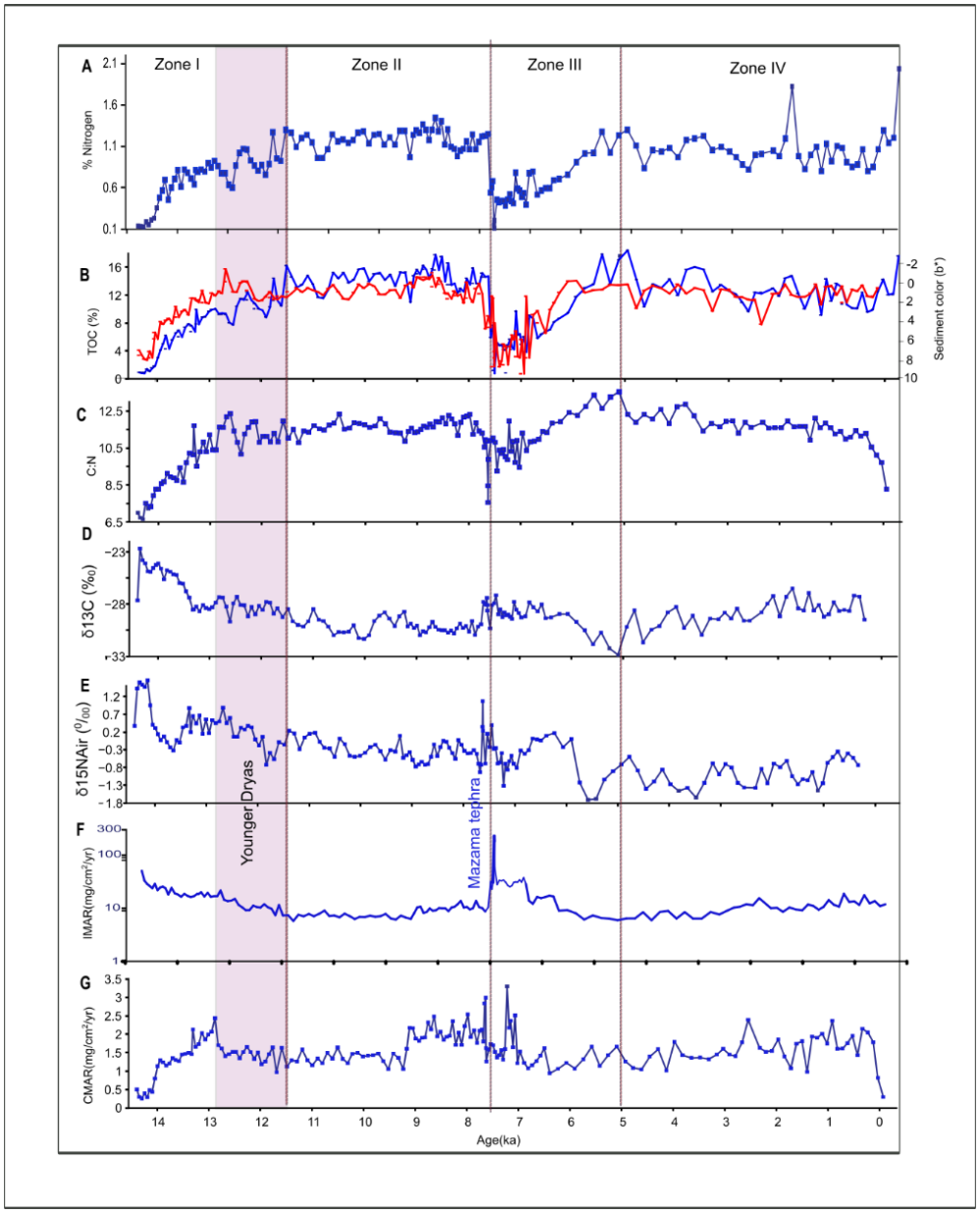


Figure 4. 3 (A) Total nitrogen (%N); (B) Total organic carbon (%C: blue line) and sediment color (b*: red line); (C) C: N ratio; (D) $\delta^{13}C$; (E) $\delta^{15}N$; (F) IMAR (mg/cm$^2$/yr); (G) CMAR (mg/cm$^2$/yr). Solid vertical grey lines mark the boundaries between Late-Glacial, early Holocene pre-Mazama, middle Holocene post-Mazama, and late Holocene.

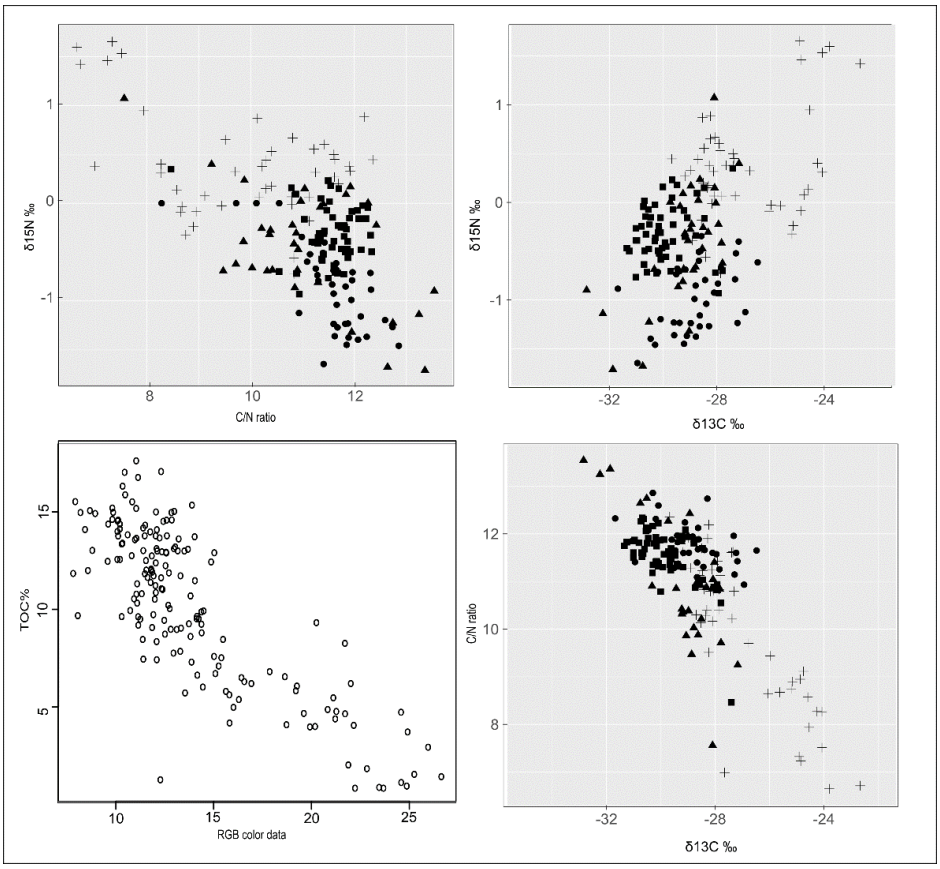


**Figure 4. 4 Cross-plots of Gold Lake geochemical data highlighting relationships between** A) $\delta^{15}N$ and C/N ratio; B) $\delta^{15}N$ and $\delta^{13}C$; C) total organic carbon (TOC%) and RGB color data; D) C/N ratio and $\delta^{13}C$. Late Glacial (marked as a plus sign), early Holocene pre-Mazama (marked as square), middle Holocene post-Mazama (marked as a triangle), late Holocene (marked as a circle).

## Gold III-Middle Holocene-Post-Mazama (700-450 cm; ca. 7.5-5 ka)

The most significant geochemical change observed in zone 3 was a decrease in TOC (1.3% to 0.8%) after the Mazama eruption, a continuation of the decrease from 17.0 % to 1.3% across the Llao Rock tephra in zone II. TOC concentration remains low until 6.2 ka (0.8% to 9.0%) and then increases to 17.7%, the highest value in the record. The C/N ratio decreases to a value of 7.5 after the Mazama eruption and then starts to increase and reaches the highest level (13.5) in the record at 5.5 ka to 5 ka, while $\delta^{13}C$ reaches the lowest level in the core during the same period (-32.9‰).

CMAR fluctuates greatly across the Llao Rock and Mazama tephra but overall declines only 75% (to ca. 1.2 mg/cm$^2$/yr) before peaking at its highest level in the record at 7.2 ka. The sedimentation rate was highest after the Mazama eruption and remained high until 6.5 ka and then fluctuated between 0.33 to 0.13 cm/yr. After 6.5 ka, the sedimentation rate decreases and reaches 0.05 cm/yr at ~5.2 ka. The inorganic mass accumulation rate was high directly after the Mazama tephra but declined from 183.3 to 6.0 mg/cm$^2$/yr through this zone (Fig. 4.3).

Organic content increased from 10 to 33% during this time, while the sedimentation rate (0.06-0.33 cm/yr) showed a declining trend until 5.5 ka before increasing again after 4.8 ka. As laminations abruptly end and the sediment transforms into massive sapropel around 6.4 ka, the sedimentation rate, 0.25-0.12 cm/yr until about 6.8 ka, drops to 0.062 cm/yr.

**Gold IV-Middle/Late Holocene (400-0 cm; ca. 5 ka to present)**

The greatest geochemical change observed in zone IV is the TN concentration that reaches the studied maximum stage levels in the core top at 2.0 % and fluctuates between 0.8 % to 2.0 % in this zone. The C/N ratio reaches the zone minimum value (8.2) at the core top, with values reaching 12.5 between 4.2 and 3.8 ka. During the transition from the middle to late Holocene, TN values stabilized at 5.9 ka; before that, they remained low and fluctuated between 0.1% to 1.3% in the middle Holocene. A sharp increase in TOC concentration starts at 5.9 ka (12-17%) during the middle Holocene and then remains high during this zone, with values fluctuating between 8 to 17% recorded at the core top. $\delta^{13}C$ values fluctuate between -31.7‰ to -26.5‰ during middle/late Holocene. A sharp increase in $\delta^{13}C_{org}$ is observed at ~1.7 ka, 1.4 ka, and 528 cal yr bp with -26.5‰, -26.9‰, and -27.2‰ respectively. $\delta^{15}N$ values fluctuate between -1.7‰ to -0.4‰ and reaches to this zone maximum at ~ 0.7 ka. CMAR values reach the lowest value of the studied stage (0.3) at the core top and reach the zone maximum of 2.4 at ~ 2.5 ka; overall, CMAR values remain stable and in the same range as zone III. Sedimentation rates remain low like zone II until ~1.7 ka (0.06 cm/yr to 0.01 cm/yr), and then a sharp increase in sedimentation rate is observed at ~1.6 ka, where it reaches 0.1cm/yr and then remains high until the core top (Fig. 4.2 & Fig. 4.3).

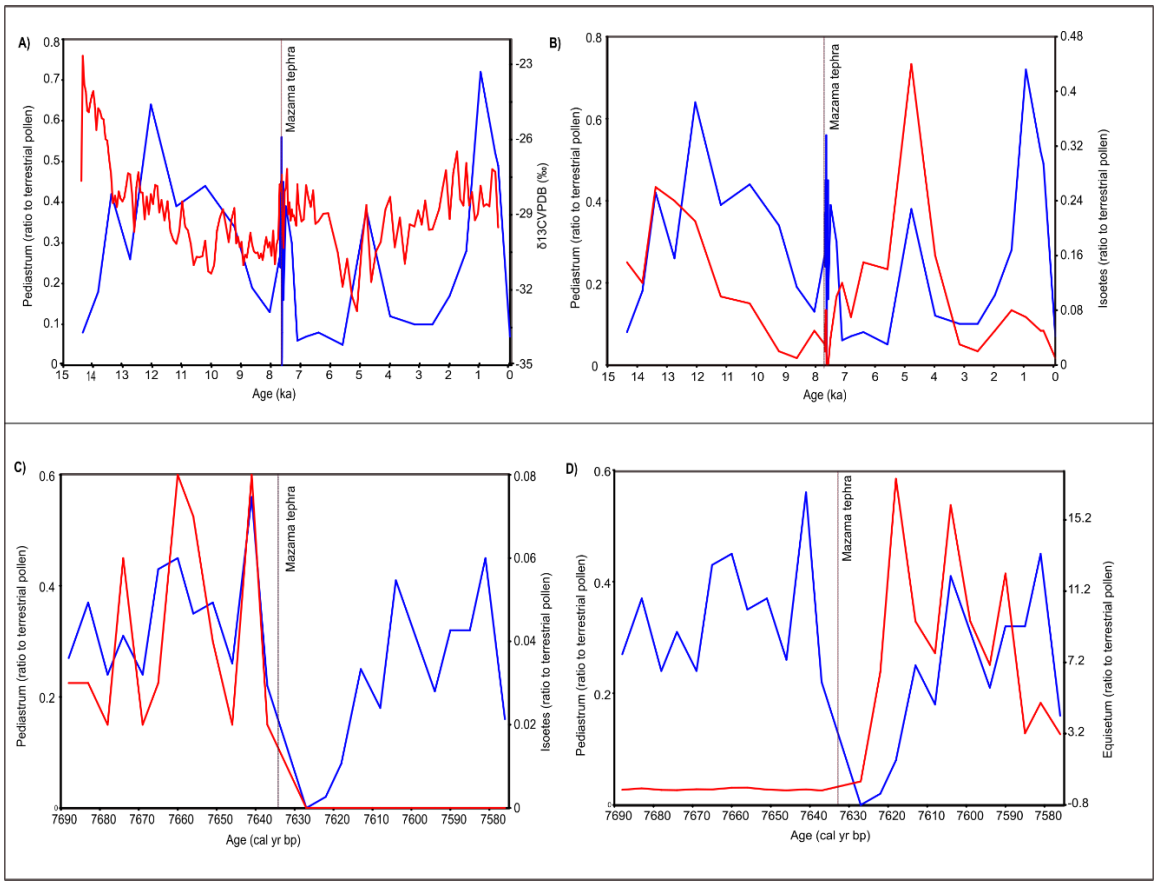


**Figure 4. 5** (A) Comparison between Pediastrum (Pediastrum represented as a ratio of terrestrial pollen counted at Gold Lake and $\delta^{13}C$; (B) Pediastrum vs. Isoetes (C) Pediastrum vs. Isoetes pre- and post-Mazama at every 1cm; (D) Pediastrum vs. Equisetum, pre- and post-Mazama at-every 1cm. Solid vertical grey lines mark the boundaries between pre- and post-Mazama. Pediastrum has been represented as a blue line, while Isoetes, equisetum, and $\delta^{13}C$ are represented as a red line.

# Discussion

## Gold I-Late-Glacial period (1302-1085 cm; ca. 14.4-11.6 ka)

The lowest values for TOC, TN, CMAR, and C/N ratio, with the highest values for $\delta^{13}C_{org}$ and $\delta^{15}N$, were noted towards the start of the Late Glacial period compared to the overall core values. At 11.8 ka, TOC and TN steadily rise, from 0.9% to 13.8% and from 0.13% to 1.27%, respectively, while $\delta^{13}C_{org}$ and $\delta^{15}N$ steadily decrease. At 12.6 ka, the C/N ratio increases and stays high for the remainder of this zone, whereas the lowest CMAR values were found near the base of the core, which increased from 0.2 mg/cm2/yr at 14.2 ka to 2.4 mg/cm$^2$/yr at 12.8 ka.

This pattern represents the development of soil and terrestrial growth around lakes following Younger Dryas (Diefendorf et al., 2008).

Two primary sources that contribute to lake organic matter are aquatic phytoplankton, which produces organic matter with C/N ratios of 4-10, while terrestrial matter has a C/N >20; thus, C/N ratios between 10 and 20 represents a mixture of terrestrial and aquatic. This ratio could be used to determine the relative abundance of allochthonous and autochthonous organic matter (Meyers, 1990, 1994). Most organic matter (more than 50%) at Gold Lake is aquatic, as shown by C/N values <10 for most parts of the core. During the Late Glacial period, the C/N ratio of Gold Lake varied between 7-13, representing most of the organic matter coming from the aquatic productivity. After deglaciation, as the lake was established, a forest was established with more open vegetation around Gold Lake (Baig & Gavin, 2023). Late Glacial sediment of Gold Lake has the highest $\delta^{13}C_{org}$ and $\delta^{15}N$ values with the lowest C/N ratio compared to the remainder of the core, which indicates that primary productivity at Gold Lake is dominated by aquatic phytoplankton in the lake (Kemp et al., 1977). In addition, $\delta^{15}N$ and $\delta^{13}C_{org}$ are positively correlated with each other (r=0.51), and both are negatively correlated with C/N (r=-0.60 and –0.79, respectively). Periods of high productivity increase the relative amounts of aquatic vs. terrestrial organic matter. High productivity also can increase the 13C of the DIC pool in lake water because aquatic plants prefer to take up $^{12}C$ during photosynthesis, leaving dissolved inorganic poles enriched in $^{13}C$, which increases positive $\delta^{13}C$ as primary productivity increases (Meyers & Lallier-Vergès, 1999). Meanwhile, a high 15N may indicate greater nitrogen cycling associated with higher dissolved nitrate concentrations (Talbot, 2001). Higher primary productivity at Gold Lake during deglaciation is in agreement with findings from Jenny Lake, Wyoming (Larsen et al., 2016) and other alpine lake systems in the Rocky Mountains (Slemmons & Saros, 2012). It has been postulated that a high level of inorganic nitrogen is present in meltwater from glaciers, but its source is not well known (Baron et al., 2009; Saros et al., 2010). Similar patterns were observed at Lake Ontario, where an increase in algal productivity accompanied increased $\delta^{15}N$ values (Silliman et al., 1996), as Gold Lake had increased algal productivity with higher $\delta^{15}N$ values.

Glacial sediments were laid down during a period of regional deglaciation, when large glaciers still occurred within the watershed, and subglacial erosion and meltwater transport would have been the primary mechanisms responsible for delivering sediment to the lakes (Karlén, 1981). Two cirque basins within the Gold Lake watershed may have contained ice during the Late Glacial, providing glacial meltwater for centuries. Glaciers in the Gold Lake watershed were providing nitrogen and other nutrients, resulting in high productivity that's driving up $\delta^{13}C_{org}$. However, if glaciers in the watershed reformed during the Younger Dryas, they did not have an effect on 15N or other sediment properties. Changes in aquatic productivity and the terrestrial environment both drive isotope fluctuations in lacustrine sediment records (Diefendorf et al., 2008). Changes in the $\delta^{15}N$ values from high to low during the transition from glacial to non-glacial period represent a relationship between $\delta^{15}N$ and glacier melt water (Larsen et al., 2016). During the glacial period, high $\delta^{15}N$ in the lake suggests a source pool of isotopically enriched N produced on, in, or below the glacier (Talbot, 2001). During the early Holocene, 15N started to decrease and fluctuated around lower values, which might reflect changes in the source and composition of nitrogen being supplied to the lake (Talbot, 2001). A similar decreasing pattern of 15N was found at Jenny Lake in Wyoming (Larsen et al., 2016). Aquatic phytoplankton preferentially assimilates 14N from the lake's dissolved inorganic nitrogen (DIN) pool during photosynthesis, enriching the remaining $\delta^{15}N$ of the residual DIN pool over time. When phytoplankton production rises, aquatic organic matter $\delta^{15}N$ levels rise gradually (Wada & Hattori, 1978). According to Gu et al. (1996), low $\delta^{15}N$ values could be found in lakes despite their status of productivity from low to high because of the presence of cyanobacteria that fix N from the atmosphere, thus decreasing 15N in bulk organic matter.

TOC represents a bulk value of organic matter not affected by remineralization during sedimentation (Meyers, 2003). TOC is overall negatively correlated with $\delta^{13}C_{org}$ ($r=-0.72$). Low TOC occurred during the Late Glacial period when the forest was not fully established after deglaciation. During this period, the lake water was likely cold but nutrient-rich, so both diatom and glacial silt may be a reason for lowering the percent carbon by diluting organic matter. Diatom productivity has a significant role in depressing % carbon, as seen later in the record following the Llao Rock and Mazama tephra. During the Late Glacial, high silica and other

cations were likely entering the lake from freshly exposed rocks after deglaciation. Sand, gravel, and silt provided silica nutrients for diatom to grow rapidly. In order to remove the effect of a diatom and silt dilution on %TOC, CMAR was calculated. However, CMAR is near zero at the base of the core and gradually increases until the start of Younger Dryas and starts to decline and remains steady until 9 ka. While we note that CMAR is low at the core base (suggesting lower productivity), the low CMAR may be an artifact of the age-depth model. As there is no radiocarbon age constraining the age of the core base, the sedimentation rate may be higher at the core base than the estimated sedimentation rate based on our extrapolated age model.

In summary, the Gold Lake core base was composed of silt and clay for 50 cm (14.4–13.8 ka) during the Late Glacial period when glaciers were retreating. $\delta^{15}N$ is very high because glaciers are melting and delivering high $\delta^{15}N$. The zone's sedimentation rate peaked (0.11 cm/year) early on and decreased to its lowest point (0.07 cm/year) near the zone top (Baig & Gavin, 2023).

**Gold II-Early Holocene-Pre-Mazama (1060-860cm; ca. 11.6-7.7 ka)**

The TOC, TN, and C/N ratios reached the zone's lowest values before the Mazama eruption, although higher than in the Late Glacial period. $\delta^{15}N$ values declined from 0.35 to -0.93 over the zone, while $\delta^{13}C_{org}$ varied around -31.6‰ to -28.0 ‰ and reached the zone maximum on the top samples (-27.4‰). CMAR values were at the second highest levels (2.9 to 3) throughout the studied stages prior to the Mazama eruption (Fig. 4.3 & Fig. 4.4). The highest sedimentation rate (0.33 cm/yr) was recorded prior to the Mazama eruption, while the base of the zone had the lowest sedimentation rate (0.04cm/yr) (Baig & Gavin, 2023). Pollen data indicate that early Holocene vegetation was more open (Baig & Gavin, 2023). The level of organic content remained high after an abrupt increase at ~ 13.2 ka; however, after the Llao Rock tephra, LOI decreased to 14% from its high of 37% at 9.2 ka (Baig & Gavin, 2023). The evidence shows productivity slowly increasing during the early Holocene.

An increasing pattern of TOC concentration (10 to 15%) and in CMAR (1.0 to 3 mg $cm^2$/yr) suggests an increase in input from terrestrial organic matter (Cohen, 2003). During this transition, $\delta^{13}C$ values decreased from -28.4‰ to -31.4‰, which may also be the result of increased input from the terrestrial organic material, which is isotopically lighter (Talbot &

Laerdal, 2000). However, at the top of the zone, just after Llao Rock tephra, C/N declines and $\delta^{13}C$ increases, suggesting increased input from aquatic organic matter. $\delta^{15}N$ values were negative except at a few depths where they increased (11.2 ka, 10.8 ka, and the top sample of the core with values 0.18 % and 0.35‰ respectively) that might be due to the effect of isotopically lighter soil nitrogen into lake DIN pool (Peters et al., 1978) and might be due to the fixation of atmospheric nitrogen by cyanobacteria (Hecky & Kling, 1981; Peters et al., 1978) that kept the values very negative at Gold Lake throughout Holocene. Reports show that Gold Lake has a higher concentration of Cyanobacteria (Johnson et al. 1985).

**Gold III-Middle Holocene-Post-Mazama (700-450 cm; ca. 7.5-5 ka)**

After the Mazama eruption, TOC dropped from 1.3% to 0.8%, remained low until 6.2 ka (2-9%), and rose to 11–18%, the highest value in the core. The C/N ratio declined to 7.5 after the Mazama eruption. Then it starts to increase up to the highest level (13.2 to 13.5) of this zone at 5.5 ka to 5 ka, whereas $\delta^{13}C$ reaches the lowest values recorded for this zone ( -31.87 to -32.85) (Fig. 4.3 & Fig. 4.4). These changes are consistent with the lake ecosystem responding to the impact of tephra deposition, Tephra can alter aquatic ecosystems' physical and chemical properties and affect aquatic organisms due to changes in habitat and available nutrients (Egan et al., 2016). The Gold Lake record shows the sensitivity of the lake system to this sudden change (Payne & Egan, 2019).

Due to the deposition of 78 cm of Mazama tephra at Gold Lake, the sedimentation rate increased to 6-7 times higher than the remainder of the core (Baig & Gavin, 2023). During this time, aquatic productivity increased as silica ($SiO_2$) was added to the water column from tephra particles (Barker et al., 2000) that facilitated the production of silicious organisms (Hickman & Reasoner, 1994). Diatom, as one of the major primary producers in the aquatic environment, is highly sensitive to environmental change (Mackay et al., 2003) and is an excellent proxy to assess the impact of tephra deposition on lacustrine ecosystems. This increase in productivity is documented by an increased value of $\delta^{13}C$ (-30.2‰ to -27.2‰) that started to increase at 7.7 ka after Llao Rock eruption and remained high until 5.7 ka, where varves end abruptly in the Gold Lake core (Meyers & Lallier-Vergès, 1999).

The algae Pediastrum and spores from littoral aquatic plants reveal additional immediate impacts of the tephra deposition. After the Llao Rock and Mazama tephra, *Pediastrum* and 13C increased discretely (Fig 4.5), which indicates high algal productivity. Similar patterns were observed by (Haberle et al., 2000) at Laguna Miranda Lake, Chile, and Egan et al. (2016) at Moss Lake, Washington, where Pediastrum increased after tephra deposition with the influx of nutrients. Other changes include an abrupt increase in *Equisetum* and a complete loss of *Isoëtes*. These changes are consistent with the burial of the littoral habitat. Equisetum's long rhizomes may have been able to penetrate through the tephra and rapidly colonize the littoral zone (Antos and Zobel 1985). In contrast, the short root systems of Isoëtes resulted in the temporary extirpation of this species.

After the Mazama eruption, CMAR values plummeted 50% and then fluctuated between 0.94 and 3.2, whereas the sedimentation rate was highest and remained high until 6.5 ka, fluctuating between 0.33 and 0.13, and dropped to 0.05cm/yr at ~ 5.2 ka (Baig & Gavin, 2023). At this stage, TOC, TN, and C/N ratios are lowest at the core bottom and highest at the core top (0.84% to 17.7%, 0.11% to 1.3%, and 7.56 to 13.6 respectively), whereas $\delta^{15}N$ values are highest at the bottom and lowest at the top (1.07 to -1.71), and $\delta^{13}C_{org}$ levels lowest at the core top and highest at 7.5ka, 7.1ka, and 6.8ka (-27.82 to -27.17).

**Gold IV-Middle/Late Holocene (400-0 cm; ca. 5 ka to present)**

The most notable geochemical shift detected during the middle/late Holocene is the increase in TN concentration, which reaches this zone's highest level of 2.1% at the core top. Before the shift from the middle to the late Holocene, TN levels were low and fluctuated between 0.1% and 1.3%. The relative amount of terrestrial organic matter peaked at the start of the zone (C/N= 13.5), though still indicating >50% algal organic content (Meyers & Lallier-Vergès, 1999). The highest values of TN towards the core top and especially at the sediment-water interface may be due to increased human activities around the lake (Kemp et al., 1977) or due to the effects of early diagenesis of labile organic matter (with a higher N content), which may have the effect of reducing C/N over the first decade after deposition (Brahney et al., 2014). Throughout the middle to late Holocene, $\delta^{13}C$ values fluctuate between -while $\delta^{15}N$ value reaches the zone maximum value (-0.35‰) at 722 cal yr bp. The lowest C/N ratio (8.2) was

found at the top, while the highest ratios were recorded at 4.2 ka and 3.8 ka (12.5 and 12.8, respectively). At the core top, CMAR values drop to the lowest point for the studied stage (0.3) and reach the zone's highest value (2.4) at ~2.5 ka.

Aquatic productivity indicators increased over this zone after reaching a minimum at 5 ka. $\delta^{13}C$ increased from 31.7‰ to -26.5‰ and reached the zone maximum (-26.48 ‰) at ~ 1.7 ka, as IMAR increased, and C/N decreased. Productivity indicators for the past 2000 yr are greater than occurred in the early Holocene and close to the post-Mazama varve period. The low productivity likely represents the loss of Si fertilization as tephra is buried in sediment and organic soils develop. The millennial-scale increase in productivity may reflect climatic factors, such as increased late Holocene precipitation and nutrient delivery to the lake or autogenic processes of nutrient accumulation and recycling within the lake (Cohen, 2003). There is little other evidence of climatic drivers of millennial-scale trends in productivity. The lower $\delta^{15}N$ values, especially after 5.4 ka, can be related to increased input from terrestrial input with an increasing C/N ratio (Arcagni et al., 2015) along with cyanobacteria which have higher N content compared to other phytoplankton (Gu & Alexander, 1996). The existence of cyanobacteria, which can fix nitrogen from the atmosphere and so increase the lake's productivity, is one argument that may be put forward for this. According to the Oregon Lake Atlas study, Cyanobacteria are found in Gold Lake. The isotopic nitrogen levels in Gold Lake are notably negative, which is rare for temperate lakes (McLauchlan et al., 2013). It is interesting to observe that the nitrogen levels are only positive at the lake's bottom. Therefore, the C/N ratio and $\delta^{15}N$, which are inversely correlated (r=-0.42), both reflect the cyanobacterial remains in the sediment. This interpretation is consistent with cyanobacteria causing the low $\delta^{15}N$ values in Gold Lake. However, additional investigation may provide insight into this interpretation and the drivers of cyanobacteria presence in Gold Lake.

## Conclusion

Our detailed geochemical analysis of Gold Lake lacustrine sediment provides information about paleo-productivity during major climatic events of the Late Glacial and Holocene and volcanic eruptions. A C/N ratio between 8 and 13 indicates that Gold Lake organic matter has more than 50% of the algal organic content. During the Late Glacial period, when it was affected

by receding glaciers and soil was not very well developed, it has the highest $\delta^{13}C_{org}$ and $\delta^{15}N$ values with the lowest C/N ratio compared to the remainder of the core, which indicates that primary productivity at Gold Lake is dominated by aquatic phytoplankton in the lake. Higher aquatic productivity is due to adding nutrients to the lake due to the supply of glacial melt water. Increasing C/N rations preceding and through the Younger Dryas represent soil development and vegetation structure in the newly deglaciated landscape. Higher early Holocene C/N ratios, with low $\delta^{13}C_{org}$, remained constant until the Llao Rock eruption at Gold Lake. The deposition of 78 cm of Mazama tephra at Gold Lake raised the sedimentation rate to 6-7 times faster than the rest of the core. During this time, aquatic productivity rose as silica from tephra particles entered the water column. During the late Holocene, the highest values of TN represented an increase in the load of terrestrial organic matter and human activities around the lake. After low productivity ($\delta^{13}C$ < -30‰, C: N>12), the late Holocene returned to high aquatic productivity similar to the post-Mazama period and higher than during the early Holocene. This detailed record of aquatic productivity significantly contributes to understanding climate change and ecosystem changes in the Oregon High Cascades. More detailed studies at higher temporal resolution (ca. 1 cm or 10 yr) resolution, including diatoms taxonomic identification, will add more explanation to the existing paleo productivity record and the impact of several factors contributing to it.

## References


Adrian, R., Deneke, R., Mischke, U., Stellmacher, R., & Lederer, P. (1995). A long-term study of the Heiligensee (1975-1992). Evidence for effects of climatic change on the dynamics of eutrophied lake ecosystems. *Archiv Fur Hydrobiologie*, *133*(3), 315–337. https://doi.org/10.1127/ARCHIV-HYDROBIOL/133/1995/315

Arcagni, M., Rizzo, A., Campbell, L. M., Arribére, M. A., Juncos, R., Reissig, M., Kyser, K., Barriga, J. P., Battini, M., & Guevara, S. R. (2015). Stable isotope analysis of trophic structure, energy flow and spatial variability in a large ultraoligotrophic lake in Northwest Patagonia. *Journal of Great Lakes Research*, *41*(3), 916–925. https://doi.org/10.1016/J.JGLR.2015.05.008

Baig, J., & Gavin, D. G. (2023). Postglacial vegetation and fire history with a high-resolution analysis of tephra impacts, high Cascade Range, Oregon, USA. *Quaternary Science Reviews*, *303*, 107970. https://doi.org/10.1016/j.quascirev.2023.107970

Barker, P., Telford, R., Merdaci, O., Williamson, D., Taieb, M., Vincens, A., & Gibert, E. (2000). The sensitivity of a Tanzanian crater lake to catastrophic tephra input and four millennia of climate change.

*Http://Dx.Doi.Org/10.1191/095968300672848582*, *10*(3), 303–310. https://doi.org/10.1191/095968300672848582

Baron, J. S., Schmidt, T. M., & Hartman, M. D. (2009). Climate-induced changes in high elevation stream nitrate dynamics. *Global Change Biology*, *15*(7), 1777–1789. https://doi.org/10.1111/J.1365-2486.2009.01847.X

Battarbee, R. W., Jones, V. J., Cameron, N. G., Carvalho, L., & JUGGINS, S. (2002). Diatoms. In K. (eds) T. E. C. U. L. S. D. in P. R. Smol, J.P., Birks, H.J.B., Last, W.M., Bradley, R.S., Alverson (Ed.), *Diatoms. In: Smol, J.P., Birks, H.J.B., Last, W.M., Bradley, R.S., Alverson, K. (eds) Tracking Environmental Change Using Lake Sediments. Developments in Paleoenvironmental Research* (pp. 155–190). Springer. https://doi.org/https://doi.org/10.1007/0-306-47668-1_8

Blaauw, M., & Christen, J. A. (2011). *Bacon manual – v 2.3.9.1*. 1–15.

Cohen, A. S. (2003). The Geological Evolution of Lake Basins. *Paleolimnology: The History and Evolution of Lake Systems*.

Dean, W. E. (1999). The carbon cycle and biogeochemical dynamics in lake sediments. Journal of paleolimnology, 21, 375-393.

Debret, M., Desmet, M., Balsam, W., Copard, Y., Francus, P., & Laj, C. (2006). Spectrophotometer analysis of Holocene sediments from an anoxic fjord: Saanich Inlet, British Columbia, Canada. *Marine Geology*, *229*(1–2), 15–28. https://doi.org/10.1016/J.MARGEO.2006.01.005

Deng, Y. N., Rioual, P., Jones, V. J., Sun, C., & Mingram, J. (2023). A palaeoecological study investigating the impacts of multiple tephra depositions on a lacustrine ecosystem in Northeast China, using diatoms as environmental indicators. Journal of Paleolimnology, 70(1), 1-22.

Diefendorf, A. F., Patterson, W. P., Holmden, C., & Mullins, H. T. (2008). Carbon isotopes of marl and lake sediment organic matter reflect terrestrial landscape change during the late Glacial and early Holocene (16,800 to 5,540 cal yr B.P.): A multiproxy study of lacustrine sediments at Lough Inchiquin, western Ireland. *Journal of Paleolimnology*, *39*(1), 101–115. https://doi.org/10.1007/s10933-007-9099-9

Dunnette, P. V., Higuera, P. E., Mclauchlan, K. K., Derr, K. M., Briles, C. E., & Keefe, M. H. (2014). Biogeochemical impacts of wildfires over four millennia in a Rocky Mountain subalpine watershed. *New Phytologist*, *203*(3), 900–912. https://doi.org/10.1111/nph.12828

Egan, J., Fletcher, W. J., Allott, T. E. H., Lane, C. S., Blackford, J. J., & Clark, D. H. (2016). The impact and signi fi cance of tephra deposition on a Holocene forest environment in the North Cascades , Washington , USA. *Quarternary Science Reviewternary Science Review*, *137*, 135–155.

Egan, J., Staff, R., & Blackford, J. (2015). A high-precision age estimate of the Holocene Plinian eruption of Mount Mazama, Oregon, USA. *Holocene*, *25*(7), 1054–1067. https://doi.org/10.1177/0959683615576230

Faegri K, PE, K., & K, K. (1989). *Textbook of Pollen Analysis*. Wiley.

Gu, B., & Alexander, V. (1996). Stable carbon isotope evidence for atmospheric CO2 uptake by cyanobacterial surface scums in a eutrophic lake. *Applied and Environmental Microbiology*, *62*(5), 1803–1804. https://doi.org/10.1128/AEM.62.5.1803-1804.1996

Gu, B., Schelske, C. L., & Brenner, M. (1996). Relationship between sediment and plankton isotope ratios (δ13C and δ15N) and primary productivity in Florida lakes. *Canadian Journal of Fisheries and Aquatic Sciences*, *53*(4), 875–883. https://doi.org/10.1139/f95-248

Haberle, S. G., Szeicz, J. M., & Bennett, K. D. (2000). Late Holocene vegetation dynamics and lake geochemistry at Laguna Miranda, XI Region, Chile Dinámica vegetaciónal y geoquímica lacustre del Holoceno tardío en Laguna Miranda, XI Región, Chile. BMC.

Hecky, R. E., & Kling, H. J. (1981). The phytoplankton and protozooplankton of the euphotic zone of Lake Tanganyika: Species composition, biomass, chlorophyll content, and spatio-temporal distribution. *Limnology and Oceanography*, *26*(3), 548–564. https://doi.org/10.4319/LO.1981.26.3.0548

Hickman, M., & Reasoner, M. A. (1994). Diatom responses to late Quaternary vegetation and climate change, and to deposition of two tephras in an alpine and sub-alpine lake Yoho National Park, British Columbia. *J Paleolimn*, *11*(2), 173–188. https://doi.org/10.1007/bf00686864

Hodell, D. A., & Schelske, C. L. (1998). Production, sedimentation, and isotopic composition of organic matter in Lake Ontario. *Limnology and Oceanography*, *43*(2), 200–214. https://doi.org/10.4319/LO.1998.43.2.0200

Hu, F. S., Finney, B. P., & Brubaker, L. B. (2001). Effects of holocene Alnus expansion on aquatic productivity, nitrogen cycling, and soil development in southwestern Alaska. *Ecosystems*, *4*(4), 358–368.

Jellison, R., Anderson, R. F., Melack, J. M., & Heil, D. (1996). Organic matter accumulation in sediments of hypersaline Mono Lake during a period of changing salinity. *Limnology and Oceanography*, *41*(7), 1539–1544. https://doi.org/10.4319/LO.1996.41.7.1539

Johnson, D. M., R.R., P., D.R., L., J.W., S., M.E., N., & A.L., and S. (1985). *Atlas of Oregon lakes*. Oregon State University Press.

Karlén, W. (1981). Lacustrine Sediment Studies. A Technique to Obtain a Continous Record of Holocene Glacier Variations. *Source: Geografiska Annaler. Series A, Physical Geography*, *63*(4), 273–281.

Kemp, A. L. W., Thomas, R. L., Wong, H. K. T., & Johnston, L. M. (1977). Nitrogen and C/N ratios in the sediments of Lakes Superior, Huron, St. Clair, Erie, and Ontario. *Canadian Journal of Earth Sciences*, *14*(10), 2402–2413. https://doi.org/10.1139/e77-205

Larsen, D. J., Finkenbinder, M. S., Abbott, M. B., & Ofstun, A. R. (2016). Deglaciation and postglacial environmental changes in the Teton Mountain Range recorded at Jenny Lake, Grand Teton National Park, WY. *Quaternary Science Reviews*, *138*, 62–75. https://doi.org/10.1016/j.quascirev.2016.02.024

Mackay, A. W., Jones, V. J., & Battarbee, R. W. (2003). Approaches to Holocene climate reconstruction using diatoms. In *Mackay A, Battarbee R, Birks J, Oldfield F (eds) Global Change in the Holocene* (pp. 294–309). Routledge, London.

McLauchlan, K. K., Craine, J. M., Oswald, W. W., Leavitt, P. R., & Likens, G. E. (2007). Changes in nitrogen cycling during the past century in a northern hardwood forest. *Proceedings of the National Academy of Sciences of the United States of America*, *104*(18), 7466–7470. https://doi.org/10.1073/PNAS.0701779104

Meyers, P. A. (1990). Impacts of late Quaternary fluctuations in water level on the accumulation of sedimentary organic matter in Walker Lake, Nevada. *Palaeogeography, Palaeoclimatology, Palaeoecology*, *78*(3–4), 229–240. https://doi.org/10.1016/0031-0182(90)90216-T

Meyers, P. A. (1994a). Preservation of elemental and isotopic source identification of sedimentary organic matter. In *Chemical Geology* (Vol. 114).

Meyers, P. A. (1994b). Preservation of elemental and isotopic source identification of sedimentary organic matter. *Chemical Geology*, *114*(3–4), 289–302. https://doi.org/10.1016/0009-2541(94)90059-0

Meyers, P. A. (2003). Applications of organic geochemistry to paleolimnological reconstructions: A summary of examples from the Laurentian Great Lakes. *Organic Geochemistry*, *34*(2), 261–289. https://doi.org/10.1016/S0146-6380(02)00168-7

Meyers, P. A., & Lallier-Vergès, E. (1999). Lacustrine sedimentary organic matter records of Late Quaternary paleoclimates. *Journal of Paleolimnology*, *21*(3), 345–372. https://doi.org/10.1023/A:1008073732192

Payne, R. J., & Egan, J. (2019). Using palaeoecological techniques to understand the impacts of past volcanic eruptions. *Quaternary International*, *499*, 278–289. https://doi.org/10.1016/j.quaint.2017.12.019

Peters, K. E., Sweeney, R. E., & Kaplan, I. R. (1978). Correlation of carbon and nitrogen stable isotope ratios in sedimentary organic matter. *Limnol. Oceanogr*, *23*(4), 598–604. https://doi.org/10.4319/lo.1978.23.4.0598

Peterson, B. J., & Howard, R. W. (1987). Sulfur, carbon, and nitrogen isotopes used to trace organic matter flow in the salt-marsh estuaries of Sapelo Island, Georgia l. *Limnol. Oceanogr*, *32*(6), 1195–1213. https://doi.org/10.4319/lo.1987.32.6.1195

Reimer, P. J., Austin, W. E. N., Bard, E., Bayliss, A., Blackwell, P. G., Bronk Ramsey, C., Butzin, M., Cheng, H., Edwards, R. L., Friedrich, M., Grootes, P. M., Guilderson, T. P., Hajdas, I., Heaton, T. J., Hogg, A. G., Hughen, K. A., Kromer, B., Manning, S. W., Muscheler, R., … Talamo, S. (2020). The IntCal20 Northern Hemisphere Radiocarbon Age Calibration Curve (0–55 cal kBP). *Radiocarbon*, *62*(4), 725–757. https://doi.org/10.1017/RDC.2020.41

Saros, J. E., Rose, K. C., Clow, D. W., Stephens, V. C., Nurse, A. B., Arnett, H. A., Stone, J. R., Williamson, C. E., & Wolfe, A. P. (2010). Melting alpine glaciers enrich high-elevation lakes with reactive nitrogen. *Environmental Science and Technology*, *44*(13), 4891–4896.

Schnurrenberger, D., Russell, J., & Kelts, K. (2003). Classification of lacustrine sediments based on sedimentary components. *Journal of Paleolimnology*, *29*(2), 141–154. https://doi.org/10.1023/A:1023270324800

Sea, D. S., & Whitlock, C. (1995). Postglacial Vegetation and Climate of Cascade Range, central oregon. *Quater*, *43*, 370–381.

Silliman, J. E., Meyers, P. A., & Bourbonniere, R. A. (1996). Record of postglacial organic matter delivery and burial in sediments of Lake Ontario. *Organic Geochemistry*, *24*(4), 463–472. https://doi.org/10.1016/0146-6380(96)00041-1

Slemmons, K. E. H., & Saros, J. . (2012). Implications of nitrogen-rich glacial meltwater for phytoplankton diversity. *Limnol. Oceanogr*, *57*, 1651–1663.

Talbot, M. R. (2001). Nitrogen isotopes in paleolimnology. In J. P. (Eds. L. W. M. Smol (Ed.), *Tracking Environmental Change Using Lake Sediments, Physical and Geochemical Methods* (pp. 401–439). Kluwer, Dordrecht.

Talbot, M. R., & Johannessen, T. (1992). A high resolution palaeoclimatic record for the last 27,500 years in tropical West Africa from the carbon and nitrogen isotopic composition of lacustrine organic matter. *Earth and Planetary Science Letters*, *110*(1–4), 23–37. https://doi.org/10.1016/0012-821X(92)90036-U

Talbot, M. R., & Laerdal, T. (2000). The Late Pleistocene-Holocene palaeolimnology of Lake Victoria, East Africa, based upon elemental and isotopic analyses of sedimentary organic matter . *Journal of Paleolimnology*, *23*, 141–164.

Teranes, J. L., & Bernasconi, S. M. (2000). The record of nitrate utilization and productivity limitation provided by 15 N values in lake organic matter-A study of sediment trap and core sediments from Baldeggersee, Switzerland. *Limnol. Oceanogr*, *45*(4), 801–813.

Wada, E., & Hattori, A. (1978). Nitrogen isotope effects in the assimilation of inorganic nitrogenous compounds by marine diatoms. *Geomicrobiology*, *1*(1), 85–101. https://doi.org/10.1080/01490457809377725

Zolitschka, B., Francus, P., Ojala, A. E. K., & Schimmelmann, A. (2015). Varves in lake sediments - a review. *Quaternary Science Reviews*, *117*, 1–41. https://doi.org/10.1016/j.quascirev.2015.03.019

# V. CONCLUDING SUMMARY

In this dissertation, a multiproxy approach was used to study vegetation change, fire history, the impact of Mazama tephra, lake paleo productivity, and paleotemperature reconstruction to present a complete picture of climate change and its impact on aquatic and terrestrial ecosystems around the Gold Lake by using lacustrine sediment from the Gold Lake, Oregon. Paleotemperature reconstruction using chironomid head capsules is the first attempt in Oregon using the IMW data set developed by Haskett & Porinchu (2014).

The Gold Lake pollen and charcoal research reveals vegetation and fire response to major climatic and disturbance events like the Late Glacial, Holocene, and volcanic eruptions. High charcoal peaks in the Late Glacial period correlated with increased open vegetation and warm temperatures that provided forest fire fuel. Less moisture and climate circumstances that inhibited herbaceous and shrub cover, which provides surface fuel for major fires, may have reduced fires in the early Holocene. Unlike other Pacific Northwest locations, the High Cascades Range may have been fuel-limited or supported a low-severity fire regime during the early Holocene. Mazama tephra affected both arboreal and non-arboreal taxa, where arboreal taxa's relative abundance changed, but non-arboreal taxa's composition changed. Frequent low-magnitude charcoal peaks and greater NAP abundance suggest the tephra promoted a millennium-long low-severity fire regime. More significant charcoal peaks reflected more catastrophic fires throughout the late Holocene when forest density increased. The tephra's spatial pattern and species-specific effects on plants and fire require more high-resolution studies to understand this significant event in Pacific Northwest paleoenvironmental history.

Chironomid-based quantitative reconstructions are rare and developing in the US. Gold Lake midge-inferred MJAT predicts a cold condition during the Late Glacial period with ~10.6 °C, 1.6 °C cooler than today. The Younger Dryas event had a lowest temperature of 9.4 °C and an increasing temperature trend through the early Holocene. Thermophilus taxa increased as the early Holocene temperature reached 12.0 °C at 9.2 ka. The middle Holocene was colder than the early Holocene. At ~2.5 ka, the Northeast Pacific sea surface temperature increased by 1.0 °C, as inferred by alkenone SST (Barron et al., 2003). The late Holocene at Gold Lake was the warmest period of the Holocene and provided clear evidence of rising temperature during the Medieval

Climatic Optimum (MCA), yet sample resolution was insufficient to address the MCA and Little Ice Age (LIA). Although poorly collected (multi-centennial intervals), chironomid MJAT history revealed Mazama tephra's effect on temperature and a late Holocene temperature trend. This shows that more studies, particularly Pacific Northwest lakes, and higher temporal resolution, are needed to contextualize future climatic changes. The IMW training data set was statistically suitable for Gold Lake history, but expanding it to the Pacific Northwest will improve its temperature reconstruction from Pacific Northwest lakes.

Gold Lake's high-resolution geochemical investigation of lacustrine sediment provides varying degrees of paleo productivity during major climatic events. Gold Lake data shows that aquatic phytoplankton dominated primary productivity during the Late Glacial period when the soil was poorly developed, and glacial meltwater nutrients increased lake productivity. Early Holocene C/N ratios with low $\delta^{13}C_{org}$ values stayed consistent until the Llao Rock eruption at Gold Lake, indicating soil development and vegetation structure in the newly deglaciated terrain. Mazama tephra deposited at Gold Lake accelerated sedimentation by 6-7 times, and due to silica from tephra particles, aquatic productivity increased. During the late Holocene, TN values increased due to terrestrial organic materials and human activity near the lake. Late Holocene had higher aquatic productivity than the post-Mazama period than the early Holocene. This extensive aquatic production record helps explain climate and ecosystem changes in the Oregon High Cascades. Having high-resolution studies, including diatoms, will add more explanation to the record presented here and will be helpful for other studies carried out in the region.

Through a comprehensive analysis of Gold Lake, this dissertation offers a unique approach that provides a fuller understanding of climate change's impact on aquatic and terrestrial ecosystems. Utilizing a multi-proxy approach, such as vegetation changes, fire history, paleo productivity, and temperature reconstructions, we were able to gather highly detailed information on the recovery process following the tephra's impact on vegetation and fire. This study's findings can be utilized for future research in the region, and it underscores the importance of conducting multiproxy studies at multiple sites to comprehend climatic events on a larger scale.

# SUPPLEMENTARY DOCUMENTS

## Supplementary for Chapters II, III, and IV

**Figure S. 1** Lines scan image of all cores from Gold Lake, annotated with tie points between parallel drives. Tie points on individual cores are shown with red lines, while links to other drives are shown with red dash lines.78 cm of Mazama tephra is also included in this image. Each core is given a specific name based on the drive I & II and core number (GOLD18-1A-1P-1 & GOLD18-2A-1P-1), i.e., Gold18 (Gold Lake cored in 2018):1A/2A (Drive 1 & 2):1-13P (number of core):1(Number of holes to recover cores from Gold Lake). The column starts, and the endpoint shows the integrated stratigraphic order of drives I and II. This figure image is included separately.

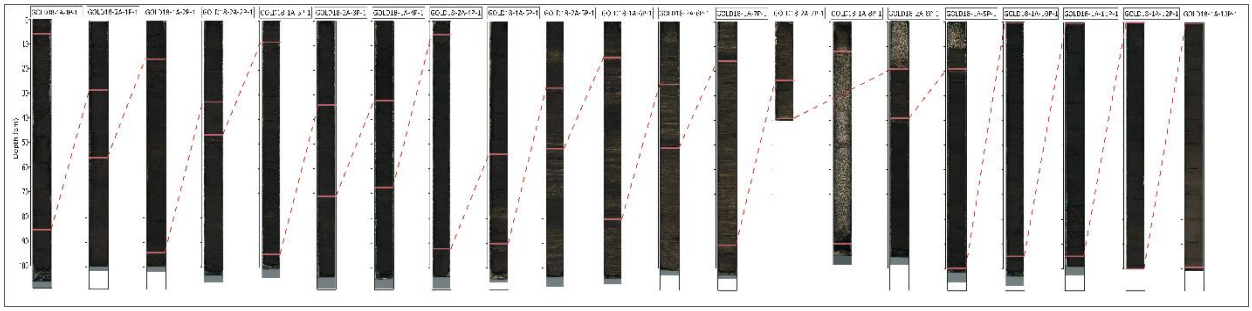

**Table S. 1** Electron microprobe analysis of tephra chemistry from Gold Lake 241 cm. 23 shards were analyzed at the Washington State University Peter Hooper GeoAnalytical Lab. Glass composition is reported in weight % oxides, normalized to 100%. Using their tephra geochemistry database, the analysis produced a match to the Rock Mesa tephra from South Sister with a dissimilarity coefficient of 0.99.

Sample: Gold IC 241

| | Average | Standard deviation |
|---|---|---|
| $SiO_2$ | 76.66 | 0.30 |
| $Al_2O_3$ | 12.95 | 0.16 |
| $Fe_2O_3$ | 1.30 | 0.07 |
| $TiO_2$ | 0.19 | 0.02 |
| $Na_2O$ | 3.94 | 0.16 |
| $K_2O$ | 3.76 | 0.11 |
| MgO | 0.16 | 0.03 |
| CaO | 0.93 | 0.10 |

| | | |
|---|---|---|
| Cl | 0.11 | 0.02 |
| Total | 100.0 | |

**Table S. 2** Details of Livingstone core drives and initial core description, Gold Lake, Oregon.

| LAKE CORE SECTION | **Measured depth in the field (cm)** | **Recovered core length (meter)** | **Top and base of** section (cm) | **START AND ENDPOINT** | **Core description** | TIE POINT BETWEEN DRIVE I & II |
|---|---|---|---|---|---|---|
| DRIVE I A JB-GOLD18-1A-1P-1 | 1240-1340 | 1 meter | 35-131 | 40-122 | The entire core is dark brown, with light brown patches and dark black patches, a firm white band at 102cm | 120cm-move to IIA, where sediment was slightly lighter and had the same tie point in IIA |
| DRIVE IIA JB-GOLD18-2A-1P-1 | 1300-1400 | 1 meter | 94-192 | 122-149 | Dark brown sediment with lighter bands, white patches, Brownish red gyttja | 149cm-Abrupt change to a lighter brown; move to IB |
| DRIVE IB JB-GOLD18-1A-2P-1 | 1340-1440 | 1 meter | 133-229 | 149-227 | Uniform dark brown sapropel with light diatom bands, light brown at some points, dark blue bands, dark blue bands at 163 and 167, white bands at 151, 152, black band at 166-167, a dark blue band with white patches between 200-205 | 227cm to IIB, dark brown sediment after lighter color sediment |
| DRIVE IIB JB-GOLD18-2A-2P-1 | 1400-1500 | 1 meter | 194-291 | 227-239 | Reddish brown organic gyttja, micro tephra band at 50cm | 240-241cm(1 cm tephra layer-Rock Mesa eruption) |
| DRIVE IC JB-GOLD18-1A-3P-1 | 1440-1540 | 1 meter | 229-330 | 239-326 | Alternate layers of light and dark brown bands, blue bands at some point, white patches | 326cm-abrupt color change into the dark brown |
| DRIVE IIC JB-GOLD18-2A-3P-1 | 1500-1600 | 1 meter | 292-392 | 326-363 | Possible lamination at the bottom, 92cm light brown streak | 363cm-1/2 cm ark blue band |
| DRIVE ID JB-GOLD18-1A-4P-1 | 1540-1640 | 1 meter | 329-428 | 363-399 | Uniform dark brown with light bands and BBB layers (blue, brown, black) | 399cm-light brown color- an abrupt change |
| DRIVE IID JB-GOLD18-2A-4P-1 | 1600-1700 | 1 meter | 391-491 | 399-483 | The whole core is uniformly dark brown sediment with light bands at some depth, Brownish red organic | 483cm-light molted, black, blue, brown bands |
| DRIVE IE JB-GOLD18-1A-5P-1 | 1640-1740 | 1 meter | 429-527 | 483-519 | Dark brown sediment with patches of light brown and irregular depths, thick lamination from 502-510cm, pinkish sediment at some point | 519cm-thick laminations |
| DRIVE IIE JB-GOLD18-2A-5P-1 | 1700-1800 | 1 meter | 491-591 | 519-542 | laminations | 542cm-thick laminations |

| | | | | | | |
|---|---|---|---|---|---|---|
| DRIVE IF<br>JB-GOLD18-1A-6P-1 | 1740-1840 | 1 meter | 528-627 | 542-608 | Classic chemically created varves. Diatoms might have gone crazy after Mazama; high silica content from tephra. | 608cm-dark blue bands with white and dark brown bands from 602-608cm |
| DRIVE IIF<br>JB-GOLD18-2A-6P-1 | 1800-1900 | 1 meter | 592-691 | 608-642 | Highly laminated | 642cm-1cm dark brown band followed by alternate white and brown bands |
| DRIVE IG<br>JB-GOLD18-1A-7P-1 | 1840-1940 | 1 meter | 628-724 | 642-718 | Varves all the way down, more laminations, years of forest succession after a fire | 718cm-1/2cm dark blue band |
| DRIVE IIG<br>JB-GOLD18-2A-7P-1 | 1900-2000 | 1 meter | 692-791 | 718-732 | Large lapilli tephra lost, 732 is the endpoint because tephra was lost, 41cm above tephra (59cm) was recovered.<br>As Mazama tephra recovered in I-H is 78cm, the next starting point on drive IH is 810cm. | 732cm, (732+78cm of Mazama tephra=810 next starting point on IIH) start of Mazama tephra layer |
| DRIVE IH | 1940-2040 | 94 cm | Drive IH was not split due to having 78cm of tephra | | First 12 cm varves, Organic matter after Mazama shows a huge ecological shift,<br>Organic at bottom<br>Lapilli, 1cm fragment at top,<br>5-8cm mixed tephra and sediment,<br>8-60cm coarse tephra<br>60-81cm much coarser<br>81-93cm laminated sediment,<br>Between 47-48cm and 52-56cm black boundaries. | |
| DRIVE IIH<br>JB-GOLD18-2A-8P-1 | 2000-2100 | 1 meter | 792-880 | 811-831 | Some dark banding,<br>No more drive II cores due to the time limit, so we stopped here | 811- a mix of tephra and sediment. Dark sediment followed by varves |
| DRIVE I-I<br>JB-GOLD18-1A-9P-1 | 2040-2140 | 97cm | 811-911 | 831-911 | Firm brown sediment | 832-1cm Llao Rock eruption ash layer |
| DRIVE IJ<br>JB-GOLD18-1A-10P-1 | 2140-2240 | 1 meter | 912-1008 | 911-1007 | All brown firm sediment, a smear of tephra at bottom | 911-Uniform dark brown sediment |
| DRIVE IK<br>JB-GOLD18-1A-11P-1 | 2240-2340 | 1 meter | 1008-1104 | 1007-1103 | Two white macro-organic layers around 85cm, all mucky brown sediment | 1007cm-Uniform dark brown sediment followed by a black band |
| DRIVE IL<br>JB-GOLD18-1A-12P-1 | 2340-2440 | 1 meter | 1104-1203 | 1103-1202 | Possible micro varves | 1103cm-Thick lamination followed by a white layer |
| DRIVE IM<br>JB-GOLD18-1A-13P-1 | 2440-2540 | 1 meter | 1203-1302 | 1202-1302 | Possible glacial transition at 50-60cm, very grey at 92cm, dark brown at 96cm, silty at the end, and could not push more to get core, stopped coring | 1202cm-Alternative bands of very dark grey and reddish-brown sediment |

## Supplementary for Chapter IV

**Table S 4. 1** Physico chemical parameters measured during the fieldwork at Gold Lake

| Depth | Dissolved oxygen (%) | Temperature (°C) | Conductivity (µS/cm) |
|---|---|---|---|
| 0 | 81 | 18.1 | 42 |
| 1 | 78 | 18.2 | 41.7 |
| 2 | 77 | 18.2 | 41.3 |
| 3 | 88 | 15.8 | 39.3 |
| 4 | 85 | 12.8 | 35.8 |
| 5 | 78 | 10.5 | 30.8 |
| 6 | 53 | 8.2 | 32.6 |
| 7 | 38 | 7.2 | 33.4 |
| 8 | 28 | 6.6 | 33.4 |
| 9 | 28 | 6.4 | 33.7 |
| 10 | 19 | 6.1 | 34.2 |
| 11 | 15 | 5.9 | 34.4 |
| 12 | 12.8 | 5.9 | 34.5 |